UC Santa Cruz

UC Santa Cruz Electronic Theses and Dissertations

Title

Characterizing the function of the Helicobacter pylori chemoreceptor TlpA, its role in regulating gastric localization, and effect on inflammation in vivo

Permalink

https://escholarship.org/uc/item/0n82b4f2

Author

Johnson, Kevin Scot

Publication Date

2021

Copyright Information

This work is made available under the terms of a Creative Commons Attribution License, availalbe at https://creativecommons.org/licenses/by/4.0/

Peer reviewed|Thesis/dissertation

eScholarship.org Powered by the California Digital Library
University of California

UNIVERSITY OF CALIFORNIA
SANTA CRUZ

CHARACTERIZING THE FUNCTION OF THE *HELICOBACTER PYLORI* CHEMORECEPTOR TLPA, ITS ROLE IN REGULATING GASTRIC LOCALIZATION, AND EFFECT ON INFLAMMATION *IN VIVO*

A dissertation submitted in partial satisfaction
of the requirements for the degree of

DOCTOR OF PHILOSOPHY

in

MICROBIOLOGY AND ENVIRONMENTAL TOXICOLOGY

by

Kevin S. Johnson

September 2021

The Dissertation of Kevin S. Johnson is approved:

_____
Professor Karen M. Ottemann, Chair

_____
Professor Victoria Auerbuch Stone

_____
Professor Fitnat Yildiz

_____
Professor Martha Zúñiga

_____
Peter F. Biehl
Vice Provost and Dean of Graduate Studies

Table of Contents

List of Figures

List of Tables

ABSTRACT

Characterizing the function of the *Helicobacter pylori* chemoreceptor TlpA, its role in regulating gastric localization, and effect on inflammation *in vivo*

Kevin S. Johnson

Helicobacter pylori is a ubiquitous bacterial pathogen, colonizing half of the world's population. Stomach colonization leads to inflammation development, called gastritis. Depending on the severity of gastritis, more serious diseases can develop, such as peptic ulcers or gastric cancer. To successfully colonize the gastric niche, *H. pylori* uses chemotaxis. Through this system, proteins called chemoreceptors sense a variety of beneficial and harmful conditions, regulating the localization and fitness of *H. pylori* in the gastric niche. The *H. pylori* chemoreceptor TlpA alters host inflammation through an unknown mechanism. To better understand this phenotype, this thesis characterizes 1) the sensing profile of TlpA and 2) how TlpA affects the host immune response and the localization of *H. pylori in vivo.*

TlpA has a dCache_1 periplasmic sensing domain and previous studies have identified two signals sensed by this chemoreceptor. It has become appreciated that dCache_1 sensor domains can bind diverse sets of ligands, and ligand binding can occur through either the membrane-proximal or -distal subdomain. To better understand what signals TlpA may be responsible for sensing *in vivo*, we performed an extensive screen for novel TlpA ligands using ligand binding arrays and surface

plasmon resonance. TlpA-dependent chemotactic responses towards hits from this screen were characterized using a temporal, live-cell tracking assay. Novel TlpA chemoattractants were identified, and their binding was characterized using *in silico* molecular docking experiments and *in vitro* SPR assays with TlpA membrane-proximal and -distal subdomain point mutants. Roles in ligand binding were identified for each subdomain. Additionally, an antagonistic TlpA ligand was identified, which blocked the normal chemotaxis response to TlpA chemoattractants. Antagonistic ligands are an emerging theme in signal transduction and may play a role in regulating chemotactic responses *in vivo*. In total, these studies provide a clearer understanding of the signals sensed by TlpA, the role of dCache_1 subdomains in ligand binding, and identifies a potential mechanism for regulating chemotactic responses.

To better understand how TlpA affects host inflammation, we performed detailed, longitudinal colonization studies in an *in vivo* murine model over 8-months. Throughout this period, we determined total colonization loads, assessed gland colonization, measured inflammation via histology, and performed flow cytometry to analyze the innate and effector $CD4^+$ T-cell populations recruited to the stomach during infection. We found that TlpA attenuates inflammation in the corpus of the stomach at 5-month post-infection, which is associated with a decreased Th17 frequency. In addition, TlpA altered the timing of transient increases in inflammation. Also, in agreement with other reports, TlpA is not required for WT colonization levels overall in the stomach. However, TlpA

regulates the localization of *H. pylori* within the gastric glands of the corpus and antrum. This regulation is most prominent during the first month of infection. From this work, we propose a possible link between TlpA regulated gland colonization and inflammation development.

The regulation of host inflammation is critical for controlling *H. pylori* disease outcomes. In total, this work furthers our understanding of this process by characterizing the sensing capabilities of TlpA and providing a detailed understanding of the localization and immune response affected by TlpA during colonization. This work lays the groundwork for future studies aiming to understand how the chemotaxis system of *H. pylori* alters disease outcomes and could potentially lead to the development of novel chemotaxis-related therapeutics.

ACKNOWLEDGEMENTS

This dissertation would not have been possible without the mentorship, encouragement, and support of so many important people in my life.

I want first to thank Karen Ottemann. I first got to work for Karen when I was a young, timid undergraduate student TAing her METX 119L class. Her encouragement and mentorship gave me a sense of reassurance and validation that was so critical for me at the time. She has continued to instill confidence in me throughout my graduate career, and she has been instrumental in my development as a scientist. I truly cannot say enough great things about Karen. She is a fantastic scientist, she is deeply empathetic to her students, and she is an excellent mentor. I feel a deep sense of gratitude to Karen, and it has been a privilege to work for her.

I want to thank Vicki Auerbuch Stone for sparking my interest in microbiology and allowing me to explore it as a career possibility. During my undergrad, I took her METX 119 class. This class uniquely captivated my interest in a way that no other class had, and it led me to explore the world of microbiology further. Most critically, Vicki allowed me the opportunity to be an undergraduate researcher in her lab. I appreciate the mentorship and support I received from Vicki and my graduate student mentor, Miles Duncan. In addition, my labmates from the Auerbuch Stone Lab, Walter, Jessica, Leah, Hahn, Natalia, and the undergrads, made it such a welcoming, fun, and supportive environment to grow as a young scientist. It was a true privilege to work for Vicki, and I am very grateful to her.

I want to thank all my lab mates from the Ottemann Lab. When I joined the lab, Samar, Kieran, Daniella, and Christina were so welcoming and introduced me to the world of *H. pylori*. They were very generous with their time mentoring me during the beginning of my graduate career. Throughout my time in the lab, it has been a pleasure getting to work with, mentor, and learn from all the present and past lab members I overlapped with, including Christina, Skander, Shaui, Raymond, Aaron, Xiaolin, Frida, Yazzy, Francesca, Cande, and Jashwin. I want to thank Megan Pryce especially. I couldn't have asked for a better undergraduate student to mentor. I appreciate the dedication she put into her research, and she helped my thesis work tremendously by piloting and developing new chemotaxis assays and making TlpA point mutants. I also want to thank Christina Yang especially. We performed all our mouse experiments together and she managed to help make long *in vivo* days fun. I deeply valued her expertise and discussions about our work together.

My thesis work would not have been possible without the expertise and support of many great collaborators, mentors, and committee members, to whom I am deeply grateful. Victoria Korolik, Bassam Elgamoudi, Thomas Haselhorst, Freda E.-C. Jen, and Christopher Day provided essential expertise to study chemoreceptor-ligand interactions. Karen Guillemin and Emily Sweeney provided helpful feedback and insights about TlpA ligand-binding. Isabelle Arnold was very generous with her time and taught me how to isolate leukocytes from gastric tissue and perform flow cytometry. Also, her discussions about the immune response to

H. pylori have been crucial for my *in vivo* work. Dr. Elliot Carter provided histology grades for all my *in vivo* work. Atesh Worthington, Donna Poscablo, Elektra Robinson, and Bari Holm Nazario provided essential support and advice for flow cytometry experiments. I also want to thank my thesis committee of Fitnat Yildiz, Vicki Auerbuch Stone, and Martha Zúñiga. I am very grateful for the advice and feedback I have received from them, which has greatly improved the quality of my dissertation.

I want to thank my partner, Elektra Robinson. I cannot imagine having a more loving, supportive, and beautiful person to share my life with. Elektra has taught me so much, and I would not be the person I am today without her. She is there for me on my best days and my worst. She always believes in me, even when I do not. Her infectious joy for life never fails to put a smile on my face, and I look forward to everything thing life brings us in the future. She also happens to be a fantastic scientist who always inspires me through her work. I also want to thank her family. Her parents, Roula and Lee, and her siblings, Anastasia and Tasos, have welcomed me into their families with open arms, and I am thankful for all their support.

I want to thank the pets from my family and friends who have given copious amounts of emotional support: Serra, Charlie, Oreo, Calypso, Mani, Atom, Xander, Chester, Maia, Blu, Whiskey, and Luna.

Lastly, I want to thank my parents, Scot and Sylvia Johnson. They have provided an essential foundation of love and support throughout my life that has

allowed me to pursue my passions freely. While they will admit they do not fully understand what I do in the lab, they have always been my biggest cheerleaders. I love them deeply, and while cliche, words can not describe how much they mean to me. I would not be where I am today without them, and I am forever grateful to them. Also, I want to thank all my family members: my Grandpa and Grandma Johnson, Grandma Kralevich, and my Aunts, Uncles, and Cousins. Thank you all for your love and support throughout my life. I love you all.

The text of this dissertation includes reprints of the following previously published material: Kevin S. Johnson and Karen M. Ottemann, "Colonization, localization, and inflammation: The roles of *H. pylori* chemotaxis *in vivo*," Current Opinion in Microbiology, 2018, Volume 41, Pages 51-57; Kevin S. Johnson, Bassam A. Elgamoudi, Freda E.-C. Jen, Christopher J. Day, Emily Goers Sweeney, Megan L. Pryce, Karen Guillemin, Thomas Haselhorst, Victoria Korolik, and Karen M. Ottemann, "The dCache Chemoreceptor TlpA of *Helicobacter pylori* Binds Multiple Attractant and Antagonistic Ligands via Distinct Sites," mBio, 2021, Volume 12, Issue 4. Karen M. Ottemann directed and supervised this research which forms the basis of Chapters 1 and 2 of this dissertation.

CHAPTER 1- Colonization, localization, and inflammation: The roles of *Helicobacter pylori* chemotaxis *in vivo*

An earlier version of this chapter was published (Johnson and Ottemann, 2018).

1.1 Abstract

Helicobacter pylori is a gram-negative bacterium that infects half of the world's population, causing gastritis, peptic ulcers, and gastric cancer. To establish chronic stomach infection, *H. pylori* utilizes chemotaxis, driven by a conserved signal transduction system. Chemotaxis allows *H. pylori* to sense an array of environmental and bacterial signals within the stomach, guiding its motility towards its preferred niche within the gastric mucosa and glands. Fine-tuned localization, regulated by the chemotaxis system, enables robust colonization during the acute stage of infection. During chronic infection, chemotaxis helps maintain bacterial populations and modulates the host immune response. Given its importance in host colonization and disease, chemotaxis is an attractive target for future treatments against *H. pylori* infections.

1.2 Highlights

- The *H. pylori* chemotaxis system includes classical and auxiliary chemotaxis proteins
- *H. pylori* senses several host and bacterial ligands through four chemoreceptors

- Chemotaxis is critical for colonization during acute infection
- Chemotaxis modulates host inflammation during chronic infection

1.3 Introduction

Helicobacter pylori is a gram-negative bacterium that has evolved a keen ability to chronically colonize the stomach, infecting roughly half of the world's population (Hooi et al., 2017a). Colonization can lead to the development of chronic gastritis, gastric and duodenal ulcers, and gastric cancers (Cover and Blaser, 2009; Plummer et al., 2015). Colonization is also linked to potential health benefits, including protection against allergic asthma, and inflammatory bowel and esophageal diseases, presumably though modulating effector T-cell populations or gastric acid production (Arnold et al., 2011a; Blaser et al., 2008; Parsonnet, 2014; Salama et al., 2013). The beneficial and pathogenic aspects of *H. pylori* require colonization; therefore, an important goal is to understand the molecular basis of the bacterial factors that promote chronic infection.

H. pylori colonizes the primate stomach, a harsh environment. The stomach lumen ranges between pH 1-5 (Fimmel et al., 1985), conditions at which *H. pylori* is viable for only ~30min (Schreiber et al., 2005). Additionally, stomach contents are cleared regularly, and the gastric mucosa undergoes constant turnover (Atuma et al., 2001). Accordingly, *H. pylori* must rapidly initiate colonization and localize where the environment is more hospitable. These hospitable niches are found close to the gastric epithelium, within 15μm from the gastric epithelial cells (Schreiber et al., 2004), and deep within gastric glands (Howitt et al., 2011).

H. pylori colonization is promoted by chemotaxis, the focus of this review. Chemotaxis is a process that enables *H. pylori* to sense environmental signals and regulate its motility to move away from harmful conditions and towards favorable ones (Wadhams and Armitage, 2004). Chemotaxis promotes colonization and plays a role in modulating host immune responses (McGee et al., 2005; Rolig et al., 2011; Williams et al., 2007). In addition to chemotaxis, *H. pylori* utilizes a suite of colonization factors, including urease, cell shape, adhesins, the Cag pathogenicity island type four secretion system, and the toxin VacA. Readers are referred to several excellent recent reviews on these topics (Keilberg and Ottemann, 2016; Polk and Peek, 2010; Salama et al., 2013; Sgouras et al., 2015).

1.4 The *H. pylori* signal transduction system transforms ligand presence into a swimming response

Chemotaxis signal transduction systems allow bacteria to direct their motility (Colin and Sourjik, 2017; Wadhams and Armitage, 2004; Wuichet and Zhulin, 2010). Such systems are widespread, present in ~50% of bacterial species, highlighting the strong fitness advantage they confer (Wuichet and Zhulin, 2010). The chemotaxis system of *H. pylori* contains core chemotaxis proteins found in all chemotaxis systems and auxiliary ones found in only some (Figure 1.1). The core chemotaxis proteins are the chemoreceptors (TlpA, TlpB, TlpC, and TlpD), the CheW coupling protein, the CheA kinase, and the CheY response regulator (Tomb et al., 1997; Wadhams and Armitage, 2004). The *H. pylori* auxiliary chemotaxis proteins include three CheV-type coupling proteins (CheV1, CheV2, and CheV3),

the CheZ phosphatase, and the unique chemotaxis protein ChePep, which localizes CheZ to the cell poles (Abedrabbo et al., 2017; Howitt et al., 2011; Lertsethtakarn et al., 2015; Lertsethtakarn and Ottemann, 2010; Andrew C Lowenthal et al., 2009; Pittman et al., 2001; Terry et al., 2006). Environmental signals are sensed either directly or indirectly by chemoreceptors and are relayed to the histidine kinase CheA via the CheW or CheV1 coupling proteins (Abedrabbo et al., 2017; Wadhams and Armitage, 2004). Currently, the role of CheV2 and CheV3 are unknown. Chemicals sensed as repellents activate CheA's auto-phosphorylation, and this phosphoryl group is subsequently passed to CheY via histidine-to-aspartate phosphorelay (Jiménez-Pearson et al., 2005). Phosphorylated CheY interacts with the flagellar motor, causing it to rotate clockwise and the bacteria to reverse or change direction (Lam et al., 2010; Andrew C. Lowenthal et al., 2009). Alternatively, attractants squelch CheA's auto-phosphorylation; non-phosphorylated CheY does not interact with the motor, and the bacteria swim straight without direction changes. Mutants in any one of these proteins are non-chemotactic (Che^-) to varying degrees and with different swimming behavior. Accordingly, *cheW*, *cheA*, *cheY*, *cheV1*, and *cheV2* mutants are all Che^-, displaying straight swimming phenotypes, likely because they do not produce phosphorylated CheY (Foynes et al., 2000; Andrew C Lowenthal et al., 2009; Terry et al., 2006, 2005). *cheZ*, *chepep*, *cheV3* mutants are also Che^-, but display hyper-reversal phenotypes, apparently because they produce high amounts of phosphorylated CheY (Howitt et al., 2011; Lertsethtakarn et al., 2015; Andrew C Lowenthal et al.,

2009; Terry et al., 2006). Readers are referred to several excellent reviews of this system for more molecular details (Keilberg and Ottemann, 2016; Lertsethtakarn et al., 2012, 2011).

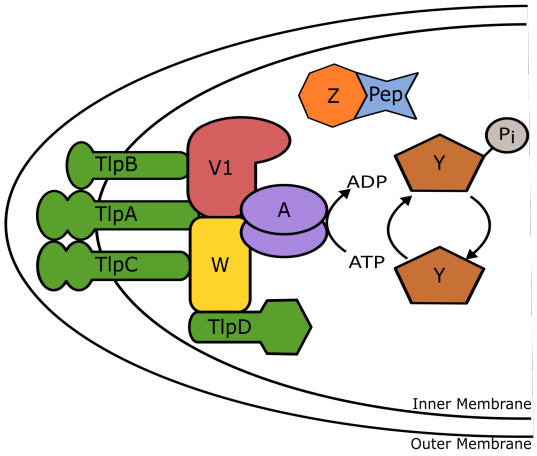

Figure 1.1- *H. pylori* chemotaxis system.
Chemotactic signals are sensed by the chemoreceptors TlpA, TlpB, TlpC, and TlpD. Signals are relayed through the coupling protein CheW (W) or the auxiliary CheV-type coupling protein CheV1 (V1) to the histidine kinase CheA (A). Repellents promote CheA auto-phosphorylation, while attractants squelch CheA auto-phosphorylation. Phosphorylated CheA passes its phosphoryl group to the CheY (Y) response regulator via histidine to aspartate phosphorelay. Phosphorylated CheY interacts with the flagellar motor and is dephosphorylated by CheZ phosphatase (Z), in complex with ChePep (Pep). CheV2 and CheV3 are not depicted as their role in this system are unknown.

1.5 *H. pylori* senses multiple host and bacterially-generated conditions as repellents and attractants

H. pylori senses specific chemicals and conditions via three transmembrane chemoreceptors with periplasmic sensing domains—TlpA, TlpB, TlpC— and one cytoplasmic receptor, TlpD (Andermann et al., 2002; Croxen et al., 2006; McGee et al., 2005; Schweinitzer et al., 2008). The signals of these chemoreceptors and

their distribution likely play a driving role in the localization of *H. pylori in vivo*. Thus, efforts have been made to determine *H. pylori*'s sensing profile.

H. pylori experiences multiple repellent conditions. Several of these are host generated, including acidic pH, reactive oxygen species (ROS), and bile (Collins et al., 2016; Croxen et al., 2006; Worku et al., 2004). The acidic stomach lumen is toxic to *H. pylori* (Fimmel et al., 1985; Schreiber et al., 2005). Accordingly, acid is a potent chemorepellent, with TlpA, TlpB, and TlpD playing roles in sensing (Croxen et al., 2006; Goers Sweeney et al., 2012; Huang et al., 2017), and TlpC playing a role in modulating the acid response (Sanders et al., 2013). Currently, there is only a mechanistic proposal for how TlpB senses acid via amino acids that are variably protonated (Goers Sweeney et al., 2012). Another signal, ROS (Collins et al., 2016), is produced by host epithelial and immune cells (Grasberger et al., 2013; Handa et al., 2010; Naito and Yoshikawa, 2002). TlpD senses ROS via an unknown mechanism (Collins et al., 2016). Bile acids are toxic to *H. pylori* and are sensed via unknown chemoreceptor(s) (Hänninen, 1991; Worku et al., 2004). Bile is released from the gallbladder into the duodenum (Behar, 2013). The repellent and toxic properties of bile may explain why *H. pylori* does not colonize this region (Hänninen, 1991; Rolig et al., 2012; Worku et al., 2004).

H. pylori is also repelled by the self-generated, quorum-sensing molecule autoinducer-2 (AI-2) and responds to its own electron transport chain (ETC) (Rader et al., 2011; Schweinitzer et al., 2008). AI-2 is sensed by TlpB as a chemorepellent, in a manner dependent on the periplasmic proteins AibA and AibB (Anderson et

al., 2015; Rader et al., 2011). A repellent response to AI-2 may promote dispersion of *H. pylori in vivo*. *H. pylori* also senses disruptions to the ETC via TlpD, but the physiological change required to induce this sensing is unknown (Behrens et al., 2016, 2013; Schweinitzer et al., 2008)

In addition to chemorepellents, many of which are harmful to the bacterium, *H. pylori* also senses several beneficial chemoattractants. One of these chemoattractants, urea, is sensed by TlpB (Huang et al., 2015; Mizote et al., 1997; Nakamura et al., 1998; Worku et al., 2004). In non-infected individuals, urea is available at concentrations between 5-21 mM within the stomach (Neithercut et al., 1993) and is hydrolyzed by *H. pylori* urease into ammonia and bicarbonate to buffer its local environment (Salama et al., 2013). Arginine is sensed as a chemoattractant by TlpA (Cerda et al., 2003, 2011; Worku et al., 2004) and is an essential amino acid for *H. pylori* (Nedenskov, 1994; Reynolds and Penn, 1994). In both urea and arginine chemotaxis, chemoattraction may help *H. pylori* find key nutrients while also directing it toward the epithelial surface.

There are several additional chemotactic signals that have not been extensively studied. For example, *H. pylori* uses chemotaxis to migrate to the site of gastric damage (Aihara et al., 2014). However, the exact host-derived chemicals that direct this response are unknown. Another attractant that has not been mapped to a chemoreceptor is cholesterol (Wunder et al., 2006).

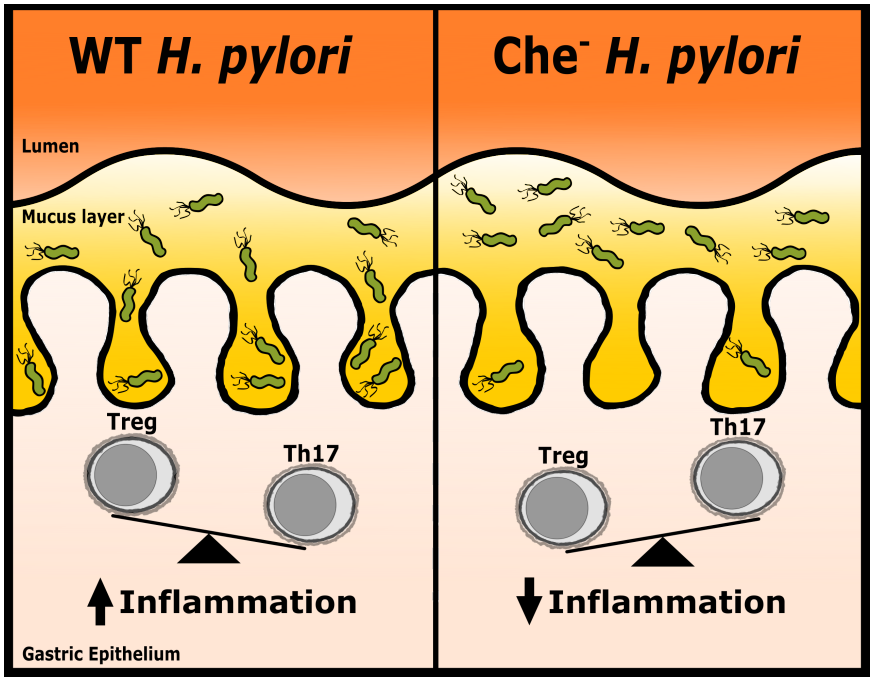

Figure 1.2- Chemotaxis promotes localization and modulates inflammation *in vivo*.
Wild-type (WT) *H. pylori* robustly colonizes gastric glands early during infection, and can replicate and spread between glands. Conversely, non-chemotactic (Che$^-$) *H. pylori* fail to colonize gastric glands to the same degree. Concurrently, WT *H. pylori* initiates a proinflammatory immune response, with a substantial T-helper 17 cell (Th17) response, while non-chemotactic *H. pylori* promotes a dampened immune response, skewed toward T-regulatory cells (Tregs).

1.6 Chemotaxis during *in vivo* colonization

Che$^-$ *H. pylori* mutants have severe colonization defects (Figure 1.2) and appear to interact with host tissue differently based on their aberrant inflammatory responses (Figure 1.2). These aspects are discussed in the following sections.

1.6.1 Chemotaxis is required for wild-type colonization

Chemotaxis is required for wild-type (WT) level colonization of the stomach, based on studies using a variety of Che$^-$ mutants lacking CheA, CheY, CheW, or ChePep. In some cases, Che$^-$ mutants did not colonize at all (Foynes et

al., 2000; McGee et al., 2005), and in others, they colonized poorly (Aihara et al., 2014; Keilberg et al., 2016; Rolig et al., 2012, 2011; Terry et al., 2005; Williams et al., 2007). Che$^-$ mutants require 100-fold more bacteria to initiate colonization (Terry et al., 2005); thus, some studies might have employed *H. pylori* doses that were below the infectious dose. Overall, these results show that chemotaxis is critical during the initial stages of infection, particularly with low infectious doses, such as could be experienced during natural infection.

1.6.2 Chemotaxis during early infection

For roughly the first three months of infection, chemotaxis is critical. During this period, Che$^-$ mutants display significant colonization defects that are greater in one region, the antrum (Rolig et al., 2012; Terry et al., 2005). The murine stomach is extensively invaginated into over 25,000 glands. Gastric glands in the corpus and antrum contain distinct cell types (Yang and Ottemann, 2019), which are explained in greater detail in Chapter 3. Che$^-$ mutants fail to robustly colonize these niches, especially within the antrum (Howitt et al., 2011; Keilberg et al., 2016; Sigal et al., 2015). During the first month of a WT infection, the number of glands infected and the amount of *H. pylori* per gland increases. Che$^-$ mutants, however, infect few glands initially and fail to promote this same population expansion between and within glands (Keilberg et al., 2016).

1.6.3 Chemotaxis during chronic infection

A hallmark of *H. pylori* colonization is its ability to achieve chronic infection. The role of chemotaxis during the chronic stage has been more difficult

to evaluate. However, it seems that in the absence of challenge by WT, Che$^-$ *H. pylori* can achieve WT levels of colonization as early as one month post-infection, maintaining comparable levels up to six months post-infection and presumably longer (Keilberg et al., 2016; Rolig et al., 2012; Terry et al., 2005; Williams et al., 2007). During the chronic stage of infection, Che$^-$ *H. pylori* colonize gastric glands in the corpus and antrum, while WT populations also colonize the mucus layer of the corpus (Keilberg et al., 2016). Additionally, Che$^-$ mutants have been observed to be less closely associated with the gastric epithelium during this stage (Williams et al., 2007).

1.6.4 Competition

Che$^-$ *H. pylori* have general colonization defects when they are the sole infecting strain, with even greater colonization defects observed during competition experiments. When mice are infected with equal doses of WT and Che$^-$ *H. pylori*, the Che$^-$ mutant is outcompeted by over 1000-fold (Andermann et al., 2002; Terry et al., 2005). If the infections are given sequentially, a secondary WT infection can displace a primary population of Che$^-$ *H. pylori*, nearly displacing the entire gland population of Che$^-$ bacteria. In contrast, a secondary WT infection is unable to displace a primary population of WT, a phenotype termed colonization resistance (Keilberg et al., 2016; Terry et al., 2005). This finding suggests that chemotaxis is needed to maintain colonization during chronic colonization, especially when WT *H. pylori* are present.

1.6.5 Role of chemoreceptors for colonization

Chemoreceptors head the chemotaxis signal transduction system. Accordingly, several studies have examined the *in vivo* phenotypes of chemoreceptor mutants. Loss of individual chemoreceptors alters the sensing profile of *H. pylori* but does not cause a complete loss of chemotactic ability. Specifically, bacteria would lose the ability to sense some compounds, perhaps biasing bacteria towards or away from signals sensed by the remaining chemoreceptors. Such a change could lead *H. pylori* towards more inhospitable environments.

tlpA and *tlpC* mutants colonize mice to WT levels during single strain infections but are outcompeted by WT during competition infections (Andermann et al., 2002). This phenotype suggests that WT either exacerbates or alters the environment to reveal the mutant's defect. One possible mechanism is that WT outcompetes the mutant for finding nutrients, an idea that would fit well with the function of TlpA for finding the essential amino acid, arginine (Cerda et al., 2003, 2011; Nedenskov, 1994). Another possibility is that the WT causes a host response that the mutant cannot avoid. While the exact reason why WT outcompetes *tlpA* and *tlpC* mutants are unknown, these phenotypes provide clear support for the importance of TlpA and TlpC *in vivo*.

tlpB mutants have either no defects or subtle ones that appear more pronounced later in infection (Croxen et al., 2006; Huang et al., 2015; Rolig et al., 2012; Williams et al., 2007). Interestingly, *tlpB* mutants are not outcompeted by

WT (McGee et al., 2005; Williams et al., 2007), suggesting that WT does not exacerbate or reveal the mutant's defect. Because this mutant is not outcompeted, this suggests that TlpB's signal, urea, is found at levels that are not limiting for *H. pylori*, an idea that fits well with its relatively high (mM) levels (Neithercut et al., 1993). The late infection defects observed for *tlpB* mutants could be related to enhanced inflammation (see below) or to defects associated with AI-2 chemotaxis (Rader et al., 2011; Williams et al., 2007)

In single strain infections, *tlpD* mutants have substantial colonization defects early in infection, greater than Che$^-$ *H. pylori* (Behrens et al., 2013; Rolig et al., 2012). Additionally, *tlpAD* double mutants have an even greater colonization defect and are defective in antral gland colonization (Huang et al., 2017). Treatment of *tlpAD*-infected mice with omeprazole, which blocks acid production, rescues *H. pylori* levels to that seen in *tlpD* single strain infections (Huang et al., 2017; Rolig et al., 2012). This result suggests the inability to sense acid via TlpA and D reduces *in vivo* fitness, and indicates the remaining colonization defect in *tlpD* infections is potentially due to an inability to sense ROS or changes in its ETC activity (Collins et al., 2016; Schweinitzer et al., 2008).

1.6.6 Role of auxiliary chemotaxis proteins in colonization

Loss of the auxiliary chemotaxis proteins creates *H. pylori* mutants that are either fully or partially Che$^-$ (Howitt et al., 2011; Lertsethtakarn et al., 2015; Andrew C Lowenthal et al., 2009; Pittman et al., 2001). Likewise, mutants lacking the CheVs or ChePep display colonization defects that range from severe, similar

to fully Che$^-$ mutants, to less severe (Howitt et al., 2011; Andrew C Lowenthal et al., 2009; Sigal et al., 2015). Overall, the data support the idea that auxiliary proteins can have as substantial an effect as core proteins.

1.6.7 Chemotaxis modulates host inflammation

Host inflammation is a major disease outcome of *H. pylori* colonization. Inflammation occurs upon recognition of microbial-associated molecular patterns (MAMPs) or damage-associated molecular patterns (DAMPs) by local monocytes, macrophages, and epithelial cells. These cells release pro-inflammatory cytokines and chemokines, the latter of which recruit neutrophils and antigen-presenting cells, including macrophages and dendritic cells, to the site of infection (Soehnlein and Lindbom, 2010; Wilson and Crabtree, 2007). Dendritic cells release cytokines and process and present *H. pylori* antigens, priming T-cell differentiation (Josefowicz et al., 2012; Larussa et al., 2015; Peek et al., 2010; Salama et al., 2013; Shiu and Blanchard, 2013; Soehnlein and Lindbom, 2010; Wilson and Crabtree, 2007). *H. pylori* colonization induces the differentiation of pro-inflammatory T-helper 1 (Th1) and T-helper 17 (Th17) cells and anti-inflammatory T-helper 2 (Th2) and T-regulatory cells (Tregs) (Larussa et al., 2015; Peek et al., 2010; Salama et al., 2013; Wilson and Crabtree, 2007). The degree of host inflammation is modulated by the balance of effector T-cell populations. *H. pylori* induces inflammation via its intimate interaction with the gastric epithelium and the production of virulence factors such as the type 4 secretion system, CagA, NapA, and VacA (Peek et al., 2010; Salama et al., 2013; Wilson and Crabtree, 2007). The inflammatory response

to *H. pylori* colonization, however, is also modulated by chemotaxis (McGee et al., 2005; Rolig et al., 2011; Williams et al., 2007).

Chemotaxis was first shown to modulate inflammation using a *tlpB* mutant in a gerbil model of infection (McGee et al., 2005). *tlpB* mutants colonized gerbils to WT levels at four weeks post-infection, but induced only low gastric inflammation, as measured using histological enumeration of lymphocytes. While *tlpB* mutants induced less inflammation than WT, *tlpB*-infected gerbils had high neutrophil recruitment to the gastric tissue, such as seen a few days after *H. pylori* infection. This phenotype suggested *tlpB*-infected gerbils were mimicking an early stage of infection (McGee et al., 2005).

Subsequent studies extended this work to the mouse model, examining the roles of all chemoreceptors (Williams et al., 2007). Three months post-infection, Che$^-$, *tlpA*, and *tlpB* mutants induced modestly less inflammation than WT. At later time points, six months post-infection, *tlpA* and *tlpB* mutants caused high inflammation, while Che$^-$ mutants induced low inflammation. At both time points, all strains colonized to WT levels. Overall, these results made it clear that the inflammatory response was modulated by bacterial properties controlled by chemotaxis and was affected independent of overall bacterial load (Williams et al., 2007).

To gain insight into why Che$^-$ mutants induce less inflammation, Rolig *et al*. (2011) examined the specific immune cell populations recruited to the stomach. While Che$^-$ mutants induce less histologically-evident inflammation, the total

number of $CD4^+$ T-cells recruited was equivalent between mice infected with WT or Che^- *H. pylori* two months post-infection (Rolig et al., 2011). WT infections, however, were found to have a higher density of pro-inflammatory Th17 cells, as assessed by expression of associated genes, and an overall elevated ratio of Th17/Treg cells compared with Che^- infections. A possible explanation for the ability of WT to trigger a Th17-response came from the observation that WT infections induced more gastric tissue apoptosis than did Che^- infections (Rolig et al., 2011). Because apoptosis is a host response that can lead to the differentiation of Th17 cells (Torchinsky et al., 2009), it seemed plausible that the inability to trigger apoptosis partially explains why Che^- infections lack Th17 cells. It is still not fully understood why WT *H. pylori* induces more apoptosis and a more robust Th17 response; however, it is now known that Che^- mutants are mislocalized (Howitt et al., 2011; Keilberg et al., 2016; Williams et al., 2007). Mis-localization possibly induces modified interactions with distinct immune cell types known to sample *H. pylori*, such as dendritic cells, compared to WT infections, modulating the resulting inflammatory response. The reason for the elevated inflammation of *tlpA* and *tlpB* mutants is still under study.

1.7 Conclusions

Chemotaxis is one of several colonization factors utilized by *H. pylori* to promote chronic infection of the stomach (Foynes et al., 2000; Howitt et al., 2011; Andrew C Lowenthal et al., 2009; McGee et al., 2005; Rolig et al., 2012; Salama et al., 2013; Terry et al., 2005; Williams et al., 2007). Work over the past 20 years

strongly supports that chemotaxis helps *H. pylori* find nutrients such as urea and arginine and avoid toxic substances such as acid and ROS. The list of critical compounds sensed by *H. pylori* will undoubtedly grow as more work is done to better understand the sensing profile of each chemoreceptor. Chemotaxis plays roles in localization and modulating the host immune response. The stomach landscape is comprised of multiple niches, and studies support that chemotaxis is particularly critical for colonization during early infection, especially in the antrum, and for spread into new glands (Howitt et al., 2011; Keilberg et al., 2016; Rolig et al., 2012). During established infections, chemotaxis is less critical for colonization (Keilberg et al., 2016). Non-chemotactic *H. pylori* likely enter glands stochastically during early infection. Once in a gland, chemotaxis may not be required for growth. Instead, in late-stage infections, the role of chemotaxis in inflammation-control becomes apparent (McGee et al., 2005; Rolig et al., 2011; Williams et al., 2007). Understanding the mechanisms by which chemotaxis modulates host inflammation will facilitate our understanding of how bacteria control this important process and may lead to future treatments to modify disease outcomes. Several pathogens are motile and chemotactic. *H. pylori* is leading our understanding of the roles for this important process *in vivo*, and it will be of great interest to assess how many of the same principles translate across bacterial systems and organs.

1.8 Papers of significance

(*= Of special interest, **= Of outstanding interest)

*Lertsethtakarn et al. 2012- A review covering the *H. pylori* chemotaxis system in greater molecular detail.

**Goers Sweeney et al. 2012- The authors solved the first crystal structure of the sensing portion of the *H. pylori* chemoreceptor, TlpB. Additionally, a proposed mechanism for pH sensing by TlpB is reported.

**Huang et al. 2015- This study describes the mechanism of urea sensing by TlpB.

*Huang et al. 2017- This study uncovered the role of TlpA, TlpB, and TlpD in pH sensing and showed *tlpAD* mutants have severe colonization defects *in vivo*.

*Croxen et al. 2006- The first paper to demonstrate *H. pylori* senses acidic pH through TlpB.

*Rader et al. 2011- This study uncovers the role of TlpB in sensing the bacterial-derived signaling molecule, autoinducer-2.

*Collins et al. 2016- This study demonstrates *H. pylori* senses reactive oxygen species through TlpD.

*Schweinitzer et al. 2008- This study demonstrates *H. pylori* is capable of sensing changes in electron transport chain activity through TlpD.

*Aihara et al. 2014- This study determined *H. pylori* requires chemotaxis to localize to the site of gastric injury *in vivo* via two-photon microcopy.

**Terry et al. 2005- This is a seminal paper investigating the role of *H. pylori* chemotaxis *in vivo*. This study demonstrated that non-chemotactic *H. pylori* infect to lower levels and are defective in antral colonization, determined the infectious

dose of non-chemotactic *H. pylori*. Also, Competition experiments were performed with wild-type and non-chemotactic *H. pylori*.

**Keilberg et al. 2016, MBio- A comprehensive study of wild-type and non-chemotactic *H. pylori* population dynamics within the gastric glands and mucus layer of the antrum and corpus of the stomach over a 6-month period. Additionally, competition experiments with wild-type and non-chemotactic *H. pylori* were performed.

**Howitt et al. 2011- This study determined the auxiliary chemotaxis protein, ChePep, is required for chemotaxis, and *ChePep* mutants are unable to colonize gastric glands within the antrum. It was the first study to show chemotaxis is required for gland colonization.

*Rolig et al. 2012- This work demonstrated that non-chemotactic *H. pylori* have a general colonization defect within the antrum and that TlpD mutants, overall, have a more severe colonization defect than non-chemotactic *H. pylori*.

**Williams et al. 2007- A comprehensive study investigating the role of each *H. pylori* chemoreceptor *in vivo* over a 6-month infection. Inflammation, as scored by histology, and overall bacterial loads are measured. This work identified differential immune responses elicited by *tlpA*, *tlpB*, and *Che*$^-$ mutants.

**Rolig et al. 2011- This study investigates the host-immune responses elicited during infection with wild-type and Che$^-$ *H. pylori*. Host gene expression and flow cytometry were used to uncover the unique effector T-cell populations recruited during each infection.

CHAPTER 2- The dCache chemoreceptor TlpA of *Helicobacter pylori* binds multiple attractant and antagonistic ligands via distinct sites

An earlier version of this chapter was published (Johnson et al., 2021).

2.1 Abstract

The *Helicobacter pylori* chemoreceptor TlpA plays a role in dampening host inflammation during chronic stomach colonization. TlpA has a periplasmic dCache_1 domain, a structure that is capable of sensing many ligands; however, the only characterized TlpA signals are arginine, bicarbonate, and acid. To increase our understanding of TlpA's sensing profile, we screened for diverse TlpA ligands using ligand binding arrays. TlpA bound seven ligands with affinities in the low to middle micromolar ranges. Three of these ligands, arginine, fumarate, and cysteine, were TlpA-dependent chemoattractants, while the others elicited no response. Molecular docking experiments, site-directed point mutants, and competition surface plasmon resonance binding assays suggested that TlpA binds ligands via both the membrane-distal and -proximal dCache_1 binding pockets. Surprisingly, one of the non-active ligands, glucosamine, acted as a chemotaxis antagonist, preventing the chemotaxis response to chemoattractant ligands and acted to block binding of ligands irrespective of whether they bound the membrane-distal or -proximal dCache_1 subdomains. In total, these results suggest TlpA senses multiple attractant ligands as well as antagonist ones, an emerging theme in chemotaxis systems.

2.2 Importance

Numerous chemotactic bacterial pathogens depend on the ability to sense a diverse array of signals through chemoreceptors to achieve successful colonization and virulence within their host. The signals sensed by chemoreceptors, however, are not always fully understood. This is the case for TlpA, a dCache_1 chemoreceptor of *H. pylori* that enables the bacteria to induce less inflammation during chronic infections. *H. pylori* causes a significant global disease burden, which is driven by the development of gastric inflammation. Accordingly, it is essential to understand the processes by which *H. pylori* modulates host inflammation. This work uncovers the signals that TlpA can sense and highlights the underappreciated regulation by antagonistic chemoreceptor ligands, which is an emerging theme among chemotactic systems.

2.3 Introduction

Chemotaxis is a vital host colonization strategy used by many pathogens, including *Helicobacter pylori*, *Campylobacter jejuni*, *Borrelia burgdorferi*, *Pseudomonas aeruginosa*, *Vibrio cholerae*, and *Salmonella enterica*. How chemotaxis benefits bacteria, however, varies. Pathogens have been found to use chemotaxis to access growth-promoting nutrients, locate environmental substrates that regulate virulence gene expression, spread throughout tissue and into specific niches, and affect host interactions that control inflammation (Matilla and Krell, 2018). Chemotaxis signaling systems are highly conserved, and their widespread

presence in pathogens underscores the importance of understanding their roles in colonization (Matilla and Krell, 2018; Wuichet and Zhulin, 2010).

One pathogen that requires chemotaxis to promote infection is *H. pylori*. This Gram-negative bacterium chronically colonizes the stomach of nearly half of the world's population and ~35% of individuals in the United States (Hooi et al., 2017a). Stomach colonization results in chronic inflammation and a subset of individuals develop ulcers and gastric cancer (Cover and Blaser, 2009; Plummer et al., 2015). *H. pylori* presents a significant disease burden, with ~700,000 deaths worldwide from gastric cancer yearly (Ferlay et al., 2015). The degree of host inflammation, which drives disease severity, varies amongst infected individuals. (Arnold et al., 2011b; White et al., 2015; Wroblewski et al., 2010). We understand some *H. pylori* properties that dictate inflammation severity, such as the Cag pathogenicity island (Blosse et al., 2018; Javed et al., 2019). Still, the full compendium of *H. pylori* properties that modulate this host response is not yet understood.

H. pylori chemotaxis has been linked to host inflammation (Johnson and Ottemann, 2018; McGee et al., 2005; Rolig et al., 2011; Williams et al., 2007). Specifically, mutants missing key chemotaxis signal transduction proteins trigger less host inflammation, despite achieving normal colonization levels, while mutants missing either the chemoreceptors TlpA or TlpB cause elevated inflammation (McGee et al., 2005; Rolig et al., 2011; Williams et al., 2007). Chemoreceptors head the chemotaxis signal transduction system and dictate which signals a

bacterium responds to. Loss of individual chemoreceptors within a system alters a bacterium's sensing profile but does not cause a complete loss of chemotactic ability, presumably biasing the bacterium towards signals sensed by the remaining chemoreceptors.

H. pylori possesses four chemoreceptors—TlpA, TlpB, TlpC, and TlpD, which play non-identical roles in infection. TlpA, C, and D are required for colonization, while TlpA and B are required for inflammation control (Andermann et al., 2002; Rolig et al., 2012; Williams et al., 2007). In this work, we focus on TlpA, which plays multiple roles in promoting early but not late colonization and dampening later inflammation. At early times, 2-weeks post-infection, *H. pylori* Δ*tlpA* displays a modest colonization defect compared to wild type (WT) as the sole infecting strain, a deficiency exacerbated by WT coinfection (Andermann et al., 2002; Rolig et al., 2012; Williams et al., 2007). However, during the late stage of infection after 6 months, *H. pylori* Δ*tlpA* colonize to normal levels but induce significantly more histologically evident inflammation than WT (Williams et al., 2007).

TlpA is a transmembrane chemoreceptor with a periplasmic double Cache (dCache_1) ligand-binding domain (LBD) (Sweeney et al., 2018; Upadhyay et al., 2016). Cache domains are ubiquitous extracellular sensing domains found in both eukaryotes and prokaryotes (Upadhyay et al., 2016). Cache domains bind a wide variety of small molecules, but mostly amino acids, modified amino acids, and carboxylic acids (Upadhyay et al., 2016). Many Cache domains have been found to bind multiple ligands (Upadhyay et al., 2016). dCache_1 domains have two Cache

subdomains, a membrane-distal and -proximal subdomain, which each can bind ligands, although most commonly the ligands are bound in the membrane-distal domain (Machuca et al., 2017; Mckellar et al., 2015; Upadhyay et al., 2016). TlpA has some identified chemotaxis-active ligands, including arginine and sodium bicarbonate (Cerda et al., 2003, 2011). Additionally, TlpA has been shown to play a subtle role in sensing acidic pH, but to a much lesser extent than TlpB or TlpD (Huang et al., 2017). Whether TlpA senses additional ligands or how any of these ligands are bound, however, is unknown.

Given the sensing potential of dCache_1 chemoreceptors, we hypothesized that TlpA would be capable of sensing ligands beyond those previously reported. Knowing a full set of ligands is critical for interpreting the TlpA-associated phenotypes. In this study, we identified new TlpA ligands and characterized their binding and ability to induce a chemotactic response. Ligand binding arrays were used to screen a broad set of ligands for binding to TlpA, resulting in the identification and verification of seven TlpA specific ligands. The use of a temporal chemotaxis assay enabled us to determine that three ligands, arginine, fumarate, and cysteine, acted as TlpA-sensed chemoattractants, while the other ligands elicited no response. Molecular modeling experiments, assessment of TlpA point mutants, and SPR competition assays suggested that TlpA ligands interact with two distinct sites in TlpA. Furthermore, one of the high-affinity non-chemotactic TlpA ligands, glucosamine, blocked attractant responses to, and binding of, chemoattractant ligands, thus acting as an antagonist. Overall, our findings suggest

TlpA responds to several key *H. pylori* nutrients using both dCache_1 subdomains, with some acting as agonists and some as antagonists for a chemotaxis attractant response.

2.4 Results

2.4.1 TlpA interacts directly with multiple ligands

TlpA's LBD ($TlpA_{LBD}$) interactions with potential ligands were assessed using small-molecule arrays containing amino acids, organic acids, salts, and glycans (Supplemental Table 2.1). $TlpA_{LBD}$ bound seven small molecules: arginine, cysteine, fumarate, glucosamine, malic acid, thiamine, and alpha-ketoglutarate (Table 2.1 and Supplemental Fig. 2.1). Glycan arrays containing both simple and complex glycans were also interrogated, but no binding was detected.

We next determined $TlpA_{LBD}$ ligand binding affinity by surface plasmon resonance (SPR). Arginine, cysteine, fumarate, and glucosamine all exhibited high-affinity binding (dissociation constant [K_d] <10 μM), while malic acid, thiamine, and alpha-ketoglutarate showed lower affinities (>45 μM) (Table 2.1). Overall, these data suggest that the $TlpA_{LBD}$ can interact directly with these seven ligands, with affinities ranging from 2- 224 μM.

Table 2.1- $TlpA_{LBD}$ ligand binding analysis from ligand binding array screen and surface plasmon resonance.
Data represent the mean values (± SD) of three independent experiments (n= 3). For ligand binding array, results reported as +, positive binding; +/-, intermediate binding; -, no binding. Binding affinity (μM) was determined by SPR.

Ligand	Array	Binding affinity (μM)
Arginine	+	2 ± 0.11
Cysteine	+/-	4.7 ± 0.3
Fumarate	+	10 ± 1.53
Glucosamine	+	10.5 ± 2.8
Malic Acid	+/-	46 ± 17
Thiamine	+/-	60 ± 0.6
Alpha-Ketoglutarate	+	224 ± 11.2

2.4.2 Some TlpA ligands act as chemoattractants while others elicit no response

H. pylori chemotactic responses towards the seven putative TlpA dependent ligands were examined by a live-cell video microscopy assay that measures the temporal chemotaxis response to test ligands. In this assay, attractants eliciting fewer direction changes, and repellents more direction changes compared to basal levels (Collins et al., 2016; Goers Sweeney et al., 2012; Lertsethtakarn et al., 2015; Machuca et al., 2017; Rader et al., 2011; Schweinitzer et al., 2008; Terry et al., 2006). Several TlpA ligands were acidic in solution, leading to the appearance of significant TlpA-independent chemorepellent responses; these were cysteine, thiamine, malic acid, and alpha-ketoglutarate (Supplemental Fig. 2.2A-C). Acidic conditions are sensed by chemoreceptors other than TlpA (Croxen et al., 2006; Goers Sweeney et al., 2012; Huang et al., 2017) and potentially mask chemotactic

responses to the ligands being tested. Accordingly, the pH of the ligand stocks for cysteine, thiamine, malic acid, and alpha-ketoglutarate was neutralized using NaOH to match the pH of the water used in the mock-treated control. This treatment eliminated the confounding effect of media acidification when assessing chemotactic responses (Supplemental Fig. 2.2C). After incorporating these adjustments, we found that the addition of arginine, fumarate, or cysteine resulted in fewer direction changes for WT *H. pylori* (Fig. 2.1A, B, C), suggesting these compounds were attractants. The highest concentration tested, 10 mM, induced the most significant and robust attractant responses for each ligand (arginine, $P<0.01$; fumarate, $P<0.01$; cysteine, $P<0.001$) (Fig. 2.1A, B, C). Responses to 1 and 0.1 mM ligands were apparent but not significant when compared to the untreated control. Glucosamine, thiamine, malic acid, and alpha-ketoglutarate induced no significant direction changes at any concentration tested (Fig. 2.1D and E), suggesting they do not act as attractants or repellents.

To determine if chemoattractant responses toward arginine, fumarate, and cysteine were TlpA dependent, the same tracking experiments were repeated with a mutant lacking *tlpA* (Δ*tlpA*). The Δ*tlpA* mutant retained general chemotactic ability, producing a significant attractant and repellent response to controls dipyridyl and HCl, respectively, but failed to exhibit a chemotactic response to arginine, fumarate, or cysteine (Fig. 2.1A, B, C). These results suggest that the high-affinity ligands arginine, fumarate, and cysteine are TlpA-dependent chemoattractants.

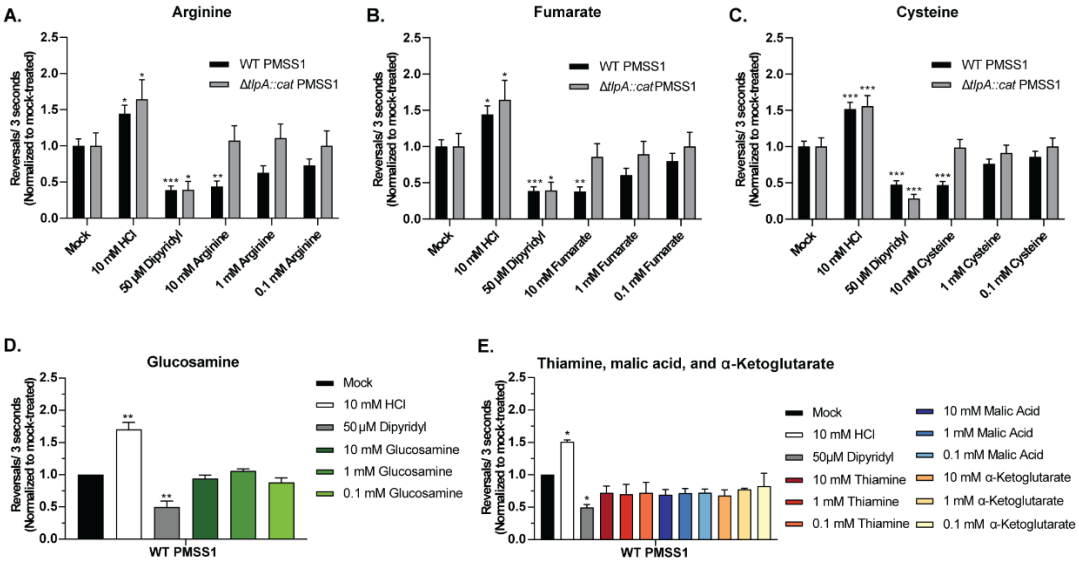

Figure 2.1- *H. pylori* responds to arginine, fumarate, and cysteine as TlpA-dependent chemoattractants in the temporal chemotaxis assay.
Cultures of *H. pylori* PMSS1 WT and Δ*tlpA* were grown overnight, back-diluted, then incubated until an OD_{600} of 0.12– 0.15 was reached. Cultures were treated with water (Mock) or with various concentrations of compounds as indicated. For Fig. 1C and E, the pH of cysteine, thiamine, malic acid, and alpha-ketoglutarate stocks was adjusted using NaOH to match the pH of the water used for the untreated control. The cells were immediately filmed, and direction changes were counted over a 3 second swimming period in at least 100 cells per treatment from 3 biological replicates. Data is normalized to the untreated control for each strain, as described in the methods. Error bars represent the standard error of the mean. *, P<0.05; **, P<0.01; ***, P<0.001, comparisons to untreated control per strain using two-way ANOVA, Dunnett's multiple comparison test.

2.4.3 TlpA has at least two ligand interaction sites.

To gain insight into how $TlpA_{LBD}$ binds ligands, a blind docking modeling experiment was carried out using AutoDock Vina (Krieger et al., 2002; Wang et al., 2016). We focused on two high-affinity ligands, arginine and fumarate. We found that these two ligands occupied two main sites, referred to as clusters (Supplemental Table 2.2), which map to the membrane-distal and -proximal dCache_1 binding pockets (Fig. 2.2A and D). Arginine was placed mostly in

Cluster D (55%, Supplemental Table 2.3), which is located in the membrane-distal dCache_1 domain. Arg-153 dominated this binding interaction with stabilization from Tyr-151 (Fig. 2.2B and C). Fumarate, in contrast, was placed mostly in Cluster A (45%, Supplemental Table 2.3), in the membrane-proximal dCache_1 domain, with Phe-203 being the most crucial residue required for interaction with fumarate (Fig. 2.2E and F). The docking experiment further revealed that although fumarate and arginine are likely to have two distinct preferred binding sites, they both can bind to their reciprocal sites. For example, 25% of the models had arginine found in fumarate's preferred Cluster A (Supplemental Table 2.3). Overall, these analyses suggest that arginine is more likely to bind the membrane-distal dCache_1 domain, while fumarate is more likely to bind the membrane-proximal dCache_1 domain, but binding to the other binding pockets is also possible.

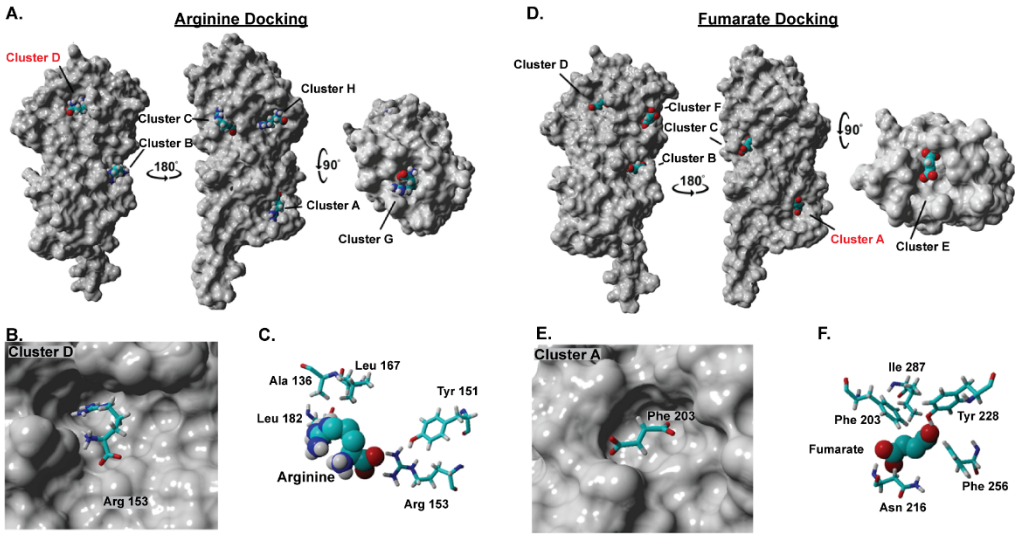

Figure 2.2- Docking analysis of TlpA and arginine or fumarate identifies several clusters that are occupied by these ligands.
Docking analysis shows several clusters occupied by **(A)** arginine and **(D)** fumarate on the surface of a space-filling version of $TlpA_{LBD}$. Cluster C and G are

biologically irrelevant due to the homodimer formation of TlpA, and Cluster B and H are poorly populated (Supplemental Table 3). **(B-C)** View of the energetically preferred bound conformation of arginine in Cluster D, the predicted membrane-distal dCache pocket, with key interacting amino acids shown. **(E-F)** View of the energetically preferred bound conformation of fumarate in Cluster A, the membrane-proximal dCache pocket, with key interacting amino acids shown.

To further study TlpA-ligand interactions, we generated $TlpA_{LBD}$ point mutants at residues in the membrane-distal (D165A, M183A) or membrane-proximal (Y228A, Y252A, D254A) binding pockets and determined the binding affinity of the resultant proteins towards all ligands (Table 2.2 and Fig. 2.3A). Mutation of either membrane-distal residue resulted in an ~10-fold decrease in the binding affinity for arginine, cysteine, fumarate, and glucosamine (Fig. 2.3B and Table 2.2). Mutation of the membrane-proximal residue $TlpA_{Y228A}$ also lead to a decrease in binding affinity for arginine, cysteine, and fumarate, but it was only 4-fold. The other mutation in the membrane-proximal site ($TlpA_{D254A}$) only affected fumarate binding (Fig. 2.3B and Table 2.2). No proximal pocket residues affected the binding affinity of glucosamine. Membrane-distal and -proximal mutations resulted in a modest ~3- 4-fold increase in binding affinity toward malic acid and thiamine compared to the WT control. Additionally, no appreciable change in binding affinity towards alpha-ketoglutarate was observed for any point mutant. Overall, TlpA binding interactions by the high-affinity ligands arginine, cysteine, fumarate, and glucosamine are most disrupted by mutations in the membrane-distal dCache_1 domain, but mutations in the membrane-proximal dCache_1 also

significantly impair fumarate, and to a lesser extent, arginine and cysteine binding, consistent with the predictions from the docking analysis.

Table 2.2- Binding affinity (μM) of $TlpA_{LBD}$ and $TlpA_{LBD}$ membrane-distal and -proximal dCache mutants to TlpA ligands.
Data represent the mean values (± SD) of three independent experiments (n= 3).

Ligand	$TlpA_{WT}$	$TlpA_{D165A}$	$TlpA_{M183A}$	$TlpA_{Y228A}$	$TlpA_{Y252A}$	$TlpA_{D254A}$
Arginine	2±0.11	12.4±0.84	22.3±5.9	8.3±1.6	4.96±1.8	3.71±0.73
Cysteine	4.7±0.3	41.9±0.4	36.1±15.7	15.7±6.6	5.5±0.8	4.58±1.5
Fumarate	10±1.5	100.5±38.9	106.1±36.6	46.6±3.9	8.5±1.7	44±8.1
Glucosamine	10.5±2.8	96±24.3	94.6±57.3	17.1±70	2.96±0.7	9.84±3.7
Malic Acid	46±17	11.9±4.3	33.6±6.2	28.6±9.4	14.2±6.2	29.3±2
Thiamine	60±0.6	43.9±14.1	18.1±1.2	29.5±12.3	35±7.3	39.3±4.3
α-ketoglutarate	224±11.2	124±7.1	256.2±27.6	295.4±27.7	289±22.6	321±21.6

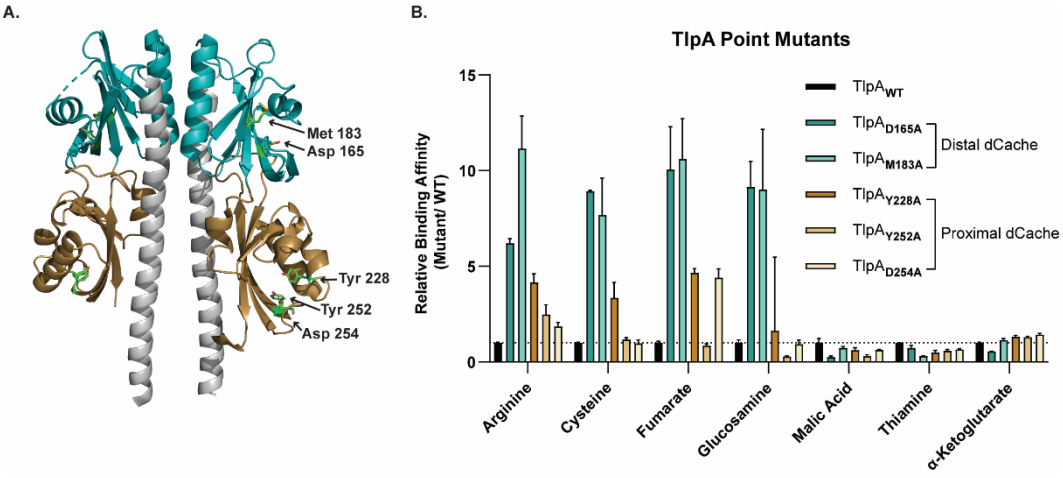

Figure 2.3- $TlpA_{LBD}$ binds chemotaxis-active ligands through the membrane-distal or -proximal dCache subdomains.
(A) A ribbon diagram of $TlpA_{LBD}$ as a homodimer. The membrane-distal and membrane-proximal dCache domains are colored teal and gold, respectively. Residues that were mutated to alanine are highlighted in each region to make $TlpA_{D165A}$, $TlpA_{M183A}$, $TlpA_{Y228A}$, $TlpA_{Y252A}$, and $TlpA_{D254A}$. **(B)** The relative binding affinity [K_d] for each ligand to $TlpA_{LBD}$ membrane-distal and -proximal dCache point mutants relative to WT $TlpA_{LBD}$. E.g., mutation of D165 to A resulted in a ~ 6-fold decrease in arginine binding affinity compared to WT binding. Data represented the mean values and standard error of the mean of three independent experiments (n=3).

2.4.4 $TlpA_{LBD}$ binds arginine and fumarate through distinct binding sites.

The above data suggest that $TlpA_{LBD}$ can bind ligands in both dCache_1 subdomain binding pockets. To further analyze the possibility of two distinct binding sites for chemotaxis-active ligands in $TlpA_{LBD}$, we employed a competition SPR (A-B-A) binding assay focused on arginine and fumarate because they were both chemoattractants and predicted to bind different sites preferentially. In this assay, the competition for binding to $TlpA_{LBD}$ between arginine and fumarate is assessed by adding the ligands sequentially and monitoring whether the SPR signal changes upon the addition of the second ligand. The two ligands' binding status can be classified as either independent, shared, or preferential shared sites. For independent sites, ligand A saturates all its binding sites, and ligand B then binds to its independent site; this mode produces additive effects on the SPR signal. Shared sites, in contrast, do not produce additive/cumulative effects, *i.e.*, ligand A binds its site and then blocks ligand B from the same site. Lastly, it is also possible to have preferential shared sites where ligands share the same binding site, but the protein binds to one ligand preferentially when in equilibrium.

We first saturated $TlpA_{LBD}$ with arginine and then added fumarate. In this case, an increased response (additive effect) was observed compared to the theoretical value (Fig. 2.4). This outcome suggests fumarate and arginine bind to independent sites. Conversely, when $TlpA_{LBD}$ was saturated with fumarate, arginine did not produce an additional response compared to the theoretical value (Fig. 2.4). This result suggests that fumarate prevented arginine binding, either

because arginine competed with fumarate at the same site(s), or that fumarate caused an allosteric effect that prevents arginine binding, a common occurrence in sensory proteins (Biemann and Koshland, 1994). Overall, the docking and competitive SPR data support the hypothesis that there are two binding sites with possible cooperative interactions or overlap between them.

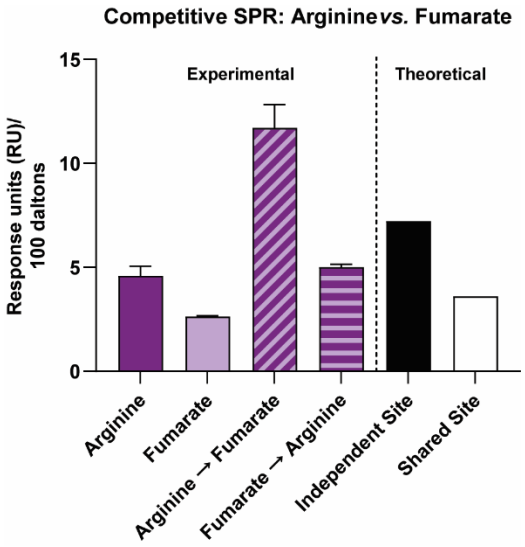

Figure 2.4- SPR competition analysis indicates the presence of two distinct binding sites for TlpA ligands.
SPR competition analysis of binding by arginine and fumarate to WT $TlpA_{LBD}$. Compounds were used at concentrations 10x their respective K_d. Arginine, response to arginine only; Fumarate, response to fumarate only; Arginine → Fumarate, fumarate response after saturation with arginine; and Fumarate → Arginine, arginine response after saturation with fumarate. The theoretical value is responses units (RU) values based on mathematical theory: Independent Site is the sum of individual responses; Shared Site is the sum of individual responses divided by the number of individual responses. All response data was normalized 100 Da molecular weight for each analyte allowing direct comparison of responses.

The docking analysis and competition SPR assay suggested that arginine and fumarate bind to distinct $TlpA_{LBD}$ sites, therefore we sought to further characterize TlpA-ligand interactions using Saturation Transfer Difference (STD)

NMR spectroscopy, which can measure protein-ligand interactions and ascertain which part of a ligand interacts with the receptor protein (Haselhorst et al., 2009; Mayer and Meyer, 1999). When $TlpA_{LBD}$ bound fumarate, a significant STD NMR signal was detected, consistent with the two ethylene protons interacting with the protein (Fig. 2.5A). Similarly, when $TlpA_{LBD}$ bound arginine, significant STD NMR signals were observed (Fig. 2.5B). On arginine, the relative STD NMR effects showed the H-3 and H-4 protons on the side chain received the largest saturation transfer from the protein protons, indicating arginine interacts with $TlpA_{LBD}$ around its middle carbon side chain region (Fig. 2.5B). These results, therefore, provide additional confirmation that TlpA interacts with fumarate and arginine, mostly along the carbon chain backbones in each ligand.

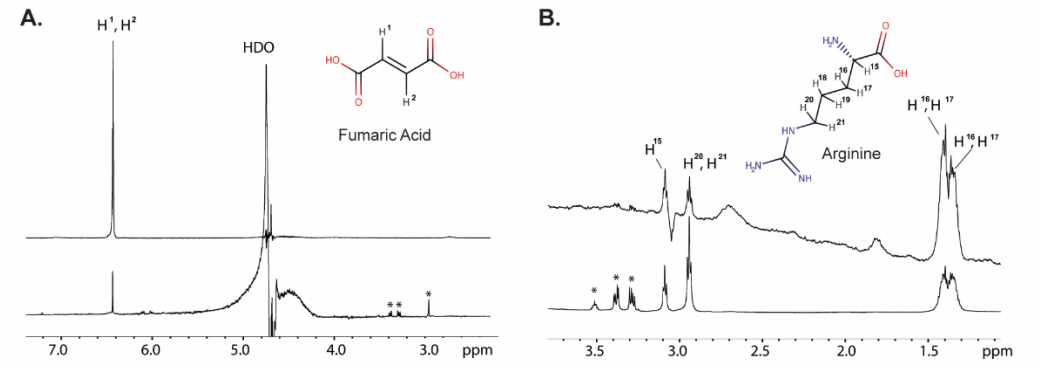

Figure 2.5- STD NMR analysis supports $TlpA_{LBD}$ binds fumarate and arginine.
^{1}H NMR spectra are shown at the bottom for **(A)** fumarate and **(B)** arginine. The STD NMR spectra are shown on top acquired at 600 MHz, 289 K with an on-resonance of -1 ppm and off-resonance of 33 ppm and a total saturation time of 2 sec.

2.4.5 A non-chemotaxis active TlpA ligand can antagonize chemoattractant responses

It was surprising to find a high affinity direct binding ligand, glucosamine, which bound to the membrane-distal dCache_1 subdomain (Fig. 2.3) that did not elicit a chemotaxis response (Fig. 2.1D). Previous reports on ligand interactions with chemoreceptors in *E. coli* and *P. aeruginosa* suggested that some ligands bind chemoreceptors as antagonists, blocking normal chemotactic responses toward chemotaxis-active ligands (Bi et al., 2013; Martín-Mora et al., 2018). Consequently, we tested whether glucosamine could block binding of the chemotaxis-active TlpA ligands arginine and fumarate, using a competitive SPR assay. Of note, the other non-chemoactive TlpA ligands, malic acid, thiamine, and alpha-ketoglutarate were not affected by either membrane-proximal or -distal dCache_1 domain point mutants (Fig. 2.3), therefore we hypothesized they would be unable to effect binding of chemotaxis-active TlpA ligands, as they do not appear to bind through the same sites. The results showed that when glucosamine was added following saturation with arginine or fumarate, the response was not additive, suggesting glucosamine competed with both arginine and fumarate (Fig. 2.6A and B). However, when arginine or fumarate were added to $TlpA_{LBD}$ following initial saturation with glucosamine no additive response was observed (Fig. 2.6A and B). This result suggests that glucosamine can prevent binding of both ligands to $TlpA_{LBD}$.

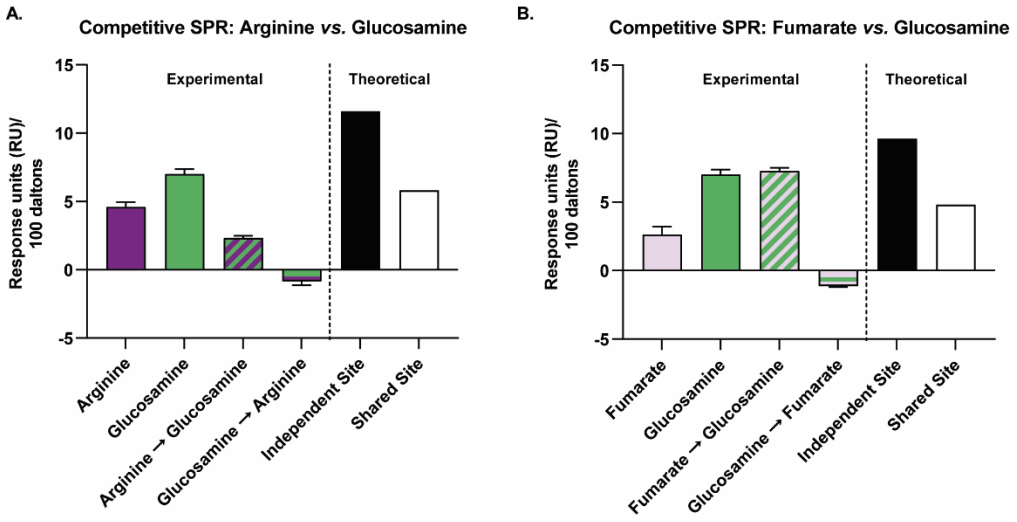

Figure 2.6- SPR competition analysis demonstrates glucosamine blocks bindings of TlpA chemoattractants.
Data from SPR competition analysis of binding of arginine, fumarate, and glucosamine to WT $TlpA_{LBD}$ are shown. Compounds were used at concentration 10x their respective K_d values. **(A)** Arginine, response to arginine only; Glucosamine, response to glucosamine only; Arginine → Glucosamine, response to glucosamine following saturation with arginine; Glucosamine → Arginine, response to arginine following saturation with glucosamine. **(B)** Fumarate, response to fumarate only; Glucosamine, response to glucosamine only; Fumarate → Glucosamine, response to glucosamine following saturation with fumarate; Glucosamine → Fumarate, response to fumarate following saturation with glucosamine. The theoretical values are response units (RU) values based on mathematical theory. All response data was normalized 100 Da molecular weight for each analyte allowing direct comparison of responses.

Consequently, we tested whether glucosamine affected *H. pylori* chemotaxis by developing a ligand competition tracking assay between non-chemotaxis active and chemotaxis-active TlpA ligands. This assay is a modified version of our live-cell video microscopy assay where the addition of a chemotaxis-active ligand is followed by the addition of a non-chemotaxis active ligand 10-seconds later and vice versa. Using this approach, we determined that glucosamine addition prevented the chemoattractant response towards arginine, fumarate, and

severely blunted the response to cysteine (Fig. 2.7). This response was decreased regardless of whether glucosamine was added prior to or after the addition of the chemoattractant. In total, these results suggest that glucosamine blocks chemotaxis-active ligand binding and acts as a TlpA chemotaxis antagonist.

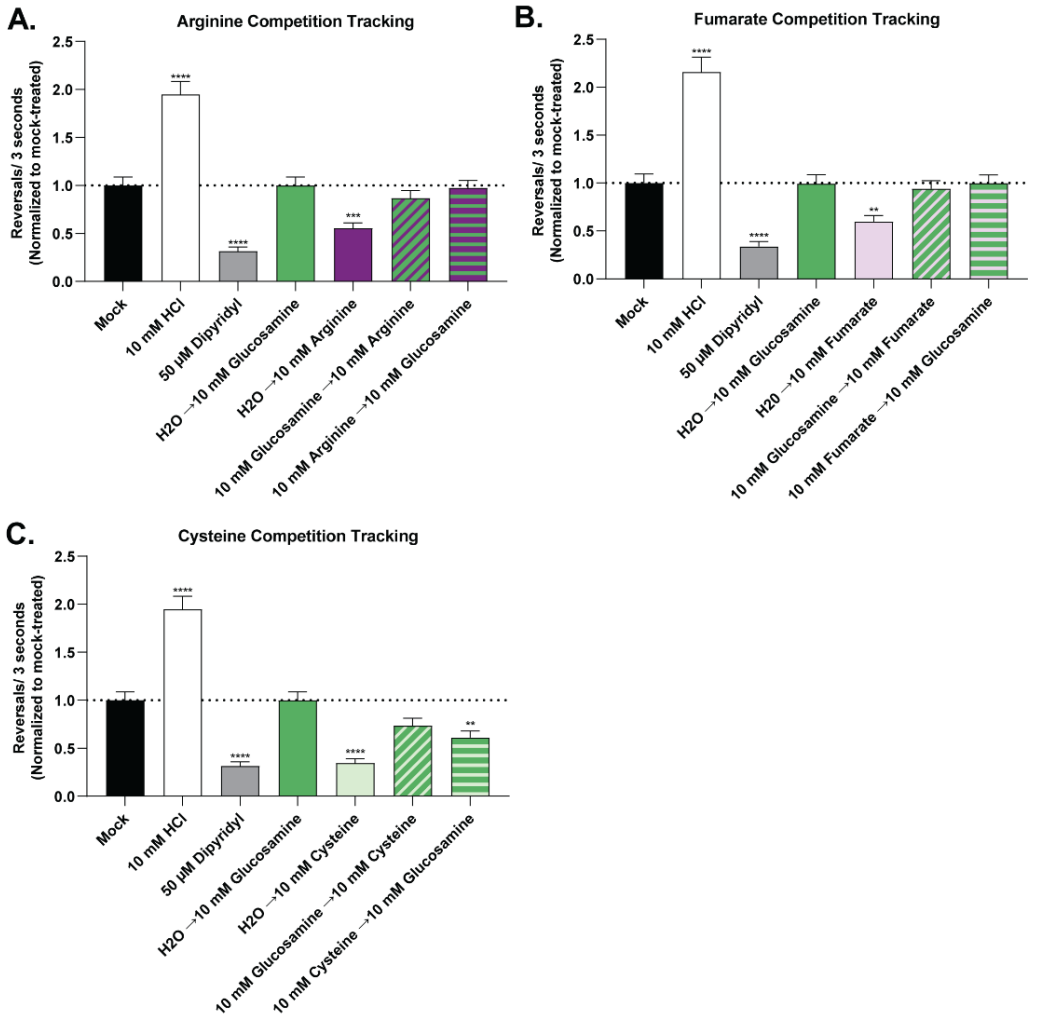

Figure 2.7- Ligand competition tracking experiment between chemoactive and non-chemoactive TlpA ligands.
Cultures of *H. pylori* PMSS1 WT were grown in BB10 overnight and then back-diluted as described in Fig. 1. Cultures were mock-treated or with various concentrations of compounds as indicated. The pH of the cysteine stock was adjusted using NaOH to match the pH of the water used for the untreated control.

The cells were immediately filmed, and direction changes were counted over a 3 second swimming period in at least 100 cells per treatment from 3 biological replicates. Repellents increase in direction changes, as exemplified by the control repellent HCl, while attractants decrease direction changes as exemplified by the control attractant dipyridyl. Data is normalized to the untreated control for each strain, as described in the methods. Error bars represent the standard error of the mean. *, $P<0.05$; **, $P<0.01$; ***, $P<0.001$, comparisons to untreated control per strain using two-way ANOVA, Dunnett's multiple comparison test.

2.5 Discussion

We report the identification of several ligands specific for *H. pylori* dCache_1 chemoreceptor TlpA, including confirmation of previous reports that TlpA interacts with arginine (Cerda et al., 2003, 2011). Arginine, along with fumarate and cysteine, functioned as TlpA-sensed chemotaxis attractants. Furthermore, these chemotaxis-active ligands appeared to interact with the membrane-distal and -proximal dCache_1 domains. Finally, we found that glucosamine acts as a chemotaxis antagonist, blocking TlpA binding and responses to multiple attractants.

2.5.1 TlpA can bind a broad set of ligands with diverse biological functions

TlpA bound a broad set of molecules ranging from the amino acid arginine with a large, charged side chain, the amino acid cysteine with a smaller polar side chain, organic acids including fumarate, malic acid, and alpha-ketoglutarate, the large vitamin thiamine, and the amino sugar glucosamine. Ultimately, our data suggest that only some of these ligands bind within the canonical dCache_1 binding pockets, including all those that affected chemotaxis. Thus, these results agree with

previous reports showing that individual dCache chemoreceptors can sense diverse types of ligands (Rahman et al., 2014; Ud-Din et al., 2020).

The three molecules that elicited a chemotaxis response, arginine, fumarate, and cysteine, have been shown to have important biological roles in *H. pylori* biology. Arginine is an essential amino acid for *H. pylori* under *in vitro* growth conditions (Nedenskov, 1994), and *H. pylori* uses arginine to promote acid tolerance and dampen host immune responses (Alam et al., 2018; Gobert and Wilson, 2016; Mcgee et al., 1999; Valenzuela et al., 2014). Fumarate is predicted to be an alternative terminal electron acceptor for growth under anaerobic respiration (Mendz et al., 1995), and the associated enzyme, fumarate reductase, is essential for *H. pylori* colonization *in vivo* (Ge et al., 2000). Additionally, fumarate is highly depleted when *H. pylori* is co-cultured with gastric organoids, consistent with the prediction that it is preferentially used *in vivo* (Keilberg et al., 2020). Lastly, cysteine is an essential amino acid for some strains of *H. pylori* (Nedenskov, 1994). These ligands have been shown to be present in the stomach during infection via metabolomics studies (Keilberg et al., 2020; Nishiumi et al., 2017), however, the exact concentration of these ligands are not known. Each chemotaxis-active TlpA ligand is important for critical cellular functions for *H. pylori*, therefore the ability to sense these ligands is likely a survival-linked evolutionary adaptation.

2.5.2 TlpA appears to use both binding pockets

dCache_1 chemoreceptors contain two potential ligand-binding pockets in each Cache subdomain. Previous work showed dCache_1 chemoreceptors sense

chemotaxis-active ligands through either subdomain, but as of yet, not both (Machuca et al., 2017; Mckellar et al., 2015). In contrast, our data suggests that TlpA might bind ligands in both Cache subdomains. Ligand binding locations, suggested by docking prediction analysis, placed fumarate within the membrane-proximal subdomain and arginine within the membrane-distal subdomain. These location assignments were further supported by $TlpA_{LBD}$ point mutants of residues within the predicted dCache_1 membrane-distal (D165A and M183A) and membrane-proximal (Y228A, Y252A, D254A) subdomains. All membrane-distal subdomain mutations led to a decreased binding affinity for the chemotaxis-active ligands, arginine, fumarate, cysteine, as well as the antagonist ligand glucosamine. These findings suggest that the membrane-distal site is important for chemotaxis signaling, as seen in other dCache_1 receptors (Mckellar et al., 2015; Upadhyay et al., 2016). It has been shown that individual dCache_1 receptors can bind aliphatic, small polar, and large positively charged amino acids through a single subdomain due to the malleable nature of dCache_1 receptors that can accommodate ligands of different sizes and charges (Ud-Din et al., 2020). Thus, it is plausible the membrane-distal subdomain could be able to accommodate these diverse ligands.

Our data also suggest that the membrane-proximal subdomain plays a role in the TlpA ligand binding. Site-directed mutagenesis of the membrane-proximal subdomain, as well as the membrane-distal one, decreased fumarate binding. This outcome suggests that the point mutations either directly disrupted ligand binding or altered long-range interactions in the protein that influence ligand binding

affinities. Additionally, our data showed that fumarate blocked arginine binding, despite having similar binding affinities. Of note, arginine binding to the membrane-proximal domain was affected by the membrane-proximal domain point-mutant $TlpA_{Y228A}$, while fumarate is affected by both $TlpA_{Y228A}$ and $TlpA_{D254A}$ membrane-proximal domain point-mutants, which supports docking analysis predictions suggesting fumarate preferentially binds to the membrane-proximal domain, while arginine preferentially binds the membrane-distal domain. Several models could account for these findings. One is that fumarate binds at the membrane-proximal site and creates an allosteric change that prevents ligand binding at the membrane-distal site. Alternatively, the amino acid changes in the proximal site could affect ligand affinities at the distal site. Finally, a third possibility is that arginine binds at both sites, and proximal site binding is affected by the proximal mutations. It will be interesting to dissect whether there is cooperative interactions, distinct site binding, or simultaneous site binding. Regardless, while cooperativity between subdomains in dCache_1 chemoreceptors has not yet been observed, it is well documented that four-helix bundle types of chemoreceptors have negative cooperativity between their two binding sites (Biemann and Koshland, 1994). It furthermore is not yet known which site is required for chemotaxis. Overall, our data suggests that TlpA may use both dCache_1 subdomains to bind ligands.

2.5.3 TlpA chemotaxis responses can be antagonized.

We were somewhat surprised to find a high-affinity binding TlpA ligand, glucosamine, that did not elicit a chemotaxis response yet appeared to bind the membrane-distal dCache_1 subdomain. Indeed, we found that glucosamine occluded chemotaxis-active TlpA ligands from binding and inhibited the normal chemoattractant responses towards arginine, fumarate, and cysteine. This response was observed whether glucosamine was added before or after the addition of the TlpA chemoattractants, suggesting glucosamine may have a very high on-rate for binding TlpA compared to arginine, fumarate, or cysteine. Two studies have reported high-affinity chemoreceptor ligands that acted as antagonists by blocking chemotaxis-active ligand binding (Bi et al., 2013; Martín-Mora et al., 2018), and Cache receptor antagonists have been reported for a histidine kinase (Busch et al., 2007). Martín-Mora and colleagues showed that binding of the attractant malic acid to the *P. aeruginosa* sCache chemoreceptor PA2652 was inhibited by either citraconic acid or D,L- methylsuccinic acid, and subsequently chemoattractant responses towards malic acid were decreased (Martín-Mora et al., 2018). Another of these studies described finding diverse ligands for the *E. coli* four-helix bundle chemoreceptor Tar, and reported a high-affinity ligand, *cis*-1,2-cyclohexane-dicarboxylic acid also acted as an antagonist for aspartate chemotaxis. *cis*-1,2-cyclohexane-dicarboxylic acid competed for aspartate binding and blocked intracellular kinase activity (Bi et al., 2013). We expect there will be more discoveries of these types of chemo-modulatory antagonists, or maybe even

chemotaxis enhancing ligands because ligand discovery methods have changed. Specifically, previous efforts relied on chemotaxis assays, and so only chemotaxis-active ligands could be identified. In contrast, recent approaches look for direct ligand-receptor interactions at the molecular level, thus expanding our ability to identify the interacting partners (Bi et al., 2013; Ehrhardt et al., 2018; Hartley-Tassell et al., 2010; Krell, 2015; Mckellar et al., 2015).

The function of chemoreceptor antagonists is not yet known in any system (Bi et al., 2013; Martín-Mora et al., 2018). In the case of TlpA, it is possible to speculate that when confronted with abundant glucosamine, *H. pylori* benefits by not responding to arginine, fumarate, or cysteine. However, the role of glucosamine in *H. pylori* infection is unknown, although it has been shown to support the growth of some *H. pylori* clinical isolates using phenotypic Biolog plates (Lee et al., 2017). One possibility is that antagonist ligands may function as a form of adaptation, as *H. pylori* lacks the classical adaptation proteins CheR and CheB (Lertsethtakarn et al., 2011), possibly in lieu of, or in augmentation to, other adaptation systems. Chemotaxis antagonists may be useful tools to modulate chemotaxis and affect bacterial pathogenesis. In the case of TlpA, blocking its function early in infection would decrease colonization; however, a later attenuation of chemotactic responses might be predicted to enhance inflammation (Andermann et al., 2002; Rolig et al., 2012; Williams et al., 2007). Future work performing molecular dynamics experiments to understand how agonist and antagonist ligands interact with $TlpA_{LBD}$ will help to understand the function of chemoreceptor antagonists.

One caveat of this study is that experimental analyses were carried out under two different conditions. The ligand-binding work was all done with purified $TlpA_{LBD}$, while the chemotaxis studies were done with full-length TlpA that was in the context of both a membrane and its interactions with other chemoreceptors. These two different situations may lead to varying outcomes. For example, it is not clear how ligand interactions would change in the context of chemosensory array-packed receptors, which is an area for future work.

Expanding the knowledge of TlpA ligands, and how TlpA interacts with these ligands is essential for better understanding why TlpA enhances the *in vivo* fitness of *H. pylori* and alters inflammatory phenotypes driven by *H. pylori*. Future experiments manipulating the ability of *H. pylori* to sense specific TlpA ligands will be useful to understand whether all or a subset of TlpA ligands play a role in driving these *in vivo* phenotypes (Andermann et al., 2002; Rolig et al., 2012; Williams et al., 2007). Furthermore, this work provides another example (Bi et al., 2013; Martín-Mora et al., 2018) of a chemotaxis system having antagonistic ligands, operating through a distinct type of chemoreceptor ligand-binding domain. These results suggest an interesting possible mechanism for regulating responses to multiple chemotactic ligands in a nutrient-rich environment using agonist and antagonist ligands.

2.6 Methods

2.6.1 TlpA construct design and protein purification

The periplasmic portion of TlpA ($TlpA_{LBD}$), amino acids 28- 299, from *Helicobacter pylori* SS1 was cloned into a pBH4 expression vector (pBH4_$TlpA_{LBD}$) to generate an N-terminal 6x-His-tagged construct, with a TEV protease site, under control of IPTG (Sweeney et al., 2018). Alanine point mutants at Asp 165, Met 183, Tyr 228, Tyr 252, and Tyr 254 in $TlpA_{LBD}$ were generated via site-directed mutagenesis of pBH4_$TlpA_{LBD}$ with primers listed in Supplemental Table 4 and confirmed via restriction digest and sequencing (QuikChange, Stratagene). $TlpA_{LBD}$ and all point mutants were purified as described by Sweeney *et al.* 2018 (Sweeney et al., 2018). CD spectroscopy was used to confirm the correct folding of all proteins (Supplemental Fig. 2.3) (Elgamoudi et al., 2021).

2.6.2 Ligand binding array

Small-molecule arrays were prepared and performed as previously described (Day and Korolik, 2018). Briefly, 1 µg of purified $TlpA_{LBD}$ in PBS, pH 7.2, was incubated with a molar concentration ratio (4:2:1) of anti-His antibody (Cell Signaling), followed by incubation with a secondary antibody (Thermo Scientific) for signal amplification. The protein-antibody mix was added to an Arrayit Superepoxy III glass substrate array blocked with PBS, pH 7.2, with 1% bovine serum albumin. The glass substrate array was printed with quadruplicate spots of 148 different amino acids, salts of organic acids, and other small molecules (Supplementary Table 2.1). Unbound protein was washed away with PBS with

0.05% Tween. The arrays were scanned by a ProScan Array scanner at 488/520 nm and the results analyzed by ScanArray Express software program (Perkin Elmer). Three biological replicates were performed with a total of 12 data points for each glycan tested. Binding was classified as positive for a ligand if the relative fluorescence unit value was greater than one-fold above the mean background (defined as average background of negative control spots plus 3 standard deviations) and was statistically significant ($p < 0.005$, Students T-Test). The small molecule array slide preparation and analysis were done in accordance with MIRAGE guidelines (Liu et al., 2017) (outlined in Supplemental Table 2.5).

2.6.3 Surface Plasmon Resonance Measurements

Purified $TlpA_{LBD}$ was immobilized on a CM5 series S sensor chip and binding affinities tested using a BIAcoreTM S200 instrument (GE Healthcare) as described (Day et al., 2016; Day and Korolik, 2018; Rahman et al., 2014). Briefly, proteins were captured using an amine coupling kit (GE Healthcare), in which the carboxylmethyl dextran matrix of the sensor chip was activated by injection of a mixture of 0.2M 1-ethyl-3-[(3-dimethylamino) propyl]-carbodiimide (EDC) and 0.05 M N-hydroxysuccinimide (NHS), followed by neutralization of the remaining unreacted NHS ester groups by an injection of 1 M ethanolamine-HCl (pH 8.0). Purified $TlpA_{LBD}$ was diluted in 10 mM sodium acetate buffer pH 4.5 at a concentration of 100 μg/mL for immobilization to the chip. 8400 response units (RU) of $TlpA_{LBD}$ were captured on Flow Cell 2. As a negative control, Flow Cell 1 was a blank control undergoing the same treatment as the other flow paths, without

the protein injection. This set enabled double reference subtraction of the responses (2-1, 3-1, 4-1). The tested compounds were prepared as a stock concentration of 100- 200mM in PBS. The compounds were then diluted between 1 nM-1mM in a series of 1:10 dilutions in PBS and run over the flow cells at a flow rate of 30 µL/min. Between each sample testing, a series of buffer-only injections were run to enable double blank subtraction for the sensorgram assessment. After the initial run, based on the results, the dilution series ranged from 0.195 µM to 1 mM in 1:4 dilutions in PBS. Then the samples were run using single-cycle kinetic/affinity methods in triplicate for those compounds that showed sub-millimolar affinity after the initial binding screen. The datasets were analyzed using the BIAcore s200 evaluation software 2.0.2; sensorgrams were double reference subtracted.

2.6.4 Bacterial strains and growth conditions

For all chemotaxis assays, *H. pylori* strain PMSS1 was used (Arnold et al., 2011b). Bacteria were grown in Brucella broth (BD BBL/Fisher) with 10% heat-inactivated fetal bovine serum (FBS) (Life Technologies) (BB10), with shaking, at 37°C, under microaerobic conditions of 5% O_2, 10% CO_2, 85% N_2. The PMSS1 Δ*tlpA* mutant was created by natural transformation of wild-type PMSS1 with 5 µg of Δ*tlpA::cat* SS1 genomic DNA (Andermann et al., 2002). Chloramphenicol-resistant mutants were selected using 10 µg/ml chloramphenicol on Columbia Horse Blood Agar as previously described (Andermann et al., 2002). Mutation of *tlpA* was confirmed by PCR amplification of genomic DNA from WT PMSS1, Δ*tlpA::cat* PMSS1, and Δ*tlpA::cat* SS1 using primers TlpA_SS1_5' (TTGTCTAAAGGTTTGAGTATC)

and TlpA_SS1_3'(TTAAAACTGCTTTTTATTCAC) (This study) (Supplemental Figure 2.4).

2.6.5 Chemotaxis assays

Swimming behavior assays were done with *H. pylori* PMSS1 strains and grown in BB10 as described above. Overnight cultures were diluted to an OD_{600} of 0.1 in fresh BB10 and then incubated with shaking as above until an OD_{600} of 0.12– 0.15 was reached. Motility of these cultures was confirmed, and then they were used for chemotaxis assays by treating with L-arginine monohydrochloride (J.T. Baker, B577-05), sodium fumarate (Acros Organics, 215531000), L-cysteine hydrochloride monohydrate (RPI, C81020), D(+)-glucosamine hydrochloride (Chem-Impex International Inc., 01450), thiamine hydrochloride (Fisher BioReagents, BP892), α-ketoglutaric acid (Santa Cruz Biotechnology, SC-208504), or L-malic acid (MP Biomedicals, 102237) at a final concentration of 0.1 mM, 1 mM, 10 mM or an equal volume of H_2O as a mock-treated control (4 µl H_2O or 4 µl of ligand stock in H_2O into 96 µl culture). The number of direction changes in a bacterial swimming trajectory were enumerated over a three-second interval to determine whether each putative ligand is sensed as an attractant, repellent, or elicits no response (Collins et al., 2016; Goers Sweeney et al., 2012; Lertsethtakarn et al., 2015; Machuca et al., 2017; Rader et al., 2011; Schweinitzer et al., 2008; Terry et al., 2006). The results were compared to both a repellent control, 10 mM HCl (Fisher Chemical, A144S), which results in increased direction changes (Croxen et al., 2006; Goers Sweeney et al., 2012) and an attractant control, 50 µM

2,2'-dipyridyl (Arcos Organics, 117500250), which results in fewer direction changes (Collins et al., 2016). Each control is sensed by chemoreceptors other than TlpA (Collins et al., 2016; Croxen et al., 2006; Goers Sweeney et al., 2012; Huang et al., 2017). The pH of BB10 upon treatment was independently assessed using a Denver Instruments pH meter. Prior to realizing chemotactic responses may be due to media acidification, we resuspended all ligands in pure water. Therefore, to be able to compare results to previous experiments, we continued resuspending acidified ligands in pure water, then adjusting the pH of the resuspended ligand using NaOH. Cultures were filmed immediately after ligand addition at 400x magnification using a Hamamatsu Digital Camera C4742-95 with the μManager software (Version 1.4.22), mounted on a Nikon Eclipse E600 phase-contrast microscope. For the competition chemotaxis assay, cultures of *H. pylori* and ligands were prepared as above. However, 1 minute after the addition of a non-chemoactive ligand at a final concentration of 10 mM, a chemoactive ligand was added at a final concentration of 10 mM, and then cultures were filmed as described above. Videos were relabeled to blind the observer to the strain identity. For each sample, > 100 3-s-long bacterial tracks from three independent cultures were analyzed manually to identify stops followed by direction changes. Data for all biological replicates for each condition was combined, and the average number of direction changes in 3 seconds and standard error of the mean were calculated. For each strain, data was normalized to the untreated control for each experimental condition. Statistical

analysis of the data for treated versus untreated samples was performed using a two-way ANOVA, Dunnett's multiple comparison test.

2.6.6 SPR TlpA competition assays

SPR competition assays were performed by using a BIAcore S200 instrument and the A-B-A inject function (Elgamoudi et al., 2021). Competition A-B-A analyses were used to interrogate the specificity of the potential ligand binding site preferences of $TlpA_{LBD}$ and to unravel the nature of the ligand-sensor interactions. This assay was designed to show if a cumulative response is observed when a second analyte (B) is flown across the bound protein saturated with the first analyte (A) (Fig. 2.4). As the assay is designed to provide saturation of all analytes tested, this assay does not provide 1:1 competition to indicate which is the preferred analyte for a binding site. The proteins, wild-type $TlpA_{LBD}$ was immobilized as above. The A-B-A was used with combinations of each of the compounds (at concentration 10-fold higher than the equilibrium dissociation constant [K_d]) and PBS control, with 60-second injections of analyte A to ensure saturation or near-saturation was reached prior to competition with analyte B. The results were analyzed using BIAcore S200 evaluation software using the sensorgram mode, and data was zeroed to baseline before the initial A injection. All response data was normalized 100 Da molecular weight for each analyte, allowing direct comparison of responses. Independent Site theoretical values are calculated by taking the sum of individual responses. Shared Site theoretical values are calculated by taking the sum of individual responses divided by the number of individual responses.

2.6.7 Saturation Transfer Difference (STD) NMR

In this experiment, the entire $TlpA_{LBD}$ protein was first saturated at the protein resonances, and then excess ligand was added. As the ligand binds and releases from the receptor, saturation transfers from the protein to bound ligand. This transfer appeared as an increase in ligand intensity on epitopes that interacted with the $TlpA_{LBD}$ protein. For STD NMR experiments, samples of 25 μM $TlpA_{LBD}$ in complex with either 2.5 mM Arginine (Arg) or Fumaric Acid (Fum) in 99% D_2O were prepared. All STD NMR spectra were acquired in Shigemi tubes (Shigemi, USA) with a Bruker 600 MHz Advance spectrometer at 283 K using $^{1H}/^{13C}/^{15N}$ gradient cryoprobe equipped with z-gradients. Protein resonances were saturated at -1.0 ppm (on-resonance) and 33 ppm (off-resonance) and a total saturation time of 2 sec. A total of 512 scans per STD NMR experiment were acquired and a WATERGATE sequence was used to suppress the residual HDO signal. A spin-lock filter with 5 kHz strength and a duration of 10 ms was applied to suppress protein background. On- and off-resonance spectra were stored and processed separately, and the final STD NMR spectra were obtained by subtracting the on- and off-resonance spectra. Control STD NMR experiments were performed identically in the absence of protein.

2.6.8 Docking analysis

To evaluate a potential binding site for Arginine (Arg) and fumaric acid (Fum) to $TlpA_{LBD}$ (PDB code: 6E09). A blind docking experiment was performed using the AutoDock Vina protocol (Trott and Olson, 2009), a high-scoring molecular

docking program (Wang et al., 2016), implemented in the YASARA Structure molecular modeling package (Ver. 16.46)(Krieger et al., 2002). The blind docking experiment was set up by using the entire TlpA as-potential binding site (grid size 92.99 Å x 75.73 Å x 62.13 Å). A total number of 999 Vina docking runs were performed.

2.8 Acknowledgments

We like to thank Shuai Hu and Xiaolin Liu for their thoughtful comments on this article. The described project was supported by the National Institute of Allergy and Infectious Diseases (NIAID) grant RO1AI116946 to KMO. The funders had no role in study design, data collection, and interpretation, or decision to submit the work for publication.

CHAPTER 3- The *Helicobacter pylori* chemoreceptor TlpA regulates colonization within gastric glands and alters host inflammation

3.1 Abstract

One of the many ways *Helicobacter pylori* drives colonization and controls host inflammation is through its chemotaxis system. Chemotaxis is regulated by chemoreceptors. The *H. pylori* chemoreceptor TlpA plays a critical role in dampening chronic host inflammation via an unknown mechanism. It has become appreciated that chemotaxis and specific chemoreceptors dictate the localization of *H. pylori* in the stomach corpus and antrum. Additionally, chemotaxis affects immune responses, characterized by changes in $CD4^+$ effector T-cell populations. To better understand how *H. pylori* alters host inflammation via TlpA, we performed an 8-month study to assess inflammatory responses and colonization dynamics of wild type and a *tlpA* deficient strain. We discovered that at 5-months post-infection, TlpA dampens host inflammation in the corpus, which is associated with decreasing the Th17 cell response. Changes in inflammation are not related to overall differences in bacterial number between WT and Δ*tlpA H. pylori*; however, TlpA is required for limiting gland colonization during the acute stage of infection. The ability of *H. pylori* to limit gland colonization early in infection could be an important mechanism by which *H. pylori* influences late host inflammation.

3.2 Importance

Helicobacter pylori colonizes half of the world's population and is responsible for a significant disease burden by causing gastritis, peptic ulcers, and

gastric cancer. The development of host inflammation drives these diseases, but there are still open questions in the field about how *H. pylori* controls this process. It is known that the chemoreceptor TlpA dampens host inflammation, but it is unclear how. This work chronicles the role TlpA plays in inflammation development and the localization of *H. pylori* in the murine stomach over an 8-month time course.

3.3 Introduction

Bacterial colonization confers both beneficial and harmful effects to the host. For instance, beneficial roles of our microbiota include increasing nutrient availability, protecting against pathogens, and providing immunological benefits by producing specific metabolites and promoting particular anti-inflammatory cell types (Lazar et al., 2018). *Helicobacter pylori* is one bacterial species that confers both beneficial and harmful effects. This bacterium colonizes individuals during early childhood, often transferred from mother to child, leading to lifelong colonization of the stomach (Harris et al., 2013; Salama et al., 2013). Colonization in the early childhood period leads to immunological benefits. These benefits are characterized by the development of T-regulatory cells that in turn decrease the risk of asthma and other pathologies (Arnold et al., 2011a; Cover and Blaser, 2009; Harris et al., 2013). However, continued colonization into later life can lead to disease, including gastritis, peptic ulcers, and gastric cancer, ultimately contributing to a significant disease burden throughout the world (Cover and Blaser, 2009; Ferlay et al., 2015; Hooi et al., 2017b; Plummer et al., 2015). These

diseases are driven by stomach inflammation, making it critical to understand the mechanisms by which this bacterium manipulates host inflammation.

H. pylori forms intimate interactions with the human host, colonizing the two distinct regions of the stomach called the corpus and antrum, a pattern mimicked in murine models. Within these regions, *H. pylori* is found in the mucus layer lining the gastric epithelium, attached to gastric epithelial cells, and within gastric glands that invaginate both regions (Howitt et al., 2011; Keilberg and Ottemann, 2016; Schreiber et al., 2004; Yang and Ottemann, 2019). By all accounts, the stomach does not appear to be a hospitable niche for colonization. Its high acidity is toxic to *H. pylori* (Schreiber et al., 2005), contents of the stomach are emptied within hours of eating a solid digestible meal (Goyal et al., 2019), and the mucus layer (Atuma et al., 2001; Schreiber and Scheid, 1997) and gastric glands in which the bacteria reside are renewed in a matter of days, which is exacerbated by *H. pylori* colonization (Creamer et al., 1961; Sigal et al., 2015). Despite these challenges, *H. pylori* chronically colonizes the stomach using a variety of factors. These include virulence factors such VacA and γ-glutamyl-transpeptidase (GTT), which both lead to tolerogenic T-cells responses through effects on myeloid cell populations in the stomach (Salama et al., 2013; Zhang, 2020); the Cag PAI, which alters host cells signaling, increasing host inflammation and disease severity; adherence factors to facilitate host cell attachment; and urease to buffer the local environment of the bacteria; as well as several other factors (Keilberg and Ottemann, 2016; Salama et al., 2013).

The chemotaxis system of *H. pylori* dictates the localization of the bacteria within the stomach, which in turn promotes successful colonization and host inflammation development (Johnson and Ottemann, 2018). Chemotaxis regulates the motility of bacteria in dynamic environments, such as the stomach, in response to harmful and beneficial signals located extra- and intracellularly. These signals are sensed by chemoreceptors and are transduced through a two-component signal transduction system (Keilberg and Ottemann, 2016; Lertsethtakarn et al., 2011). *H. pylori* expresses three transmembrane chemoreceptors, TlpA, TlpB, TlpC, and one intracellular chemoreceptor, TlpD. Much work has been done to determine the sensing profile of these chemoreceptors to better understand their roles *in vivo*. Multiple attractants are sensed that are beneficial for *H. pylori* growth, including arginine, fumarate, and cysteine by TlpA; urea by TlpB; and lactate by TlpC (Cerda et al., 2003, 2011; Huang et al., 2015; Johnson et al., 2021; Machuca et al., 2017). Repellents, in contrast, are harmful to the bacteria and include acid sensed by multiple chemoreceptors, autoinducer-2 sensed by TlpB, and reactive oxygen species sensed by TlpD (Collins et al., 2016; Croxen et al., 2006; Huang et al., 2017; Perkins et al., 2019; Schweinitzer et al., 2008). The ability to sense signals through this system maximizes the fitness of the bacteria *in vivo*, as essential metabolites can be sought, and harmful host conditions can be avoided (Collins et al., 2018; Huang et al., 2017). The loss of a chemoreceptor in this system leads to the inability to sense a subset of these signals, biasing a bacterium to the signals sensed by the remaining chemoreceptors.

During colonization, these chemoreceptors play unique roles, likely due to their distinct sensing profiles. TlpA, TlpC, and TlpD are all required for colonization of the stomach to varying digress, while TlpA and TlpB are required to dampen host inflammation during chronic infection (Andermann et al., 2002; Collins et al., 2018; Rolig et al., 2012; Williams et al., 2007). The work presented here focuses on understanding TlpA's role in colonization and inflammation control *in vivo*. Previous work analyzing total tissue bacteria found that TlpA plays roles in colonization during the first two weeks of infection. Δ*tlpA H. pylori* was outcompeted by WT 50-fold in co-infections (Andermann et al., 2002) and had mild colonization defects in the antrum in single-strain infections (Rolig et al., 2012). During the later stages of infection, Δ*tlpA H. pylori* colonized to WT levels overall in the stomach at both 3- and 6-months post-infection (Williams et al., 2007). Intriguingly at late time points, e.g., 6-months post-infection, Δ*tlpA H. pylori* induced significantly more histologically measured inflammation (Williams et al., 2007). Given that host inflammation control by *H. pylori* dictates disease severity, this study aims to understand better how TlpA modulates host inflammation. (Arnold et al., 2011b; White et al., 2015; Wroblewski et al., 2010).

H. pylori inflammation is driven primarily by $CD4^+$ effector T-cells (Lundgren et al., 2005). Specifically, Th1 and Th17 cells drive pro-inflammatory responses through the production of IFNγ and IL-17a, respectively (Arnold et al., 2011b; Bamford et al., 1998; Eaton et al., 2001; Gray et al., 2013; Rolig et al., 2011). Conversely, Tregs suppress the amount of inflammation induced during

infection through the secretion of IL-10 (Arnold et al., 2011; Eaton et al., 2001; Gray et al., 2013; Rolig et al., 2011). During the acute stage of infection, several myeloid cell types are recruited to the gastric lamina propria and interact with *H. pylori*. These include $CD103^{+}$ $CD11b^{+}$ DCs, $CD103^{+}$ $CD11b^{-}$ DCs, $CD103^{-}$ $CD11b^{+}$ DCs, $MHCII^{-}$ Monocytes, $MHCII^{+}$ Monocytes, $MHCII^{+}$ Macrophages, Neutrophils, and Eosinophils (Arnold et al., 2018, 2017; Oertli et al., 2012; Zhang, 2020). These innate immune cell populations have been shown to interact with or phagocytose *H. pylori*, ultimately driving effector $CD4^{+}$ T-cell differentiation through the production of cytokines (Zhang, 2020).

Chemotaxis and chemoreceptors regulate the ability of *H. pylori* to colonize gastric glands (Collins et al., 2018; Howitt et al., 2011; Huang et al., 2017; Keilberg et al., 2016). During acute infection, non-chemotactic mutants have severe colonization defects of gastric glands in both the corpus and antrum. This gland colonization can be described in terms of the fraction of colonized glands, referred to as gland percent, and bacteria per colonized gland referred to as gland density. Non-chemotactic mutants exhibit significantly lower gland density and gland percent up to 1-month post-infection (Howitt et al., 2011; Keilberg et al., 2016). Chemoreceptors also regulate gland colonization as Δ*tlpD* and Δ*tlpAD H. pylori* have gland colonization defects 2-weeks post-infection. These phenotypes were ameliorated by reducing host ROS production or increasing stomach pH, respectively (Collins et al., 2018; Huang et al., 2017).

The ability of *H. pylori* to colonize gastric glands is important for several reasons. For one, gland colonization seems to underlie colonization resistance, the property of an initial infection preventing a second one. Specifically, non-chemotactic *H. pylori* do not colonize the glands and develop colonization resistance like WT does (Keilberg et al., 2016; Fung et al., 2019; Terry et al., 2005). Second, *H. pylori* in the glands can interact with $Lgr5^{+}$ stem cells, increasing the proliferation rate of these mammalian cells, leading to hyperplasia (Sigal et al., 2015). Lastly, gland populations may be associated with inflammation. Specifically, non-chemotactic mutants do not colonize glands and induce significantly less inflammation (Rolig et al., 2011; Williams et al., 2007). This inflammatory response is associated with a decreased pro-inflammatory Th17 cell response compared to WT *H. pylori* (Rolig et al., 2011). This data suggest that gland colonization may promote a pro-inflammatory Th17 response. Other data show that, in addition, the host T-cell response limits *H. pylori* gland infection, further supporting the connection (Carbo et al., 2014; Fung et al., 2019). Currently, it is unknown what role TlpA plays in gland colonization or how any phenotypes relate to host inflammation.

In this work, we aimed to better understand the role of TlpA in host colonization and regulation of inflammation by assessing gland and total colonization, as well as inflammation development over an 8-month infection course. Our work confirmed previous findings that TlpA is not required to maintain overall colonization levels in the stomach. However, TlpA regulates gland

colonization levels, specifically the ability of *H. pylori* to maintain WT level gland loads during early infection and to colonize glands to WT frequencies during late infection. TlpA was found to transiently attenuate inflammation in the corpus, associated with changes in Th17 cell density. Additionally, TlpA offset cyclical changes in inflammation during late infection. In total, this work suggests TlpA affects host inflammation specifically in the corpus by attenuating Th17 cell abundance, potentially through the regulation of gland colonization by TlpA.

3.4 Results

3.4.1 TlpA dampens inflammation during chronic infection

Δ*tlpA H. pylori* mutants induce high levels of inflammation at 6-months post-infection (Williams et al., 2007). The inflammation associated with Δ*tlpA* infection, however, was normal at 3-months post-infection, raising questions about the exact inflammation kinetics. Specifically, we wanted to know when Δ*tlpA* inflammation peaked and for how long (Williams et al., 2007). We thus carried out two independent, 8-month mouse colonization studies. Mice were infected orally with WT or Δ*tlpA* SS1 GFP^+ *H. pylori,* and time points at 0.5-, 1-, 2-, 3-, 4-, 5-, 5.5-, 6-, 6.5-, and 8-months post-infection were examined. Inflammation was assessed by histology of hematoxylin and eosin-stained tissue sections spanning the corpus to antrum. Inflammation grades were assigned by a pathologist (Dr. J. Elliot Carter), as done previously (Rolig et al., 2012; Williams et al., 2007), assessing the density and distribution of lymphocytic infiltration into the lamina propria of the

corpus and antrum separately. Inflammation grades were determined from the average of the two independent studies (Sup. Fig. 3.1).

Over the first 4-months of infection in the corpus, inflammation steadily increased in both WT and Δ*tlpA H. pylori* infections (Fig. 3.1A). During this period, there were no differences in the inflammation response between the two strains. At 5-months, however, Δ*tlpA H. pylori* induced significantly more inflammation ($p < 0.05$) in the corpus (Fig. 3.1A). This event was followed by a large decrease in Δ*tlpA H. pylori*-infection inflammation relative to WT at 5.5-months, however, this difference was not significant ($p = 0.1872$). The amount of inflammation induced by Δ*tlpA* then increased over the next month, reaching a maximum at 6.5-months post-infection, followed by another large decrease by 8-months post-infection. During this period, WT colonization also caused month-to-month fluctuations in inflammation, but to a lesser degree, and was temporally offset. For example, the first inflammation peak with the Δ*tlpA* mutant occurred at 5-months versus 5.5-months for WT.

In the antrum, there were no significant differences in inflammation induced between WT and Δ*tlpA* infection groups over the 8-month infection period (Fig. 3.1B). Both strains induced comparable levels of inflammation for the first 5-months of infection. At 5.5-months post-infection, the level of inflammation caused by the Δ*tlpA H. pylori* decreased (Inflammation grade ~1.5 to 0.5) and remained at a similar level until the following month. During this period, WT induced higher inflammation levels, which peaked at 6.5-months post-infection. While the level of

inflammation WT induced at this period is greater than Δ*tlpA H. pylori*, it was not significantly different (P = 0.1228) (Fig. 3.1B). Finally, at 8-months post-infection, both strains induced a similar level of inflammation (Fig. 3.1B).

Overall, these results confirm our previous report that Δ*tlpA H. pylori* induces significantly more inflammation during chronic infection (Williams et al., 2007). There are some variations in the timing, as this phenotype was previously observed at 6-month (Williams et al., 2007), while here we found elevated inflammation at 5-months post-infection (Fig. 3.1A). One new observation is that the loss of TlpA creates an *H. pylori* strain that induces high levels of inflammation in a temporal manner that is offset from WT. These phenotypes were most striking in the corpus, while in the antrum there were also subtle but not significant.

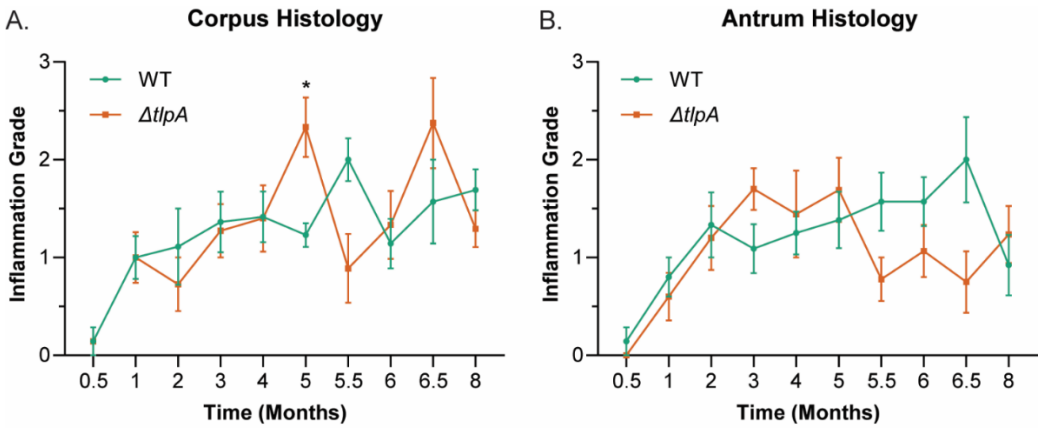

Figure 3.1- Δ*tlpA H. pylori* infections result in early inflammation peaks with offset kinetics compared to WT.
Female C57BL/6N mice (n ≥ 7 per group) were orally infected with WT SS1 GFP$^+$ or Δ*tlpA* SS1 GFP$^+$ for 0.5-, 1-, 2-, 3-, 4-, 5-, 5.5-, 6-, 6.5-, and 8-months, in two independent infections. Inflammation induced by WT SS1 GFP$^+$ or Δ*tlpA* SS1 GFP$^+$ infection groups was measured by assessing lymphocyte recruitment to the lamina propria of (A) corpus and (B) antrum via histology, as performed previously (Williams et al., 2007). Error bars represent the standard error of the mean. *,

$P<0.05$, comparisons between strains using two-way ANOVA, Šídák multiple comparison test.

3.4.2 Increased Th17 cell density is observed in Δ*tlpA H. pylori* infected during late infection

To better understand the nature of the corpus immune responses observed in Δ*tlpA H. pylori* infected mice, we assessed innate immune and effector T-cell populations by flow cytometry. Innate immune cell populations examined include, $CD103^+$ $CD11b^+$ DCs, $CD103^+$ $CD11b^-$ DCs, $CD103^-$ $CD11b^+$ DCs, $MHCII^-$ Monocytes, $MHCII^+$ Monocytes, $MHCII^+$ Macrophages, Neutrophils, and Eosinophils (Arnold et al., 2018, 2017; Oertli et al., 2012) (Sup. Fig. 3.2A). Over the period assessed, there were elevated levels of all innate immune populations relative to uninfected animals (Sup. Fig. 3.3). However, there were few differences in recruitment between WT and Δ*tlpA H. pylori* infection groups (Fig. 3.2). For example, at 6- and 8-months post-infection, there was a decrease in the frequency of eosinophils among all $CD45^+$ cells in WT-infected mice. This resulted in Δ*tlpA H. pylori* infected mice having a significantly higher frequency of eosinophils (Fig. 3.2A). There were no other significant differences in the recruitment of innate immune cell populations between infection groups.

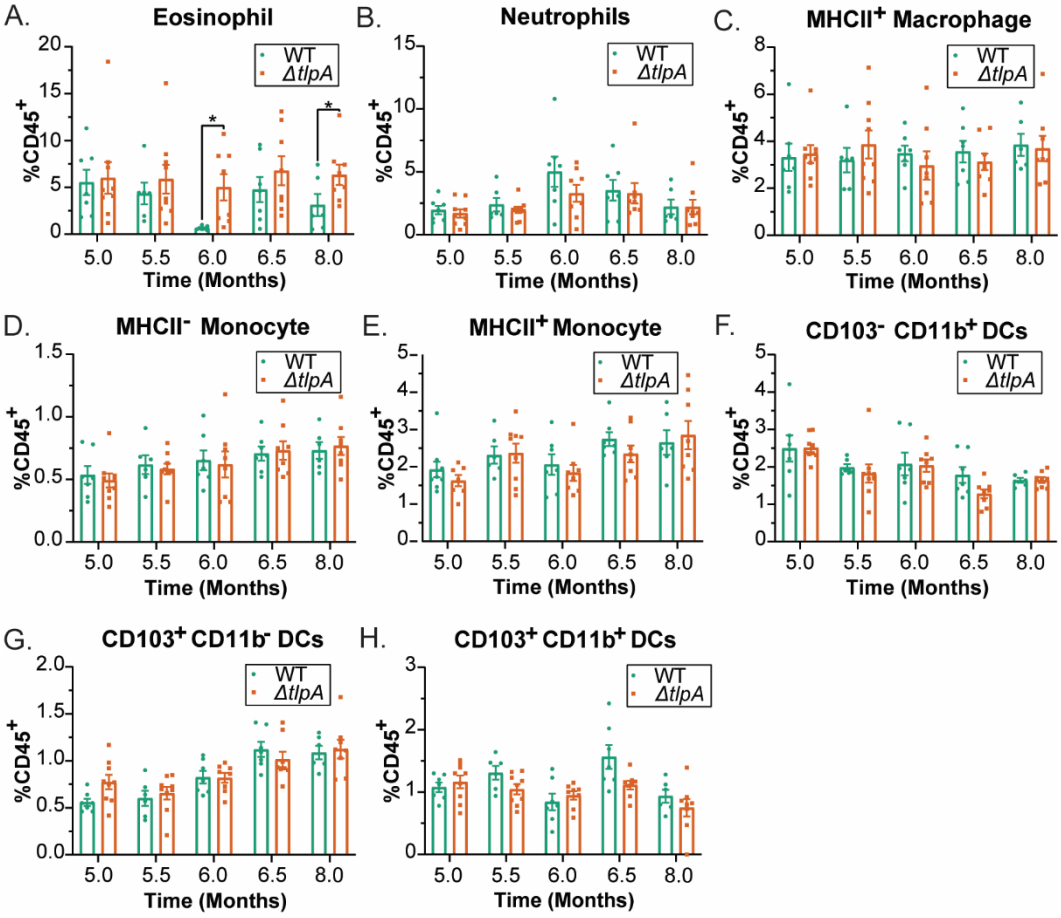

Figure 3.2- Innate immune cells recruitment during chronic infection is similar between WT SS1 and Δ*tlpA H. pylori* infected mice
Mice infected with WT SS1 GFP$^+$ or Δ*tlpA* SS1 GFP$^+$ were used to isolate corpus lamina propria leukocytes after 5-, 5.5-, 6-, 6.5-, and 8-months post-infection from the same mice as shown in Sup. Fig. 1A (n = 7- 9 per group). Analysis including uninfected mice is included in Sup. Fig. 3.2. A) neutrophils, B) eosinophils, C) MCHII$^+$ macrophages, D) MCHII$^-$ monocytes, E) MHCII$^+$ monocytes, F) CD103$^-$ CD11b$^+$ DCs, G) CD103$^+$ CD11b$^-$ DCs, and H) CD103$^+$ CD11b$^+$ DCs were analyzed by flow cytometry. Data are presented as the frequency of each cell type as the percent of all live CD45$^+$ lymphocytes. Error bars represent the standard error of the mean. *, P<0.05, comparisons between strains using two-way ANOVA, Šídák multiple comparison test.

To further compare the inflammatory response between WT and Δ*tlpA* mutants, we next focused on CD4$^+$ effector T-cell populations that are important for the development of inflammation (Lundgren et al., 2005). It has been well

established that Th1 and Th17 cells drive pro-inflammatory responses through the production of IFNγ and IL-17a, respectively (Arnold et al., 2011b; Bamford et al., 1998; Eaton et al., 2001; Gray et al., 2013; Rolig et al., 2011). Conversely, Tregs suppress the amount of inflammation induced during infection through the secretion of IL-10 (Eaton et al., 2001; Arnold et al., 2011b; Rolig et al., 2011; Gray et al., 2013). Accordingly, we assessed the recruitment of all $CD4^+$ effector T-cells ($CD4^+$ $TCR\beta^+$), Th1 ($Tbet^+$), Th17 ($Ror\gamma T^+$), and Tregs ($FoxP3^+$) (Sup. Fig. 3.2B). In both WT and Δ*tlpA H. pylori* infected mice, Th1 and Treg recruitment were equivalent throughout the period observed (Fig. 3.3A and C). However, at 5- and 8-months post-infection in Δ*tlpA H. pylori* infected mice, there was a significantly higher frequency of Th17 cells among all $CD45^+$ lymphocytes recruited to the corpus (Fig. 3.3B). At 5.5- and 6- months post-infection, Th17 cell recruitment in Δ*tlpA H. pylori* infected mice was also higher, but not significantly (Fig. 3.3B). While there were significant differences in the frequency of Th17 cells among all $CD45^+$ lymphocytes recruited, there were no differences in the absolute cell count of any effector T-cell subtype or total $CD45^+$ lymphocytes observed (Sup. Fig. 3.4A- F). This finding suggests that the frequency of each cell type among all lymphocytes recruited during infection may dictate the amount of histologically evident inflammation that is observed instead of gross numbers of a given cell type. Further analysis measuring cytokine expression from these T-cell subtypes needs to be performed to explore these connections further.

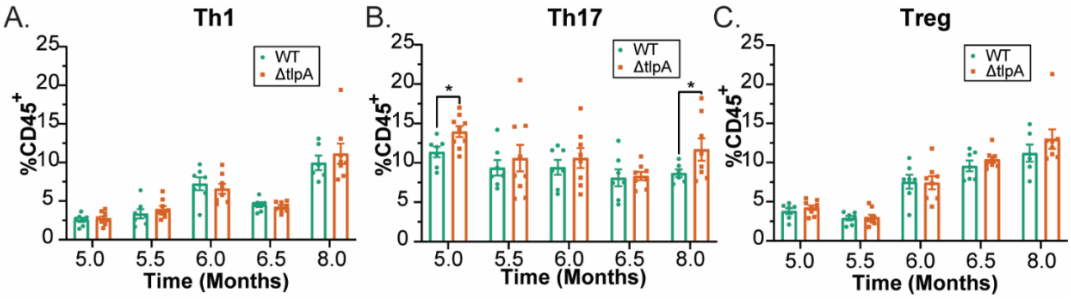

Figure 3.3- Inflammatory changes in Δ*tlpA H. pylori* infected mice are associated with an increase in the Th17 population recruited to the corpus lamina propria.
Mice infected with WT SS1 GFP$^+$ or Δ*tlpA* SS1 GFP$^+$, and lymphocytes from the corpus lamina propria were isolated at 5-, 5.5-, 6-, 6.5-, and 8-months post-infection from the same mice from Fig. 2 (n = 7- 9 per group). Analysis including uninfected mice is included in Sup. Fig. 3.3. A) Th1 (Tbet$^+$ TCRβ$^+$ CD4$^+$), B) Th17 (RorγT$^+$ TCRβ$^+$ CD4$^+$), and C) Tregs (FoxP3$^+$ TCRβ$^+$ CD4$^+$) were analyzed by flow cytometry. Data are presented as the frequency of each cell type as the percent of all live CD45$^+$ lymphocytes. Error bars represent the standard error of the mean. *, P<0.05, comparisons between strains using two-way ANOVA, Šídák multiple comparison test.

3.4.3 Gland colonization patterns of *H. pylori* are dynamic throughout a long-term infection

Having observed that TlpA influences inflammatory cell abundance in the corpus, we next assessed the colonization patterns of WT and Δ*tlpA H. pylori* in fine detail. Previous work has assessed overall tissue colonization in both strains (Andermann et al., 2002; Rolig et al., 2012; Williams et al., 2007), but there have been no detailed longitudinal studies combining inflammation development and gastric localization. Accordingly, we assessed the colonization patterns of WT and Δ*tlpA* SS1 GFP$^+$ *H. pylori* from the same samples above (Fig. 3.1) at 0.5-, 1-, 2-, 3-, 4-, 5-, 5.5-, 6-, 6.5-, and 8-months post-infection. At each time point, we enumerated corpus and antrum total colony forming units (CFU) from bulk tissue,

the average number of bacteria per gland (gland colonization), the average number of bacteria per occupied gland (gland density), and the percentage of glands occupied (gland percent) (Fig. 3.4). Of note, gland colonization is the composite of both gland density and gland percent, thus providing an overall picture of gland colonization dynamics. The latter two metrics give a contextual understanding of the overall gland colonization patterns.

WT *H. pylori* displayed a pattern in which there were significantly more total bacteria in the antrum compared to the corpus (~10 fold) until 1-month post-infection (Fig. 3.4A), as observed in previous work (Keilberg et al., 2016; Martinez et al., 2018). These differences between the corpus and antrum disappeared by 2-months post-infection. For the remainder of the time course, there were no significant differences in the total number of bacteria between these regions. While the colonization differences between regions were not significant, the antrum-located *H. pylori* displayed large population expansions and contractions from month-to-month. For instance, there was a ~60-fold increase and decrease in the antrum population from 5.5- 6.5-months post-infection, and by 8-months post-infection, there was ~20-fold less WT *H. pylori* overall in the antrum (Fig. 3.4A).

Over this time course, WT displayed obvious differences in gland colonization dynamics between the corpus and antrum. Initially, average gland colonization was equal in the two regions (Fig. 3.4B), but significantly more corpus glands were colonized (Fig. 3.4D). Antral gland colonization rapidly expanded (Fig 3.4B), with a significant increase in gland density and gland percent occupancy (Fig

3.4C-D), followed by an equally abrupt decline by 2-months post-infection (Fig. 3.4B). This decline was caused by a significant decline in gland density, although gland percent occupancy remained high (Fig. 3.4C-D). At 4-months post-infection in the antrum, there was another significant increase in gland colonization (Fig. 3.4B), caused by a significant increase in gland density within the antrum (Fig. 3.4C) and not due to an increase in gland percent occupancy (Fig. 3.4D). This expansion in the antral gland population at 4-months post-infection was transient, and by 5-months post-infection, this population declined to levels comparable to the corpus (Fig. 3.4B-C). From 3- to 8-months post-infection, there was generally a significantly higher gland percent occupancy in the corpus than in the antrum (Fig. 3.4D). Δ*tlpA H. pylori* also follow similar overall colonization trends between regions. However, Δ*tlpA H. pylori* always has higher corpus gland occupancy (Fig. 3.4E-H).

Altogether, WT *H. pylori* favors antral colonization early in infection, partially due to higher gland colonization in this region. After 2-months, overall differences between regions subside, and there is a general switch to favoring corpus gland colonization for the remainder of the time course.

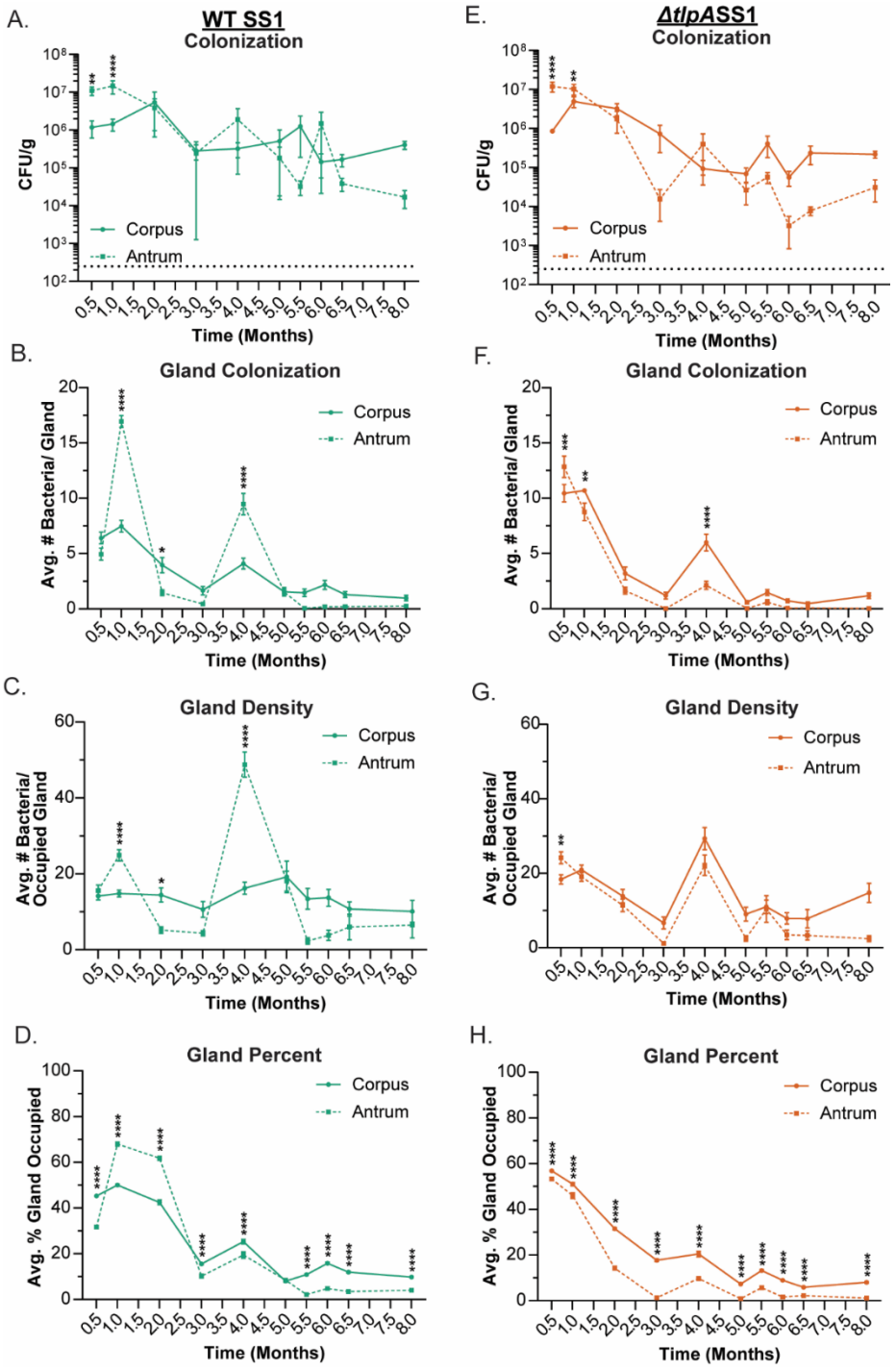

Figure 3.4- WT SS1 and Δ*tlpA H. pylori* SS1 have unique colonization patterns in the murine stomach

Colonization dynamics of WT SS1 and Δ*tlpA* SS1 within the mouse stomach were analyzed over a time course from the acute to chronic stage of infection from the

same mice from Sup. Fig. 1A-B. Female C57BL/6N mice ($n \geq 4$) were orally infected with WT SS1 GFP$^+$ or Δ*tlpA* SS1 GFP$^+$ for 0.5-, 1-, 2-, 3-, 4-, 5-, 5.5-, 6-, 6.5-, and 8-months. Total colonization levels of (A) WT and (E) Δ*tlpA* in the corpus and antrum region of the stomach was determined by homogenizing tissue and plating for colony forming units (CFU). For each strain, gland colonization phenotypes were quantified and compared between the corpus and antrum. Individual glands were isolated and GFP$^+$ bacteria were visualized using the Bacterial Localization in Isolated Glands (BLIG) method (Keilberg et al., 2016). For each mouse, 100 isolated glands from the corpus and 100 from the antrum were analyzed. (B and F) Gland colonization is the average number of WT SS1 GFP$^+$ or Δ*tlpA* SS1 GFP$^+$ per all glands analyzed in either region. (C and G) Gland density is the average number of WT SS1 GFP$^+$ or Δ*tlpA* SS1 GFP$^+$ per occupied gland. (D and H) Gland percent is the average percent of glands that are occupied by either WT SS1 GFP$^+$ or Δ*tlpA* SS1 GFP$^+$ at each time point. For all graphs, error bars represent the standard error of the mean. *, $P < 0.05$; **, $P < 0.01$; ***, $P < 0.001$; ****, $P < 0.0001$, comparisons between corpus and antrum using two-way ANOVA, Šídák multiple comparison test.

3.4.4 Sensing through TlpA alters *H. pylori* gland localization

We next compared the colonization patterns between WT and Δ*tlpA H. pylori* to better understand the colonization differences between strains (Fig. 3.5 and Sup. Fig. 3.5). At 1-month post-infection, there were significantly more ($P < 0.05$) Δ*tlpA H. pylori* CFU in the corpus compared to WT (Fig. 3.5A). At all other time points, there were no significant differences in colonization CFU between the strains in either the corpus or antrum (Fig. 3.5A and D, Sup. Fig. 3.5). These results are consistent with previous reports (Williams et al., 2007).

In corpus glands, Δ*tlpA H. pylori* showed early elevated numbers, e.g., from 0.5- 1-month post-infection (Fig. 3.5B). This increase was associated with significantly higher corpus gland percent occupancy at some time points, but at others, it was defined by higher gland density (Fig. 3.5C and D). From 2- 8-months post-infection, there were few differences in gland colonization between the strains

in either the corpus or antrum (Fig. 3.5B and F). For both strains, gland colonization steadily decreased from the peak at 1-month post-infection until 3-months post-infection in both regions (Fig. 3.5B and F). Of note, at 4-months post-infection, there was a significant increase in both WT and Δ*tlpA H. pylori* gland colonization (Fig. 3.5B and F). However, this WT gland density increase was antrum-specific, and Δ*tlpA H. pylori* increase was corpus-specific (Fig. 3.5C and G). These increases seemed fairly restricted to the individual gland level, meaning that the number of bacteria per gland increased but not the percent glands occupied. This outcome was especially apparent for the *tlpA* mutant, which did not substantially increase the percent glands occupied, while WT *H. pylori* did (Fig. 3.5D).

During the 2–8-month period, there were more limited differences in gland colonization. Δ*tlpA H. pylori,* however, consistently colonized fewer glands in both regions (Fig. 3.5D and H). At 2-, 4-, 6-, and 6.5-months post-infection in the corpus, and at 1-, 2-, 3-, 4-, 5-, 6-, and 8-months post-infection in the antrum, Δ*tlpA H. pylori* had significantly lower gland percent occupancy (Fig. 3.5D and H). One exception to this was at 5.5-months post-infection in the antrum when Δ*tlpA H. pylori* had significantly higher gland percent occupancy (Fig. 3.5H), which was associated with a non-significant increase in gland density (Fig. 3.5G).

Overall, these results demonstrate that Δ*tlpA H. pylori* have higher corpus gland colonization during the first month of infection. After this point, Δ*tlpA H. pylori* colonizes fewer glands throughout the time course (Fig. 3.5 and Sup. Fig. 3.5). Additionally, an intriguing expansion in gland colonization occurs at 4-

months post-infection for both strains in a region-specific manner, a phenotype that has not been previously reported.

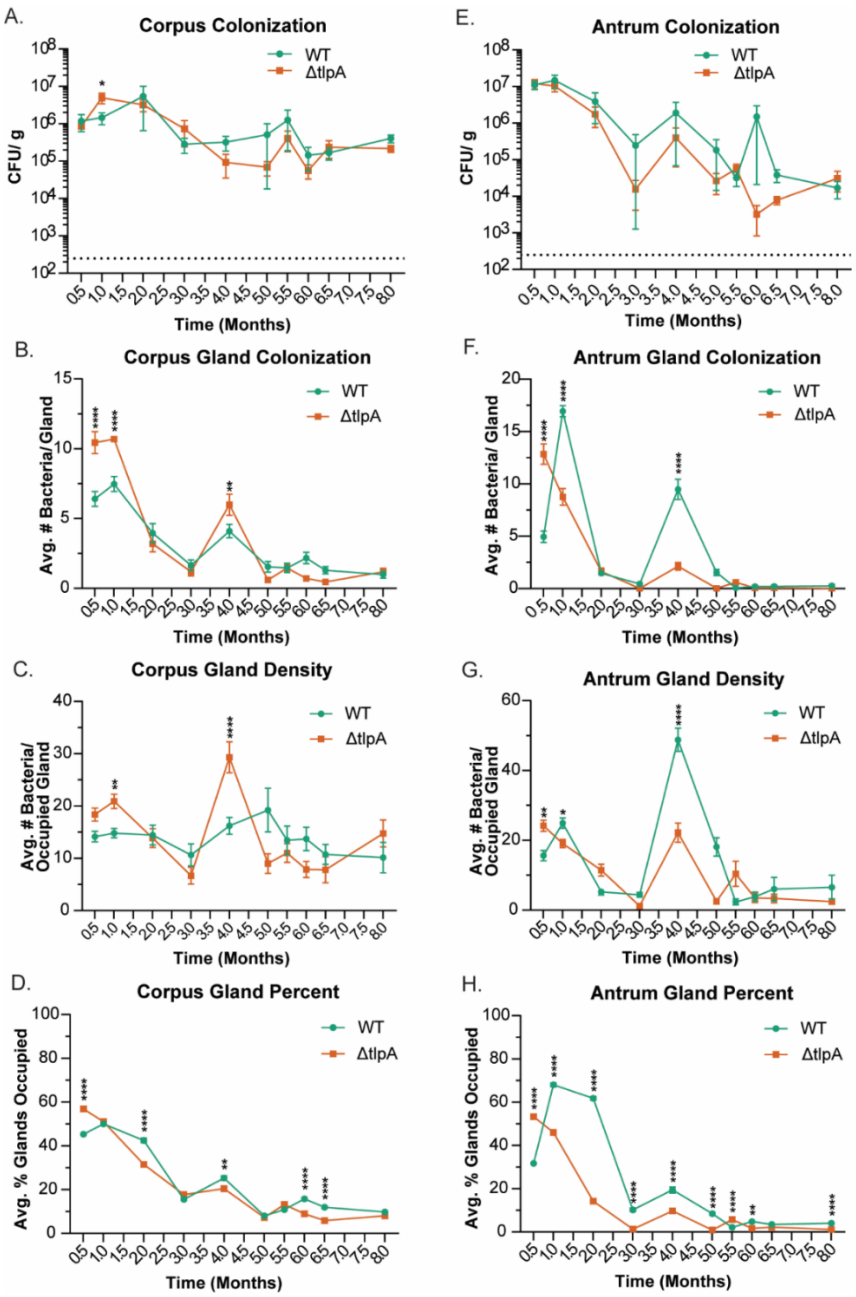

Figure 3.5- Δ*tlpA H. pylori* occupy more glands, with greater density during early infection, and colonize glands with lower frequency during late infection. Overall colonization and gland colonization phenotypes were quantified and compared between WT SS1 GFP$^+$ or Δ*tlpA* SS1 GFP$^+$ from the infection groups

from the same mice as in Fig. 4. Colonization of WT SS1 and Δ*tlpA* in the corpus was assessed for (A) total colonization, (B) gland colonization, (C) gland density, and (D) gland percent. Colonization of WT SS1 and Δ*tlpA* in the antrum was assessed for (E) total colonization, (F) gland colonization, (G) gland density, and (H) gland percent. For all graphs, error bars represent the standard error of the mean. *, P<0.05; **, P<0.01; ***, P<0.001; ****, P<0.0001, comparisons between strains using two-way ANOVA, Šídák multiple comparison test.

3.4.5 Non-chemotactic *H. pylori* induction of inflammation is associated with gland colonization phenotypes

Our results above suggest that *tlpA* mutants display elevated gland colonization compared to WT specifically in the corpus, a region that also shows a heightened inflammatory response to these mutants. This finding raised the idea that gland populations may play a role in dictating the inflammatory response. To further explore this idea, we examined a mutant with a known inability to colonize the glands in early infection, the non-chemotactic Δ*cheY H. pylori*. This mutant furthermore elicits low inflammation (Rolig et al., 2011; Williams et al., 2007). Therefore, a more detailed time course than done previously with Δ*cheY* GFP^+ *H. pylori* infected was carried out. As reported before, we documented that *cheY* mutants caused less inflammation than WT in both the corpus (Fig. 3.6A) and antrum during late infection (Sup. Fig. 3.6A). Like WT and Δ*tlpA*, Δ*cheY* induces increasing amounts of inflammation from 2- to 4-months post-infection in the corpus (Fig. 3.6A) while in the antrum, Δ*cheY H. pylori* induces similar levels of inflammation relative to WT and Δ*tlpA (*Sup. Fig. 3.6A). However, by 5-months post-infection, Δ*cheY* causes less inflammation in both regions (Fig. 3.6A and Sup. Fig. 3.6A).

Over the infection time course, there were no significant differences in total colonization levels between WT, Δ*tlpA*, and Δ*cheY* in either the corpus or antrum (Fig. 3.6B and Sup. Fig. 3.6B). However, when looking at the populations of these strains within glands, differences appear. At 2-months post-infection in the corpus and antrum, there is significantly lower gland colonization by Δ*cheY* relative to WT SS1 (Fig. 3.6C and Sup. Fig. 3.6C), due to a significantly lower gland percent occupancy by Δ*cheY* (Fig. 3.6E and Sup. Fig. 3.6E). This result suggests that previously seen early gland deficits continue to 2-months post-infection. Somewhat surprisingly, at 3-months post-infection in the corpus and antrum, there is a significant increase in gland colonization by Δ*cheY* relative to WT and Δ*tlpA*, due to a significant increase in gland density by Δ*cheY* (Fig. 3.6C-D and Sup. Fig. 3.6C-D). This expansion of Δ*cheY* in corpus glands continues at 4-months post-infection, as the gland density increases relative to the previous month and is significantly higher than WT and Δ*tlpA* (Fig. 3.6C-D). This modest expansion correlates with high inflammation at 4-months as well. In total, Δ*cheY H. pylori* accumulates to a high gland density and cause increased levels of inflammation, from 2- to 4-month post-infection.

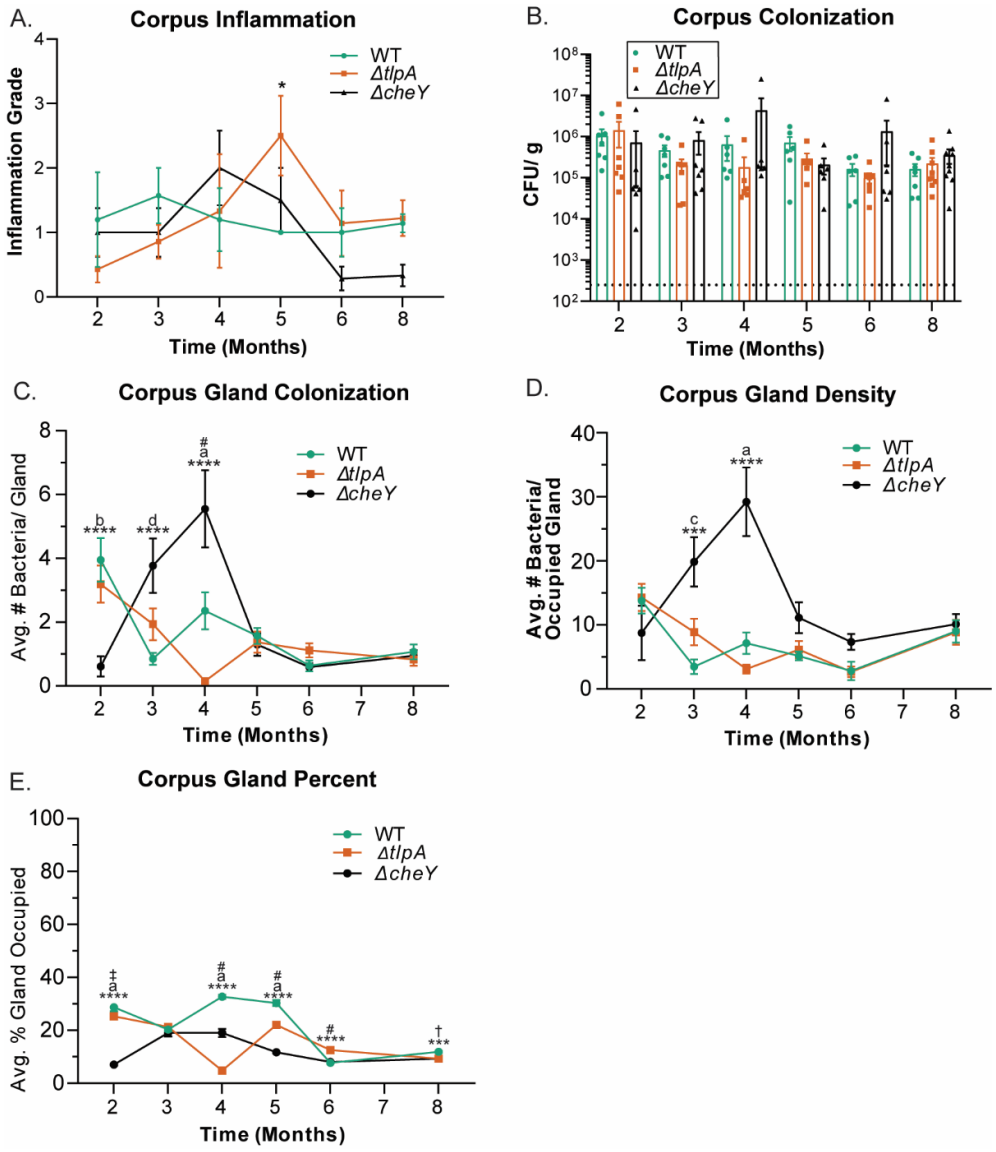

Figure 3.6- Non-chemotactic *H. pylori* induce inflammation transiently during infection, associated with increase gland density.

Colonization dynamics of WT SS1, Δ*tlpA*, and Δ*cheY* SS1 within the corpus were analyzed during the chronic stage of infection. Female C57BL/6N mice (n ≥ 3) were orally infected with WT SS1 GFP$^+$, Δ*tlpA*, Δ*cheY* SS1 GFP$^+$ for 2-, 3-, 4-, 5-, 6-, and 8-months. Data are from the same animals as in Sup. Fig. 5. (A) Inflammation by histology, (B) total colonization, (B) gland colonization, (C) gland density, and (D) gland percent were assessed. For all graphs, error bars represent the standard error of the mean. Comparisons between strains were made using two-way ANOVA, Tukey multiple comparison test. WT vs. Δ*tlpA*: a, P<0.0001; b, P<0.001; c, P<0.01; d, P<0.05. WT vs. Δ*cheY*: ****, P<0.0001; ***, P<0.001; **, P<0.01; *, P<0.05. Δ*tlpA* vs.Δ*cheY*: #, P<0.0001; †, P<0.001; ‡, P<0.01; ¥, P<0.05.

3.5 Discussion

In this work, we sought to understand how *H. pylori* influences inflammation during infection through its chemotaxis system, focusing on the chemoreceptor TlpA. Our results suggest that Δ*tlpA H. pylori* have altered late-infection inflammation kinetics that results in their inflammation being higher than WT at some time points and lower at others. This phenotype manifests in transient spikes in corpus inflammation during the late stage of infection, which is associated with an increased frequency of Th17 cells. Chemotaxis regulates the localization of *H. pylori* in the gastric mucosa. Accordingly, to better understand how inflammation may be regulated by chemotaxis, we analyzed the colonization patterns of WT and Δ*tlpA H. pylori*. During the late stage of infection, both strains have similar total colonization levels and gland colonization characteristics. However, during the early stage of infection, up to 1-month post-infection, Δ*tlpA H. pylori* colonizes more corpus glands, accumulating to higher numbers per gland than WT *H. pylori*. Early gland colonization phenotypes may dictate later inflammatory outcomes. Previous work has demonstrated that non-chemotactic *H. pylori* have severe gland colonization defects during early infection and induce less inflammation during the late stage of infection. These data suggest a possible role of early gland colonization influencing inflammation throughout infection.

3.5.1 Region-specific inflammation control

H. pylori colonizes the two major anatomical regions of the murine stomach called the corpus and antrum. The corpus is comprised of zymogenic glands, which

secrete acid, pepsinogen, hormones, and mucins, while the antrum is comprised of mucous glands, which secrete mucus and hormones (Yang and Ottemann, 2019). Due in part to the different cell types in each region, each has distinct metabolomes, creating unique microenvironment niches within the stomach (Yang and Ottemann, 2019; Keilberg et al., 2020). Likely because of these factors, *H. pylori* has distinct colonization patterns within the mucus and gastric glands of each region (Keilberg et al., 2016). Previous work demonstrated that TlpA plays a role in dampening host inflammation late during infection at 6-months post-infection (Williams et al., 2007). To expand on these studies, we wanted to assess if inflammatory outcomes of infection were widespread or region-specific.

In our experiments, we found there was no difference in inflammation between WT and Δ*tlpA H. pylori* for the first 4.5-months of infection. After this time period, the pattern changed. For example, at 5-months post-infection in the corpus, Δ*tlpA H. pylori* induced significantly elevated inflammation, a response that was reproducible and similar to that observed in the prior publication (Williams et al., 2007). This heightened inflammatory response was transient, with the inflammation decreasing rapidly by 5.5-months, and then fluctuating for the remainder of the time course. Of note, inflammation in both WT and Δ*tlpA H. pylori* infections fluctuated, but the loss of *tlpA* resulted in an offset and heightened pattern of inflammation compared to WT (Fig. 1A). Intriguing to note, TlpA appears to be under selective pressure, accumulating a high frequency of mutations in the dCache sensing domain of *tlpA* (Collins et al., 2016; Ailloud et al., 2019). While it is not

yet known how these mutations affect TlpA sensing and signaling, it is interesting that *tlpA* is one of the more highly affected loci and may be subject to mutations that change its properties and possible inflammatory-control abilities.

In this study, our latest time point was at 8-months post-infection. However, like in the human stomach, *H. pylori* can establish chronic colonization, lasting for over a year in a murine model. Colonization studies up to 15-month- post-infection with *H. pylori* SS1 have been performed, showing that mice colonized for 15-months had higher inflammation than at 6-month post-infection (Thompson et al., 2004). Given this outcome, it may be interesting to see how inflammation evolves over a more extended period. Of note, the *H. pylori* strain used, SS1, does not have a functional Cag PAI T4SS, inducing less inflammation, with lower pathology, compared to its parent strain, PMSS1 (Arnold et al., 2011b). It would also be informative to see how these inflammatory kinetics translate to another strain of *H. pylori*. The current colonization window we are examining suggests that TlpA is important for causing consistent levels of inflammation in the stomach. Following this inflammatory event at 5-months post-infection, we observed ~7- and ~17-fold colonization decreases in the corpus and antrum, respectively. It has been well established in the literature that inflammation severity and colonization levels are inversely related (Algood and Cover, 2006; Arnold et al., 2011b; Chen et al., 2001). Therefore, it is presumably advantageous for *H. pylori* to limit the amount of inflammation it induces during infection.

We characterized the Δ*tlpA*-mutant immune response using flow cytometry. We observed Δ*tlpA H. pylori* infected mice had increased Th17 cell density (Fig. 3.3B), but not any other cell type, during the period of increased inflammation at 5-months post-infection (Fig. 3.2 and Fig. 3.3A+C). Th17 cells play a major role in inflammation development during *H. pylori* colonization, primarily through the production of pro-inflammatory cytokines (Dixon et al., 2019; Serrano et al., 2013; Shiomi et al., 2008). Some of the primary cytokines include: 1) IL-17A, which promotes neutrophil recruitments through IL-8 and promotes the expression of antimicrobial peptides from epithelial cells; 2) IL-17F, which upregulates the expression of other pro-inflammatory cytokines and chemokines, inducing IL-2, TGF-β, IL-6, and GM-CSF; 3) IL-21, which promotes the proliferation of Th1 and Th17 cells, creating a positive feedback loop, and promote the proliferation of B-cells; and 4) IL-22, which acts on non-hematopoietic cells by upregulating antimicrobial peptide expression and promoting tissue repair (Dixon et al., 2019). Further work needs to be performed to determine if differences in cytokine expression are observed in Δ*tlpA H. pylori* infected mice. Interestingly, recent work has shown that arginine, a TlpA chemoattractant (Johnson et al., 2021), and the polyamine pathway are critical for maintaining Th17 pathogenicity (Wagner et al., 2021). TlpA may attenuate host inflammation by mediating a chemoattractant response towards arginine, allowing *H. pylori* to readily use it and thus limiting its availability to the host. In turn, this usage could reduce arginine uptake by Th17

cells, resulting in decreased cytokine production and pathogenicity (Wagner et al., 2021).

We also observed significantly higher eosinophil recruitment compared to WT at multiple time points in Δ*tlpA H. pylori* infected animals (Fig. 3.2A). Recently, eosinophils have been shown to play a major role during *H. pylori* colonization, as eosinophils interact with *H. pylori* in the gastric mucosa, regulating Th1 cell proliferation (Arnold et al., 2018). Th1 cells are a significant contributor to the development of pathologies that are observed during *H. pylori* colonization through the production of IFNγ (Gray et al., 2013). However, changes in eosinophil populations do not correlate with any change in Th1 recruitment during the period of observation at the 5- 8-month post-infection window (Fig. 3.2A and Fig. 3.3). Therefore, it appears that changes in the Th17 cell population may underlie the attenuation of inflammation by TlpA.

3.5.2 *H. pylori* localization throughout colonization is dynamic and regulated by chemoreceptors

Over the past decade, it has become appreciated that colonization of gastric glands by *H. pylori* is regulated by chemotaxis (Howitt et al., 2011). Non-chemotactic mutants, including Δ*cheY* and Δ*chepep*, have been shown to have severe defects in gland colonization compared to WT *H. pylori* during the first month of infection (Howitt et al., 2011; Sigal et al., 2015; Keilberg et al., 2016; Collins et al., 2018; Fung et al., 2019). A functional aspect of gland colonization is that it appears to promote colonization resistance to secondary infection, even by

matched isogenic strains (Keilberg et al., 2016; Fung et al., 2019). This may explain why non-chemotactic *H. pylori* are outcompeted by an isogenic WT strain, as they are unable to colonize gastric glands (Terry et al., 2005). In addition to general chemotaxis, specific chemoreceptors also play an essential role in regulating gland colonization.

Each chemoreceptor expressed by *H. pylori* is responsible for sensing multiple ligands and signals (Johnson and Ottemann, 2018). Accordingly, progress has been made to understand how chemoreceptors regulate the localization of *H. pylori* in the stomach. Studies with the chemoreceptor TlpD are illustrative of the roles that individual chemoreceptors can play. Δ*tlpD H. pylori* have overall colonization defects in the stomach (Rolig et al., 2012), associated with decreased gland percent but increased gland density. This colonization phenotype is ameliorated in mice defective in reactive oxygen species (ROS) production, demonstrating the importance of TlpD in sensing and initiating a chemorepellent response to ROS during infection (Collins et al., 2018). In addition to ROS, TlpD has been shown to sense pH synergistically with TlpA. Δ*tlpAD H. pylori* have a more severe overall colonization defect at 2-weeks post-infection than Δ*tlpD H. pylori* and are defective in gland colonization. These defects were improved via omeprazole treatment, a proton-pump inhibitor that increases the pH of the stomach (Huang et al., 2017). In total, this work demonstrates the importance chemoreceptors can play during colonization. The inability to sense specific signals

in the gastric environment leads to altered localization, leaving *H. pylori* susceptible to non-optimal or even toxic host conditions and immune responses.

Our studies examined the colonization patterns of both WT and Δ*tlpA H. pylori* throughout a long-term infection. We found that WT and Δ*tlpA H. pylori* have similar overall colonization trends when assessing each strain individually, comparing differences in colonization between the corpus and antrum. Both strains favor the antrum during the first month of colonization (Fig. 3.4A and E). After this point, there are no statistical differences in overall colonization between regions of the stomach when analyzing each strain independently. Δ*tlpA H. pylori* favors corpus glands throughout the infection time course, except at 0.5-months post-infection (Fig. 3.4F-G). WT, however, tends to favor antral glands 1-2-months post-infection, with either higher gland percent or density (Fig. 3.4B-D). Thus, it seems that loss of *tlpA* results in strains that are unable to thrive in the antrum, suggesting TlpA's signals are present in the antral glands or mucus layer during this period.

One striking gland colonization trend occurs at 4-months post-infection. WT *H. pylori* experience a significant increase in the antral gland population, associated with increased gland density (Fig. 3.4B-C). Δ*tlpA H. pylori* also experiences a significant increase in the gland population, but conversely, this occurs in the corpus and is significantly higher than WT (Fig. 3.4F-H and Fig. 3.5B-C). This population change suggests the gastric environment is changing at this time. While there are no differences in inflammation induced between infection groups at this time point, these population shifts occur directly before the Δ*tlpA H.*

pylori spike in inflammation at 5-months post-infection (Fig. 3.1A). The accumulation of Δ*tlpA H. pylori* within corpus glands at 4-month post-infection suggests there may be a TlpA signal present that usually directs the bacteria to exit corpus glands. There is a significant increase in WT corpus gland percent at this same time point (Fig. 3.5D), providing some support for this idea. While it may be possible for a TlpA chemoattractant, such as arginine, fumarate, or cystine, to be present outside of the glands at this time point, previous work has shown that increased gland density occurs when unable to sense a chemorepellent signal (Huang et al., 2017; Collins et al., 2018). TlpA has been shown to play a role in acid-sensing, but this function occurs primarily in cooperation with TlpD (Huang et al., 2017). Therefore, this phenotype is unlikely to be caused by an inability to sense acid, suggesting TlpA might sense additional repellents. Of note, the Δ*tlpA H. pylori* population within the corpus glands declined by 5-month post-infection (Fig. 3.4F-G and Fig. 3.5B-C). The increased Th17 response at this time point is subtle but significant. This elevated Th17 response may underlie the gland population decrease, as gland colonization is regulated by host immune responses (Carbo et al., 2014; Collins et al., 2018; Fung et al., 2019).

3.5.3 Potential link between gland colonization patterns and inflammation development

It has been demonstrated that non-chemotactic *H. pylori* mutants induce low inflammation levels at 2-month post-infection, which is characterized by a decreased Th17 response (Rolig et al., 2011). Additionally, non-chemotactic *H.*

pylori mutants have severe colonization defects during the acute stage of infection until 1-month post-infection (Keilberg et al., 2016). Our results show that Δ*tlpA H. pylori* have high gland colonization in the corpus until 1-month post-infection, characterized by increased gland density and gland percent relative to WT (Fig. 3.5B-D). A potential mechanism by which chemotaxis affects inflammatory outcomes is through controlling colonization of gastric glands during the acute stage of infection. During this period, various myeloid cell types in the stomach interact with *H. pylori*. This is critical for developing the effector T-cell response, characterized by the recruitment and proliferation of the pro-inflammatory, Th1 and Th17 cells, and the anti-inflammatory Tregs during infection (Zhang, 2020). It is plausible that situations that result in high numbers of bacteria per gland increases the chance for total or specific myeloid cells to interact with *H. pylori.* High or distinct myeloid sampling might, in turn, result in differences in T-cell priming and subsequent T-cell populations. On the other hand, non-chemotactic mutants have low gland density and occupancy compared to WT (Keilberg et al., 2016). As a result, there may be decreased T-cell priming during the early stage of infection, potentially explaining why non-chemotactic *H. pylori* induce a dampened Th17 response during infection (Rolig et al., 2011). These ideas, however, need to be explored in future experiments.

During our colonization studies, we also included Δ*cheY H. pylori*, a non-chemotactic mutant. Interestingly, despite previous reports showing that Δ*cheY H. pylori* induces less inflammation at either 2-, 3- or 6- months post-infection (Rolig

et al., 2011; Williams et al., 2007), we observed that Δ*cheY H. pylori* induces higher but not significant levels of inflammation at 4-months post-infection (Fig. 3.6A). This increase in inflammation is associated with increased gland density by Δ*cheY H. pylori* relative to WT at this same time point (Fig. 3.6C-D). Because non-chemotactic *H. pylori* cannot migrate in response to chemical gradients, they are likely trapped within gastric glands unless they can escape in a stochastic manner. This could explain why the gland density of Δ*cheY H. pylori* increases from 2- to 4-months post-infection (Fig. 3.6D). Thus, controlling gland density during infection via chemotaxis may be a mechanism by which *H. pylori* modulates inflammation.

3.6 Conclusion

This work is significant because it provides the first in-depth analysis of inflammation and colonization patterns of *H. pylori* throughout a late stage of infection. Additionally, we provide greater clarity as to the nature of inflammation control by *H. pylori* during infection and the role of chemotaxis, and the individual chemoreceptor TlpA, in this process. These findings lay the groundwork for future studies that explore these ideas.

3.7 Methods

3.7.1 Bacterial strains and culture conditions

H. pylori strains used in this study were all derived from the *H. pylori* strain SS1. They include WT, WT GFP$^+$, Δ*tlpA* GFP$^+$ (This study), Δ*cheY::cat* GFP$^+$, and

Δ*tlpA::kan-sac* (Lee et al., 1997; Keilberg et al., 2016; Rader et al., 2011). Bacteria were grown at 37°C under microaerobic conditions of 5% O_2, 10% CO_2, and 85% N_2 on solid media containing Columbia Blood Agar Base (BD), containing 5% defibrinated horse blood (Hemostat Laboratories, Dixon, CA), 50 µg/ml cycloheximide (VWR), 10 µg/ml vancomycin, 5 µg/ml cefsulodin, 2.5 U/ml polymyxin B (all from Gold Biotechnology), and 0.2% (wt/vol) beta-cyclodextrin (Spectrum Labs, Gardena, CA) (CHBA) or in Brucella broth (BD BBL/Fisher) with 10% heat-inactivated fetal bovine serum (FBS) (Life Technologies) (BB10), with shaking. Chloramphenicol-resistant mutants were selected using 10 µg/ml chloramphenicol (Gold Biotechnology) on CHBA, as previously described (Andermann et al., 2002).

The Δ*tlpA* SS1 clean deletion mutant was made by natural transformation of Δ*tlpA::kan-sac H. pylori* SS1 with pTA10, which contains a *tlpA* deletion flanked by 500 bp of the up- and down-stream regions of *tlpA* (Rader et al., 2011). Sucrose resistant colonies were selected on CHBA containing 75 µg/ml sucrose (Fisher Chemical), followed by screening for kanamycin sensitivity on CHBA with 15 µg/ml kanamycin (Gold Biotechnology). The Δ*tlpA* deletion was confirmed via PCR (TlpA_SS1_5', TTGTCTAAAGGTTTGAGTATC; TlpA_SS1_3', TTAAAACTGCTTTTTATTCAC) (Data not shown) and western blot using anti-TlpA22 (Williams et al., 2007) (Sup. Fig. 3.7). Δ*tlpA* SS1 was then transformed with the GFP expression plasmid, pTM115 ($ureA_p$-GFP *aphA3* Km^R) (Keilberg et

al., 2016). Colonies were screened for kanamycin resistance and GFP^+ fluorescence.

3.7.2 Ethics statement

The University of California Santa Cruz Institutional Animal Care and Use Committee approved all animal protocols and experiments performed (Protocol Ottek1804). Female C57BL/6N mice (*Helicobacter* free, Charles River) were housed and cared for at the University of California Santa Cruz Vivarium.

3.7.3 Animal infections

Female C57BL/6N mice (*Helicobacter* free, Charles River) were orally infected with *H. pylori* at 6 to 8 weeks of age, as done previously (Collins et al., 2018; Howitt et al., 2011). *H. pylori* SS1 strains were grown to late exponential phase (OD_{600} = ~0.75) in BB10 and were checked for GFP fluorescence and motility using a Nikon Eclipse E600 phase-contrast microscope at 400x magnification with a LED illuminator (pE-300^{white}, CoolLED) with a fluorescent filter for GFP. Motile GFP^+ cultures were concentrated to OD_{600} = 3 (~9 x 10^8 CFU/ml) by centrifugation of 1 ml culture aliquots in 1.5 ml Eppendorf Tubes at 2320 x g for 10 minutes. Culture supernatant was removed via aspiration and pellets were gently resuspended in BB10 to achieve an OD_{600} = 3. For infection, mice were scruffed and oriented at 45˚ with head and abdomen up, then orally fed 50µl of the OD_{600} = 3 culture via a pipet tip, for an inoculum of 4.5 x 10^7 CFU. Mice in the uninfected group were fed 50µl of BB10. Input inocula were plated on CHBA plates to determine the true input CFU. Two independent time course infections were performed for this study.

The infection time course reported in Figures 1- 5 included time points at 0.5- (WT and Δ*tlpA*, n = 7), 1- (WT and Δ*tlpA*, n = 7), 2- (WT and Δ*tlpA*, n = 4), 3- (WT and Δ*tlpA*, n=4), 4- (WT and Δ*tlpA*, n=7), 5- (WT, n=7; Δ*tlpA*, n=9), 5.5- (WT, n=7; Δ*tlpA*, n=9), 6- (WT, n=7; Δ*tlpA*, n=8), 6.5- (WT, n=7; Δ*tlpA*, n=8), and 8-months (WT and Δ*tlpA,* n=6). The infection time course reported in Figure 1 and 6. and Supplemental Figures 5- 6, include, 2- (WT, Δ*tlpA*, and Δ*cheY*, n=7;), 3- (WT, Δ*tlpA*, and Δ*cheY*, n=7), 4- (WT, Δ*tlpA*, and Δ*cheY*, n=6), 5- (WT, Δ*tlpA*, and Δ*cheY*, n=6), 6- (WT, Δ*tlpA*, and Δ*cheY*, n=7), and 8- months (WT, n=7; Δ*tlpA*, n=9; Δ*cheY*, n=9). From this time course, only 3 mice were used for gland analysis from 2-5- months post-infection, after which all mice from the infection group were used. For both time course infections, 3- 4 uninfected mice were included per time point. After the infection period, the mice were sacrificed by CO_2 narcosis, the stomach was removed at the stomach-esophageal junction and the antrum-duodenum sphincter, then opened by cutting along the lesser curvature of the stomach. Stomach contents were washed gently using ice-cold PBS. For dissection, a piece of tissue from the antrum to corpus was removed and stored in a histology cassette (Histoware) with sponge pads in Buffered Formalde-Fresh solution (Fisher Chemical) for histology. The remaining stomach was then separated between the antrum and corpus at the transition zone, based on tissue coloration. Each section was then divided into pieces to determine output CFU, to assess gland colonization, and for flow cytometry. To determine colonization load, tissue pieces were weighed, homogenized using the Bullet Blender (Next Advance) with 1.0 mm

zirconium silicate beads, and then plated onto CHBA plates, supplemented with 20 μg/ml bacitracin, 10 μg/ml nalidixic acid, and 15 μg/ml kanamycin, to determine CFU/g of stomach tissue.

3.7.4 Gland isolation and microscopy

Gastric glands from the antrum and corpus were isolated and *H. pylori* colonization within glands was quantified using the Bacterial Localization in Isolated Glands methods, as done previously (Collins et al., 2018; Keilberg et al., 2016). Briefly, glands were isolated by agitating dissected tissue from the antrum or corpus in PBS with 5 mM EDTA at 4˚C for 2 hours. The incubated tissue was then transferred to PBS with 1% sucrose and 1.5% sorbitol and vigorously by hand for 30 sec (both Fisher Chemical). Glands were labeled with 10 μg/ml Hoechst DNA stain (Life Technologies) and stored on ice. Glands were visualized with a Nikon Eclipse E600 microscope with a LED illuminator (pE-300^{white}, CoolLED) and fluorescent filters for 4',6'-diamido-2-phenylindole (DAPI) and GFP. At each infection time point, 100 glands from the antrum and 100 from the corpus were imaged and the number of GFP^{+} *H. pylori* per gland were manually counted. Gland colonization was calculated as the average number of bacteria per gland. Gland density was calculated by averaging the number of bacteria within occupied glands. Gland percent is calculated as the average frequency of glands occupied per mouse. Standard error of the mean was calculated for each. Statistical analysis of the data for between infection group or stomach regions at each time point was performed using two-way analysis of variance (ANOVA), Šídák multiple comparison test.

3.7.5 Histology

Tissue pieces from the antrum to corpus stored in Buffered Formalde-Fresh solution (Fisher Chemical) in histology cassettes with sponges were processed for sectioning and graded for lymphatic infiltration as done previously (Williams et al., 2007). Briefly, tissue was embedded in paraffin, sectioned (5 μm), stained in hematoxylin and eosin, and evaluated by a pathologist in a blind fashion (J. Elliot Carter). To ensure reproducibility, slides were read twice and checked to ensure identical grades were obtained. Inflammation, defined as lymphocytic infiltration, was assessed using standard methods (Eaton et al., 1995; Williams et al., 2007) and sections were given scores as follows: 0, no infiltrate; 1, mild, multifocal infiltration; 2, mild, widespread infiltration; 3, mild, widespread and moderate, multifocal infiltration; 4, moderate, widespread infiltration; and 5, moderate, widespread and severe, multifocal infiltration. Neutrophil infiltration was scored as present or absent. Sections were also assessed for atrophy according to previously defined standards (Rugge et al., 2002). Rugge *et al.* defined gastric atrophy as the loss of gastric glands in the area of the gastric mucosa being sampled. Atrophy can be associated with metaplasia, where gastric glands from a section of stomach are lost and replaced by gastric glands from a separate region of the gastric mucosa, or as atrophy without metaplasia, in which gastric glands from a section of stomach are lost with no replacement by other gastric glands and fibrosis of the lamina propria is seen. Samples negative for atrophy lack either manifestation of atrophy described. Mice from both time course infections were pooled for analysis. The

average inflammation grade and standard error of the mean was calculated for each strain per time point. Statistical analysis of the data for between strains was performed using two-way ANOVA, Šídák multiple comparison test.

3.7.6 Gastric lamina propria leukocyte isolation

Lamina propria leukocyte isolation from gastric tissue was performed as done previously (Arnold et al., 2017, 2018, 2019). Tissue pieces from the antrum and corpus were placed in 50 ml conical tubes in 5 ml RPMI (Gibco) with 10% FBS (Gibco) on ice during the dissection of the mice. Media was discarded by aspiration and replaced by 30 ml of 1x Hanks Balance Salt Solution (Gibco) with 0.5% BSA (MillaporeSigma) and 5 mM EDTA (Fisher Chemical) prewarmed to 37˚C. The tubes were then incubated horizontally at 37˚C with shaking for 1 hour at 200 rpm in a Thermo Scientific MaxQ 4000 benchtop orbital shaker. After incubation, the supernatant was removed by aspiration, the tissue resuspended in 30 ml of room temperature PBS for 2 minutes, and then the PBS was replaced with 15 ml of RPMI with 10% FCS, 500 U/ml Type IV Collagenase (Sigma-Aldrich), 0.05 mg/ml DNaseI (Gold Biotechnology) pre-warmed to 37˚C and incubated horizontally at 37˚C with shaking for 1 hr at 200 rpm in a Thermo Scientific MaxQ 4000 benchtop orbital shaker. Following incubation, the solution was pulled through a 20 ml syringe 10-15 times to finish homogenization. The supernatant containing lamina propria leukocytes was filtered through a 40 µm cell strainer (Falcon) and then 30 ml of PBS was added. Cells were collected by centrifugation in a Thermo Scientific Sorvall Legend XTR with a TX-1000 Rotor at 1500 rpm (526 x g) for 8 min, the

supernatant was discarded by aspiration, the cell pellet was resuspended in 4 ml of 80% Percoll (GE Healthcare), added to a 15 ml falcon tube, then overlayed with 4 ml of 40% Percoll. The 40/80% Percoll gradient was centrifuged for 15 min at 3000 rpm at 18˚C. The interphase, containing cells, was collected and washed with PBS with 0.5% BSA.

3.7.7 Flow cytometry

Flow cytometry was carried out as described previously (Arnold et al., 2017, 2018, 2019). For surface staining, cells were stained in PBS with 0.5% BSA with Fixable Viability Dye eFluor 780 (eBioscience) and a combination of the following antibodies: anti-mouse CD45 (PE/Cy5, 30-F11, BioLegend), CD45 (Alexa Fluor 700, 30-F11, BioLegend), CD11c (APC, N418, BioLegend), I-A/I-E (Alexa Fluor 700, M5/114.15.2, BioLegend), F4/80 (FITC, BM8, BioLegend), CD103 (Brilliant Violet 605, 2E7, BioLegend), CD11b (Brilliant Violet 421, M1/70, BioLegend), Ly-6G (PE/Dazzle 594, 1A8, BioLegend), Ly-6C (PE/Cy7, HK1.4, Biolegend), Siglec-F (PE, S17007C, BioLegend), TCRβ (PE/Cy7, H57-597, BD), or CD4 (APC, RM4-5, BioLegend). Mouse Fc Block (CD16/CD32, BD) to minimize unspecific antibody binding. For transcription factor staining, cells were fixed and permeabilized with FoxP3 Fix/Perm Buffer Set (BioLegend) following the manufacturer's instructions. Cells were stained with anti-mouse T-Bet (FITC, 4B10, BioLegend), RORγT (PE, Q31-378, BD), and FoxP3 (Pacific Blue, BioLegend, MF-14). Absolute cell counts were determined by adding CountBright Plus Absolute Counting Beads (Invitrogen) to each sample, which were analyzed

on an LSRII (BD Biosciences). Up to 300,000 cells were recorded per mouse, with some samples containing as few as 30,000 cells. Absolute counts are reported at cells/ ul. Analysis was performed using FlowJo (BD).

3.8 Acknowledgments

I would like to sincerely thank Christina Yang for her assistance and expertise with all animal work, including performing gastric gland isolations and bacterial enumeration from isolated glands. I thank Atesh K. Worthington and Elektra K. Robinson for their advice and technical support with flow cytometry experiments. I thank Raymond Lopez-Magaña and Frida Salgado for their assistance processing and plating tissue for CFU enumeration. I thank pathologist Dr. J. Elliot Carter for histology analysis and inflammation grading for all animal work. I thank Isabelle Arnold for training on how to isolate leukocytes from gastric tissue and perform flow cytometry, in addition to her thoughtful comments on this manuscript. I thank Bari Holm Nazario and the UCSC Institute for the Biology of Stem Cells Flow Cytometry Facility for technical support and training (RRID: SCR_021149). The described project was supported by the National Institute of Allergy and Infectious Disease (NIAID) grant RO1AI116946 to KMO. The funders had no role in study design, data collection, and interpretation, or decision to submit the work for publication.

CHAPTER 4- Conclusion and future directions

The ability to sense and perceive environmental signals is critical to all domains of life. In bacteria, chemotaxis systems are present in ~50% of species and enables a bacterium to direct its motility in response to harmful and beneficial environmental signals sensed by chemoreceptors (Wuichet and Zhulin, 2010). For numerous bacterial pathogens, chemotaxis and individual chemoreceptors are critical for *in vivo* colonization and pathogenesis (Matilla and Krell, 2018). One species that exemplifies this is *Helicobacter pylori*. The chemotaxis system of *H. pylori* is required for successful colonization of the stomach, and it plays a role in controlling host inflammation (Johnson and Ottemann, 2018). Previous work in our lab discovered that the *H. pylori* chemoreceptor TlpA dampens the severity of host inflammation, late in infection, through an unknown mechanism (Williams et al., 2007). Because inflammation underlies the diseases caused by *H. pylori*, we wanted to understand how TlpA plays a role in this process. This thesis provides more clarity to this question by 1) determining the sensing profile of TlpA and characterizing ligand binding interactions and 2) determining how TlpA regulates the localization of *H. pylori* in the stomach and characterizes the immune response influenced by TlpA.

5.1 The sensing profile of TlpA

To better understand the role of TlpA *in vivo*, it is crucial to know what signals this chemoreceptor is capable of sensing. It has been characterized that TlpA

senses arginine and bicarbonate, and plays a minor role in acid-sensing in combination with TlpB and TlpD (Cerda et al., 2003, 2011; Huang et al., 2017). The ligand-binding domain of TlpA adopts a dCache_1 fold, which are ubiquitous extracellular sensing domains (Sweeney et al., 2018; Upadhyay et al., 2016). dCache_1 domains are composed of tandem Cache domains, referred to as the membrane-distal and -proximal subdomains, either of which can bind multiple ligands (Machuca et al., 2017; Mckellar et al., 2015). Therefore, we reasoned TlpA might be capable of sensing additional ligands.

To discover novel TlpA ligands, we used ligand binding arrays and surface plasmon resonance (SPR). From these efforts, $TlpA_{LBD}$ was found to bind arginine, cysteine, fumarate, and glucosamine at a high affinities (K_d < 10 μM), while malic acid, thiamine, and α-ketoglutarate bound at a lower affinities (K_d > 45 μM). Chemoattractant responses, dependent on TlpA, were identified to arginine, fumarate, and cysteine. *H. pylori* elicited no chemotactic response to all other identified ligand hits. We characterized TlpA ligand binding using *in silico* docking analysis, competition SPR assays, and site-directed mutagenesis studies. We found that both the membrane-distal and -proximal subdomain play unique roles in binding distinct ligands through these experiments. Additionally, site-directed mutagenesis identified $TlpA_{LBD}$ binds glucosamine through a canonical dCache binding pocket in the membrane-distal subdomain, like the chemoactive TlpA ligands. The other non-chemoactive ligands did not bind $TlpA_{LBD}$ through a canonical binding pocket. We then explored the possibility that glucosamine might

act as a chemotaxis antagonist, an emerging concept in signal transduction systems (Bi et al., 2013; Martín-Mora et al., 2018). Glucosamine blocked TlpA chemoattractant binding *in vitro* and blocked normal *H. pylori* chemoattractant responses to arginine, fumarate, and cysteine. Together, these studies characterized glucosamine as a bona fide antagonist ligand. In total, this work greatly expanded our understanding of the sensing ability of TlpA and added a deeper understanding of the mechanisms of ligand binding through dCache_1 type chemoreceptors.

5.2 The role of TlpA *in vivo*

H. pylori chemotaxis plays a major role in colonization and inflammation development. Over the past decade, it has become appreciated that chemotaxis, and individual chemoreceptors, dictate the fine-scale localization of *H. pylori* in the mucus layer and gastric glands of the corpus and antrum throughout colonization (Howitt et al., 2011; Keilberg et al., 2016). For example, it has been shown that non-chemotactic *H. pylori* have a severe gland colonization defect early in infection and elicit less inflammation during later stages of infection (Keilberg et al., 2016; Rolig et al., 2011; Williams et al., 2007). This inflammatory phenotype is characterized by a diminished Th17 response, compared to WT *H. pylori* (Rolig et al., 2011). The *H. pylori* chemoreceptor TlpA plays an important role in dampening chronic host inflammation (Williams et al., 2007), but how this outcome is achieved is unknown.

To better understand the role TlpA plays *in vivo*, we characterized the TlpA dependent inflammatory response and the localization of *H. pylori* throughout a long-term infection. Using a WT and *tlpA* deficient strain of *H. pylori*, 8-month time course infections were performed. TlpA was required to suppress inflammation at 5-month post-infection in the corpus. After this point, TlpA plays a role in controlling transient spikes in inflammation, which is offset from WT, and changes in inflammation were associated with increased Th17 cell frequencies in the corpus. No major differences in the total number of either strain were observed in the bulk tissues. However, TlpA limited the number of *H. pylori* colonizing individual glands and the percent of glands infected early during infection. This phenotype was most striking in the corpus. From this work, we hypothesized that early gland colonization phenotypes could lead to altered inflammatory outcomes by limiting antigen sampling in the glands and subsequent T-cell activation.

To draw further connections between gland colonization and inflammation development, we examined a non-chemotactic *H. pylori* mutant (Δ*cheY H. pylori*) in more detail. It is known that Δ*cheY H. pylori* have a severe gland colonization defect early in infection and develop lower levels of inflammation during the chronic stage of infection (Keilberg et al., 2016; Rolig et al., 2011; Williams et al., 2007). However, there was limited knowledge of how Δ*cheY H. pylori* inflammation develops and colonization dynamics proceed past 1-month post-infection. Therefore, we assessed and compared the colonization patterns and inflammation outcomes dependent on chemotaxis (Δ*cheY*) and TlpA (Δ*tlpA*). We

confirmed previous reports that Δ*cheY H. pylori* induces less inflammation late in infection. Interestingly, we found that Δ*cheY H. pylori* induced increasing inflammation and gland density from 2- 4 months post-infection, which was immediately followed by a collapse in the gland population and decreased inflammation. This phenotype was unique to Δ*cheY H. pylori*. These results suggest that chemotaxis limits bacterial gland density to control aberrant inflammatory responses during infection.

In total, these results suggest that control of *H. pylori* localization via chemotaxis and TlpA may be important for regulating host immune responses.

5.3 Future directions

There are several lines of future investigation that can be explored to further our understanding of TlpA. Focusing first on TlpA sensing, we identified arginine, fumarate, and cysteine as TlpA chemoattractants. It would be informative to know where these ligands are present and their abundance during an infection *in vivo*. For example, the expression of *tlpA* is critical for limiting gland colonization during early infection. Accordingly, this implies TlpA senses either an attractant signal in the mucus layer or a repellent signal is present in the glands during this time. Previous metabolomic studies have analyzed bulk tissue. However, it would be informative to perform a metabolomic analysis comparing metabolites present in the mucus layer versus isolated glands over a 1-month infection. These studies would also help determine if and where glucosamine, the TlpA antagonist, is in the

gastric environment. The role of chemotaxis antagonists *in vivo* is currently unknown. Therefore, it is essential to know if *H. pylori* may experience this ligand in the gastric environment. Along these lines, site-directed mutants in the membrane-distal or -proximal subdomain of TlpA could also help assess which TlpA signals are important for early gland localization. It was shown that membrane-distal point mutants were more critical for arginine, cysteine, and glucosamine binding, while membrane-proximal mutants were more critical for fumarate binding. First, site-directed TlpA mutants in *H. pylori* could be created, and *in vitro* chemotaxis assays would be used to characterize which ligands each TlpA point-mutant is responsive to. Then, these TlpA point mutant strains could be used to infer which signals, or at least which dCache_1 subdomain, is critical for regulating the localization of *H. pylori in vivo*.

To better understand how TlpA regulates host inflammation, several approaches can be taken. From my findings, I hypothesize that increased gland colonization by Δ*tlpA H. pylori* early in infection leads to increased interactions with myeloid cells and T-cell priming. Therefore, a more detailed analysis of the immune response during this period would be the next step. To test this hypothesis, a flow cytometry experiment with fluorescently labeled *H. pylori* could be used to quantify the number of dendritic cells and macrophages that have encountered *H. pylori*, dependent on TlpA. If sufficient numbers of dendritic cells were observed from gastric tissues, FACS could be used to isolate dendritic cells, and *in vitro* T-cell activation experiments could be performed to assess TlpA dependent

differences in T-cell activation. To confirm whether TlpA is required early or late in infection for inflammation control, a *H. pylori* strain with *Tet*-regulation of *tlpA* expression could be generated (Debowski et al., 2013). With this strain, the expression of *tlpA* could be turned off after one month, or vice versa, to determine when *tlpA* expression is critical for inflammation control. These experiments and more could be performed to gain a better understanding of the *H. pylori* chemoreceptor TlpA. Below are additional open questions that remain to be explored.

5.4 Outstanding questions

- What TlpA signals dictate the localization of *H. pylori* and inflammation control?
- Does TlpA sense any repellent conditions?
- What is the role of a chemotaxis antagonist *in vivo?*
- Do TlpA chemoattractants directly bind to the distal or proximal domain, or do point mutants disrupt signal transduction or cause allosteric changes?
- During the early period in infection, do Δ*tlpA H. pylori* get phagocytosed at a higher rate?
- When is *tlpA* expression required for inflammation control?
- Do *tlpA* mutants have increased colonization resistance?
- Can the addition of TlpA ligands to the animal's diet affect the localization of *H. pylori*?

APPENDIX 1- Supplemental information to Chapter 2

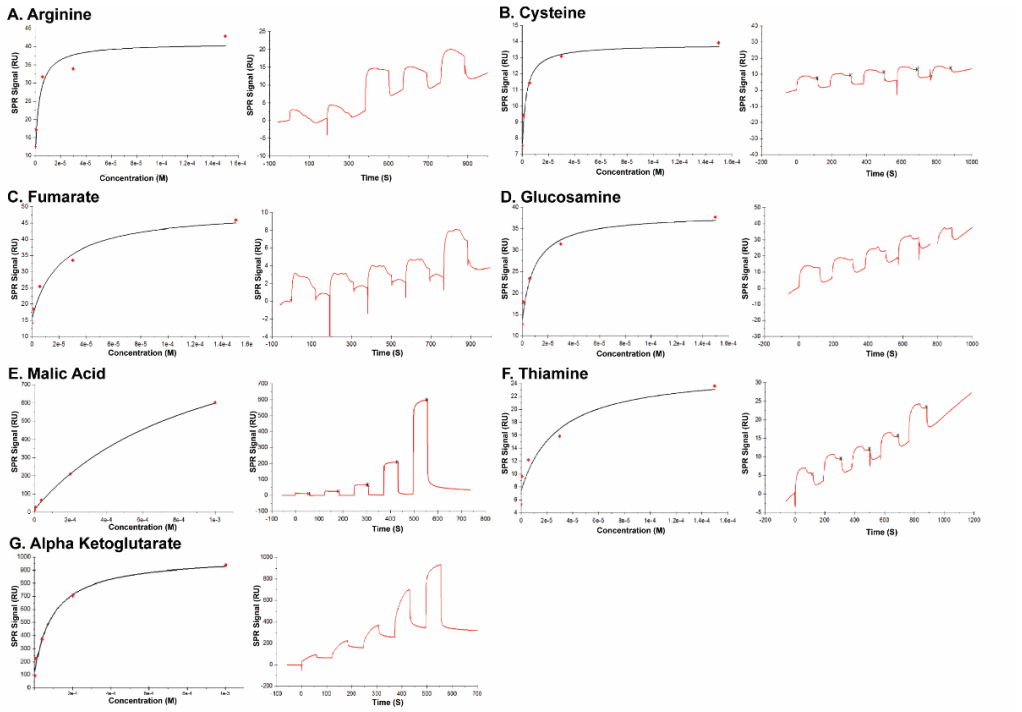

Supplemental Figure 2.1- Representative sensorgrams from surface plasmon resonance (SPR) analysis of $TlpA_{LBD}$ with A) Arginine, B) Cysteine, C) Fumarate, D) Glucosamine, E) Malic Acid, F) Thiamine, G) Alpha Ketoglutarate.

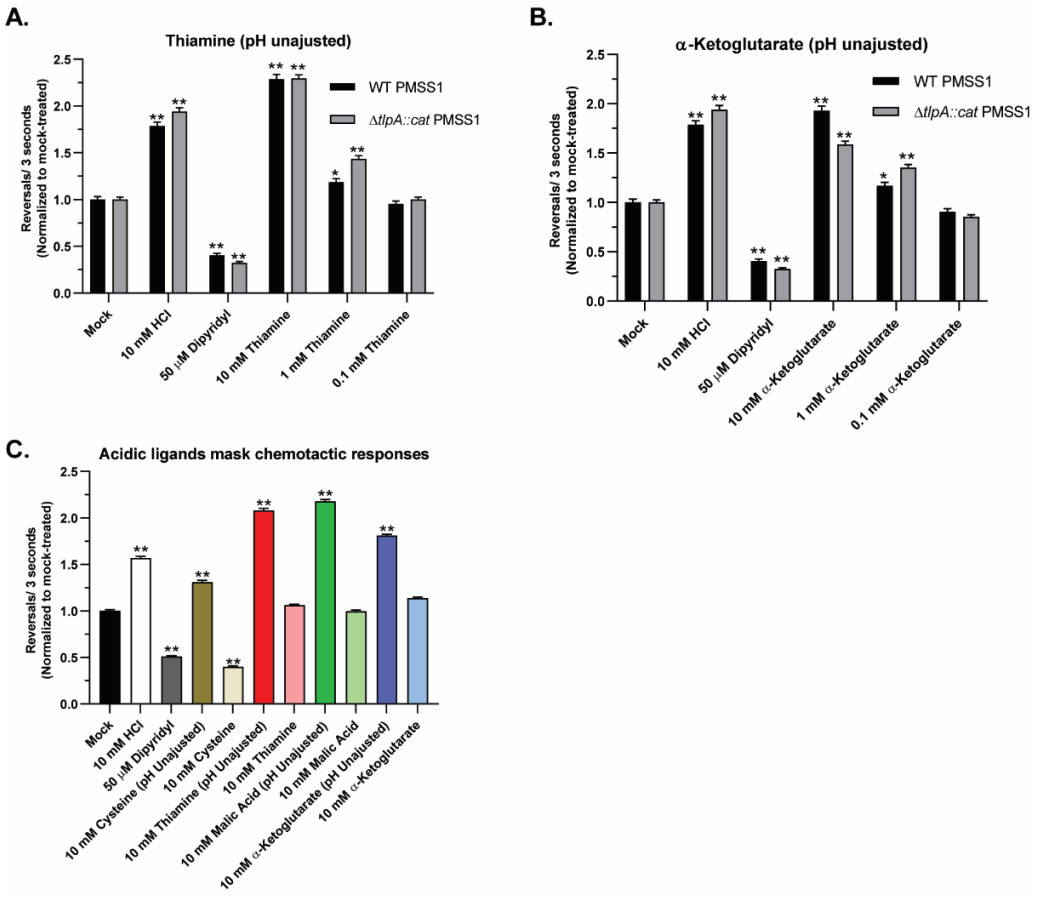

Supplemental Figure 2.2- Thiamine, alpha-ketoglutarate, cysteine, and malic acid trigger TlpA-independent repellent responses.

(A-B) Cultures of WT and Δ*tlpA::cat* PMSS1 were grown in BB10 overnight and then treated with various concentrations of thiamine or alpha-ketoglutarate. **(C)** Cultures of WT PMSS1 were grown as above and treated with 10mM pH neutralized or unadjusted thiamine, alpha-ketoglutarate, cysteine, and malic acid. For all experiments, cells were immediately filmed after ligand addition, and direction changes were counted over a 3 second swimming period in at least 100 cells per treatment. Repellents cause increases in direction changes, as exemplified by the control repellent HCl, while attractants cause fewer direction changes as exemplified by the control attractant dipyridyl. Error bars represent the standard error of the mean. *, P<0.05; **, P<0.01, comparisons to untreated control per strain using two-way ANOVA, Dunnett's multiple comparison test.

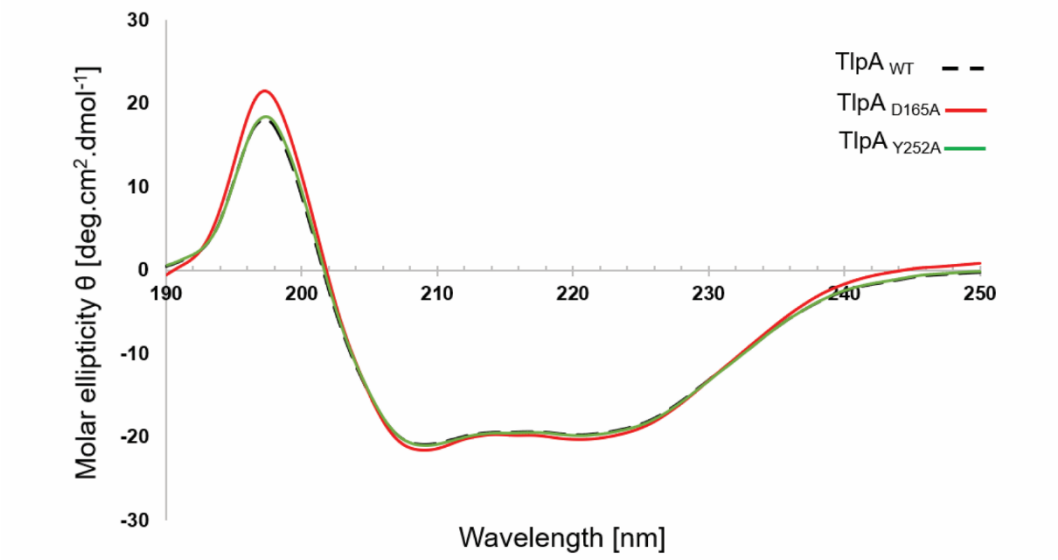

Supplemental Figure 2.3- CD spectrometry of WT $TlpA_{LBD}$ and point mutants $TlpA_{D165A}$ and $TlpA_{Y252A}$.
The far-UV CD spectra of $TlpA_{D165A}$ and $TlpA_{Y252A}$ are similar to WT $TlpA_{LBD}$, including all other $TlpA_{LBD}$ point mutants used in this study (Data not shown).

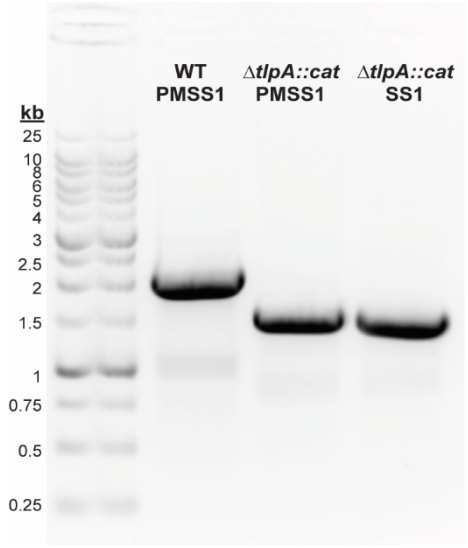

Supplemental Figure 2.4- Verification of Δ*tlpA::cat* PMSS1.
Mutation of *tlpA* was confirmed by PCR amplification of gDNA from WT PMSS1, Δ*tlpA::cat* PMSS1, and Δ*tlpA::cat* SS1 (Andermann et al., 2002) using primers TlpA_SS1_5' (TTGTCTAAAGGTTTGAGTATC) and TlpA_SS1_3' (TTAAAACTGCTTTTTATTCAC).

Supplemental Table 2.1- Amino acids, salts of organic acids, other chemotactic small molecules and glycans printed on the small molecule chemotaxis arrays.

Name	Structure/ Molecular Formula
Amino acids, salts of organic acids, + other small molecules	
Alanine	$C_3H_7NO_2$
Arginine	$C_6H_{14}N_4O_2$
Asparagine	$C_4H_8N_2O_3$
Aspartate	$C_4H_7NO_4$
Cysteine	$C_3H_7NO_2S$
Fumaric Acid	$C_4H_4O_4$
Glucosamine	$C_6H_{13}NO_5$
Glutamic acid	$C_5H_9NO_4$
Glutamine	$C_5H_{10}N_2O_3$
Histidine	$C_6H_9N_3O_2$
Isoleucine	$C_6H_{13}NO_2$
leucine	$C_6H_{13}NO_2$
Lysine	$C_6H_{14}N_2O_2$
Malic Acid	$C_4H_6O_5$
Methionine	$C_5H_{11}NO_2S$
Phenylalanine	$C_9H_{11}NO_2$
Proline	$C_5H_9NO_2$
Purine	$C_5H_4N_4$
Serine	$C_3H_7NO_3$
Succinic Acid	$C_4H_6O_4$
Thiamine	$C_{12}H_{17}N_4OS$
Threonine	$C_4H_9NO_3$
Tryptophan	$C_{11}H_{12}N_2O_2$
Tyrosine	$C_9H_{11}NO_3$
Valine	$C_5H_{11}NO_2$
α-ketoglutarate	$C_5H_6O_5$
Terminal Galactose	
Lacto-N-Biose I	Galβ1-3GlcNAc
N-Acetyllactosamine	Galβ1-4GlcNAc
β1-4galactosyl-galactose	Galβ1-4Gal
β1-6galactosyl-N-acetylglucosamine	Galβ1-6GlcNAc
β1-3galactosyl-N-acetylgalactosamine	Galβ1-3GalNAc
AsialoG$_{M1}$	Galβ1-3GalNAcβ1-4Galβ1-4Glc
Lacto-N-tetrose	Galβ1-3GlcNAcβ1-3Galβ1-4Glc
Lacto-N-neotetrose	Galβ1-4GlcNAcβ1-3Galβ1-4Glc
Lacto-N-neohexose	Galβ1-4GlcNAcβ1-6(Galβ1-4GlcNAcβ1-3)Galβ1-4Glc
Lacto-N-hexose	Galβ1-4GlcNAcβ1-6(Galβ1-3GlcNAcβ1-3)Galβ1-4Glc
Globotriose	Gala 1-4Galβ1-4Glc

Supplemental Table 2.1 Cont.

Tn Antigen	GalNAca1-O-Ser
Galactosyl-Tn Antigen	Galb1-3GalNAcα1-O-Ser
α1-3 Galactobiose	Gala1-3Gal
Linear B-2 Trisaccharide	Gala1-3Galβ1-4GlcNAc
Linear B-6 Trisaccharide	Gala1-3Galβ1-4Glc
α1-3, β1-4, α1-3 Galactotetrose	Gala1-3Galβ1-4Galα1-3Gal
β1-6Galactobiose	Galβ1-6Gal
Terminal disaccharide of globotriose	GalNAcβ1-3Gal
Receptor for pili of P. aeruginosa	GalNAcβ1-4Gal
P1 Antigen	Galα1-4Galβ1-4GlcNAc
α-D-N-acetylgalactosaminyl-1-3Gal-β1-4Glc	GalNAcα1-3Galβ1-4Glc
iso-Lacto-N-octose	Galβ1-3GlcNAcβ1-3Galβ1-4GlcNAcβ1-6(Galβ1-3GlcNAcβ1-3)Galβ1-4Glc
para-Lacto-N-hexose	Galβ1-3GlcNAcβ1-3Galβ1-4GlcNAcβ1-3Galβ1-4Glc
Terminal N`Acetyl glucosamine	
N,N'-Diacetyl chitobiose	GlcNAcβ1-4GlcNAc
N,N',N''-Triacetyl chitotriose	GlcNAcβ1-4GlcNAcβ1-4GlcNAc
N,N',N'',N'''-Tetraacetyl chitotetrose	GlcNAcβ1-4GlcNAcβ1-4GlcNAcβ1-4GlcNAc
N,N',N'',N''',N'''',N'''''-Hexaacetyl chitohexose	GlcNAcβ1-4GlcNAcβ1-4GlcNAcβ1-4GlcNAcβ1-4GlcNAcβ1-4GlcNAc
Bacterial cell wall muramyl discaccharide	GlcNAcβ1-4MurNAc
Manno se containing structures	
β1-2-N-Acetylglucosamine-mannose	GlcNAcβ1-2Man
Biannttennary N-linked core pentasaccharide	GlcNAcβ1-2Manα1-6(GlcNAcβ1-2Manα1-3)Man
α1-2-Mannobiose	Manα1-2Man
α1-3-Mannobiose	Manα1-3Man
α1-4-Mannobiose	Manα1-4Man
α1-6-Mannobiose	Manα1-6Man
α1-3, a1-6-Mannobiose	Manα1-6(Manα1-3)Man
α1-3, α1-3, α1-6-Mannopentaose	Manα1-6(Manα1-3)Manα1-6(Manα1-3)Man
Fucosylated structures	
Lacto-N-fucopentose I	Fucα1-2Galβ1-3GlcNAcβ1-3Galβ1-4Glc
Lacto-N-fucopentose II	Galβ1-3(Fuca1-4)GlcNAcβ1-3Galβ1-4Glc
Lacto-N-fucopentose III	Galβ1-4(Fuca1-3)GlcNAcβ1-3Galβ1-4Glc
Lacto-N-difucohexose I	Fucα1-2Galβ1-3(Fucα1-4)GlcNAcβ1-3Galβ1-4Glc
Lacto-N-difucohexose II	Galβ1-3(Fucα1-4)GlcNAcβ1-3Galβ1-4(Fucα1-3)Glc
H-disaccharide	Fucα1-2Gal
2'-Fucosyllactose	Fucα1-2Galβ1-4Glc
3'-Fucosyllactose	Galβ1-4(Fucα1-3)Glc
Lewis^{x}	Galβ1-4(Fucα1-3)GlcNAc
Lewis^{a}	Galβ1-3(Fucα1-4)GlcNAc

Supplemental Table 2.1 Cont.

Blood Group A-trisaccharide	GalNAcα1-3(Fucα1-2)Gal
Lactodifucotetrose	Fucα1-2Galβ1-4(Fucα1-3)Glc
Blood Group B-Trisaccharide	Galβ1-3(Fucα1-2)Gal
Lewis^{y}	Fucα1-2Galβ1-4(Fucα1-3)GlcNAc
Blood Group H Type II Trisaccharide	Fucα1-2Galβ1-3GlcNAc
Lewisb tetrasaccharide	Fucα1-2Galβ1-3(Fucα1-4)GlcNAc
Sulpho Lewis^{a}	SO_3-3Galβ1-3(Fucα1-4)GlcNAc
Sulpho Lewis^{x}	SO_3-3Galβ1-4(Fucα1-3)GlcNAc
Monofucosyl-para-Lacto-N-hexose IV	Galβ1-3GlcNAcβ1-3Galβ1-4(Fucα1-3)GlcNAcβ1-3Galβ1-4Glc
Monofucosyllacto-N-hexose III	Galβ1-4(Fucα1-3)GlcNAcβ1-6(Galβ1-3GlcNAcβ1-3)Galβ1-4Glc
Difucosyllacto-N-hexose	Galβ1-4(Fucα1-3)GlcNAcβ1-6(Fucα1-2Galβ1-3GlcNAcβ1-3)Galβ1-4Glc
Trifucosyllacto-N-hexose	Galβ1-4(Fucα1-3)GlcNAcβ1-6(Fucα1-2Galβ1-3(Fucα1-4)GlcNAcβ1-3)Galβ1-4Glc
Lacto-N-fucopentaose VI	Galβ1-4GlcNAcβ1-3Galβ1-4(Fucα1-3)Glc
Lacto-N-neodifucohexaose I	Fucα1-2Galβ1-4(Fucα1-3)GlcNAcβ1-3Galβ1-4Glc
Lacto-N-neodifucohexaose II	Fucα1-3Galβ1-4GlcNAcb1-3Galβ1-4(Fucα1-3)Glc
Trifucosyllacto-N-neoteraose I	Fucα1-2Galβ1-4(Fucα1-3)GlcNAcβ1-3(Fucα1-2)Galβ1-4Glc
Monofucosyllacto-N-neohexaose I	Galβ1-4(Fucα1-3)GlcNAcβ1-6(Galβ1-4GlcNAcβ1-3)Galβ1-4Glc
Difucosyllacto-N-neohexaose I	Galβ1-4(Fucα1-3)GlcNAcβ1-6(Galβ1-4(Fucα1-3)GlcNAcβ1-3)Galβ1-4Glc
Difucosyllacto-N-neohexaose II	Fucα1-2Galβ1-4(Fucα1-3)GlcNAcβ1-6(Galβ1-4GlcNAcβ1-3)Galβ1-4Glc
Monofucosyl(1-3)-iso-lacto-N-octaose	Galβ1-3GlcNAcβ1-3Galβ1-4(Fucα1-3)GlcNAcβ1-6(Galβ1-3GlcNAcβ1-3)Galβ1-4Glc
Trifucosyl(1-2,1-2,1-3)-iso-lacto-N-octaose	Fucα1-2Galβ1-3GlcNAcβ1-3Galβ1-4(Fucα1-3)GlcNAcβ1-6(Galβ1-3GlcNAcβ1-3)Galβ1-4Glc
Blood Group A Tetrasaccharide	GalNAcβ1-3(Fucα1-2)Galβ1-4Glc
Blood Group B pentasaccharide	Galβ1-3(Fucα1-2)Galβ1-4(Fucα1-3)Glc
Neu5Ac containing structures	
Sialyl Lewis^{a}	Neu5Acα2-3Galβ1-3(Fucα1-4)GlcNAc
Sialyl Lewis^{x}	Neu5Acα2-3Galβ1-4(Fucα1-3)GlcNAc
Sialyllacto-N-tetrose a	Neu5Acα2-3Galβ1-3GlcNAcβ1-3Galβ1-4Glc
Monosialyl, monofucosyllacto-N-neohexose	Galβ1-4(Fucα1-3)GlcNAcβ1-6(Neu5Acα2-6Galβ1-4GlcNAcβ1-3)Galβ1-4Glc
2,3'-Sialyllactosamine	Neu5Acα2-3Galβ1-4GlcNAc
2,6'-Sialyllactosamine	Neu5Acα2-6Galβ1-4GlcNAc
LS-Tetrasaccharide a	Neu5Acα2-3Galβ1-3GlcNAcβ1-3Galβ1-4Glc

Supplemental Table 2.1 Cont.

LS-Tetrasaccharide b	Galβ1-3(Neu5Acα2-6)GlcNAcβ1-3Galβ1-4Glc
LS-Tetrasaccharide c	Neu5Acα2-6Galβ1-4GlcNAcβ1-3Galβ1-4Glc
Disialyllacto-N-tetrose	Neu5Acα2-3Galβ1-3(Neu5Acα2-6)GlcNAcβ1-3Galβ1-4Glc
2,3'-Sialyllactose	Neu5Acα2-3Galβ1-4Glc
2,6'-Sialyllactose	Neu5Acα2-6Galβ1-4Glc
Colominic acid	(Neu5Acα2-8Neu5Ac)n (n<50)
Biantennary 2,6-sialylated-N-glycan-Asn	Neu5Acα2-6Galβ1-4GlcNAcβ1-2Manα1-6(Neu5Acα2-6Galβ1-4GlcNAcβ1-2Manα1-6)Manβ1-4GlcNAcβ1-4GlcNAc-Asn
Carageenan and Glycoaminoglycans (GAGS)	
Neocarratetrose-41, 3-di-O-sulphate (Na^+)	$C_{24}H_{36}O_{25}S_2Na_2$ (Mixed anomers. Tetrasaccharide of regular κ - carrageenan)
Neocarratetrose-41-O-sulphate (Na^+)	$C_{24}H_{37}O_{22}SNa$ (Mixed anomers. Derived from C1003 by removal of the non-reducing terminal 4-sulphate)
Neocarrahexose-24,41, 3, 5-tetra-O-sulphate (Na^+)	$C_{36}H_{52}O_{40}S_4Na_4$ (Mixed anomers. A hybrid sequence comprising carrageenan disaccharides in the order k-i-k, derived from the carrageenan from Chondrus crispus)
Neocarrahexose-41, 3, 5-tri-O-sulphate (Na^+)	$C_{36}H_{53}O_{37}S_3Na_3$ (Mixed anomers. Hexasaccharide of regular κ-carrageenan)
Neocarraoctose-41, 3, 5, 7-tetra-O-sulphate (Na^+)	$C_{48}H_{70}O_{49}S_4Na_4$ (Mixed anomers. Octasaccharide of regular κ-carrageenan)
Neocarradecose-41, 3, 5, 7, 9-penta-O-sulphate (Na^+)	$C_{60}H_{87}O_{61}S_5Na_5$ (Mixed anomers. Decasaccharide of regular κ- carrageenan)
ΔUA-2S → GlcNS-6S Na_4 (I-S)	$C_{12}H_{15}NO_{19}S_3Na_4$ (Predominant disaccharide produced from heparin by heparinase I and II)
ΔUA → GlucNS-6S Na_3 (II-S)	$C_{12}H_{16}NO_{16}S_2Na_3$ (Produced from heparinase II digestion of heparin and heparin sulphate)
ΔUA → 2S-GlcNS Na_3 (III-S)	$C_{12}H_{16}NO_{16}S_2Na_3$ (Produced from heparin by digestion with heparinase I and II)
ΔUA → 2S-GlcNAc-6S Na_3 (I-A)	$C_{14}H_{18}NO_{17}S_2Na_3$ (Minor component produced from heparin by heparinase II)
ΔUA → GlcNAc-6S Na_2 (II-A)	$C_{14}H_{19}NO_{14}SNa_2$ (Product of the action of heparinases II and III on heparin and heparan sulphate)
ΔUA → 2S-GlcNAc Na_2 (III-A)	$C_{14}H_{19}NO_{14}SNa_2$ (Minor product of the action of heparinase II on heparin)
ΔUA → GlcNAc Na (IV-A)	$C_{14}H_{20}NO_{11}Na$ (Produced from heparin sulphate by digestion With heparinase III)
ΔUA → GalNAc-4S Na_2 (ΔDi-4S)	$C_{14}H_{19}NO_{14}SNa_2$ (Produced from various chondroitin sulphates By the action of chondroitinases ABC, B and AC-1)

Supplemental Table 2.1 Cont.

ΔUA → GalNAc-6S Na2 (ΔDi-6S)	$C_{14}H_{19}NO_{14}SNa_2$ (Produced from various chondroitin sulphates By the action of chondroitinases ABC, AC-1 and C)
ΔUA → GalNAc-4S,6S Na_3 (ΔDi-disE)	$C_{14}H_{18}NO_{17}S_2Na_3$ (Produced from various chondroitin sulphates By the action of chondroitinases ABC, B and AC-1)
ΔUA → 2S-GalNAc-4S Na_2 (ΔDi-disB)	$C_{14}H_{18}NO_{17}S_2Na_3$ (Produced from various chondroitin sulphates by action of chondroitinase ABC and/or B. Most typically from chondroitin sulphate B (dermatan sulphate))
ΔUA → 2S-GalNAc-6S Na_3 (ΔDi-disD)	$C_{14}H_{18}NO_{17}S_2Na_3$ (Produced from various chondroitin sulphates by the action of chondroitinase ABC)
ΔUA → 2S-GalNAc-4S-6S Na_4 (ΔDi-tisS)	$C_{14}H_{17}NO_{20}S_3Na_4$ (Produced as a minor component by the action of chondroitinase ABC on various chondroitin sulphates, particularly B)
ΔUA → 2S-GalNAc-6S Na_2 (ΔDi-UA2S)	$C_{14}H_{19}NO_{14}SNa_2$ (Produced as a minor component from various chondroitin sulphates by the action of chondroitinase ABC)
ΔUA → GlcNAc Na (ΔDi-HA)	$C_{14}H_{20}NO_{11}Na$ (The only unsaturated disaccharide produced from hyaluronic acid by the action of chondroitinase ABC or AC-1)
Hyaluronan fragments (4mer)	(GlcAβ1-3GlcNAcβ1-4)n (n=4)
Hyaluronan fragments (8mer)	(GlcAβ1-3GlcNAcβ1-4)n (n=8)
Hyaluronan fragments (10mer)	(GlcAβ1-3GlcNAcβ1-4)n (n=10)
Hyaluronan fragments (12mer)	(GlcAβ1-3GlcNAcβ1-4)n (n=12)
Heparin	(GlcA/IdoAα/β1-4GlcNAcα1-4)n (n=200)
Chondroitin sulfate	(GlcA/IdoAβ1-3(±4/6S)GalNAcβ1-4)n (n<250)
Dermatan sulfate	((±2S)GlcA/IdoAα/b1-3(±4S)GalNAcβ1-4)n (n<250)
Chondroitin 6-Sulfate	(GlcA/IdoAβ1-3(±6S)GalNAcβ1-4)n (n<250)
HA - 4	(GlcAβ1-3GlcNAcβ1-4)n (n=4)
HA - 6	(GlcAβ1-3GlcNAcβ1-4)n (n=6)
HA - 8	(GlcAβ1-3GlcNAcβ1-4)n (n=8)
HA 10	(GlcAβ1-3GlcNAcβ1-4)n (n=10)
HA-12	(GlcAβ1-3GlcNAcβ1-4)n (n=12)
HA-14	(GlcAβ1-3GlcNAcβ1-4)n (n=14)
HA-16	(GlcAβ1-3GlcNAcβ1-4)n (n=16)
HA 30000 Da	(GlcAβ1-3GlcNAcβ1-4)n
HA 107000 Da	(GlcAβ1-3GlcNAcβ1-4)n

Supplemental Table 2.2- Clusters A-H and their interacting amino acids.

Cluster	Amino acids
A	PHE-203, ILE-205, VAL-211, ILE-224, TYR-228, VAL-231, ALA-234, THR-235, VAL-238, LEU-250, TYR-252, LEU-263, VAL-265, ALA-285, ILE-287
B	GLY-206, VAL-207, LYS-208, LEU-242, GLU-243, LYS-269, LEU-280, ASN-281
C	VAL-60, ASN-63, THR-64, SER-67, ALA-94, ASN-95, SER-96, HIS-97
D	SER-102, MSE-103, PHE-104, THR-114, GLU-126, ASN-133, ALA-136, ARG-153, TYR-151, LEU-167, ALA-181, LEU-182, MET-183
E	PHE-105, LYS-106, ASN-107, ARG-108, ASN-172, VAL-179
F	LYS-138, ASN-142, GLU-144, ILE-145, SER-146, SER-276, LYS-277, ASP-278
G	PRO-76, LYS-77, ASP-78, THR-79, LYS-84, PHE-105, ASN-107, ARG-108, LEU-111, ASN-172, GLU-173, VAL-179
H	SER-96, HIS-97, VAL-98, ALA-99, ARG-117, ASP-118, MSE-155, PRO-156, ASN-157, ALA-159, VAL-161, SER-187, SER-190

Supplemental Table 2.3- $TlpA_{LBD}$ docking analysis with fumarate and arginine.

	Fumarate	Arginine
Cluster	Cluster Occupation %	Cluster Occupation %
A (membrane-proximal Cache)	45	25
B	10	5
C	20	5
D (membrane-distal Cache)	10	55
E	5	-
F	10	-
G	-	5
H	-	5

Supplemental Table 2.4- Primers for site-directed mutagenesis of $TlpA_{LBD}$. Mutated codons, bolded; restriction sites used for screening clones, underlined.

Primer name	Sequence (5' → 3')
TlpA_D165A_For	GGGGCGGAAGTTTATGGAGTTGCTATTCTTTTACCTTTATTG
TlpA_D165A_Rev	CAATAAAGGTAAAAGAATAGCAACTCCATAAACTTCCGCCCC
TlpA_M183A_For	GAGGTTGTAGGGGCTTTGGCGGTTTTTATTTCCATTGACAGC
TlpA_M183A_Rev	GCTGTCAATGGAAATAAAAACCGCCAAAGCCCCTACAACCTC
TlpA_Y228A_For	GACAAACCTATCGCAGAAATTGCTAAGAGCGTACCTAAAGCC
TlpA_Y228A_Rev	GGCTTTAGGTACGCTCTTAGCAATTTCTGCGATAGGTTTGTC
TlpA_Y252A_For	CTCTAAAGCGACTTTAGAAGCTTTAGATCCCTTTAGCCATAAGG
TlpA_Y252A_Rev	CCTTATGGCTAAAGGGATCTAAAGCTTCTAAAGTCGCTTTAGAG
TlpA_D254A_For	CTAAAGCGACTCTAGAATACTTAGCTCCCTTTAGCCATAAGG
TlpA_D254A_Rev	CCTTATGGCTAAAGGGAGCTAAGTATTCTAGAGTCGCTTTAG

Supplemental Table 2.5 - Supplementary glycan microarray document based on MIRAGE guidelines (Liu et al., 2017).

Classification	Guidelines
1. Sample: Glycan Binding Sample	
Description of Sample	Sample names: TlpA protein Origin: Helicobacter pylori SS1; produced as a recombinant His -tagged protein in E. coli. Method of preparation: The preparation of TlpA is explained in the Materials and Methods section: TlpA construct design and protein purification.
Sample modifications	Sample is a His Tagged protein containing only the periplasmic receptor domain, amino acids 28-299, of the full length TlpA transmembrane protein.
Assay protocol	Please see Materials and Methods: Ligand binding array. Proteins were complexed with mouse anti-his antibody, with secondary and tertiary AlexaFluor555 antibodies (rabbit anti-mouse, goat anti-rabbit) at a molar ratio of 4:2:1. The protein/antibody complex was incubated on ice for 10 mins prior to placing on the array. Arrays were performed with 1 µg of complexed protein incubated on the array for 20 min. Arrays were then washed 3 times in Array PBS (PBS + 2 mM $MgCl_2$ + 2 mM $CaCl_2$) then dried by centrifugation for 3 min at 300 x g. Scanning was performed using an Innopsys InnoScan 1100AL and analyzed using Mapix (Innopsys). Yes/no binding was determined by six positive replicate spots in three replicate experiments. Positive binding was determined by spots being significantly greater than negative control spots by two-tailed t test.
2.1 Glycan Library	
Glycan description for defined glycans	Glycans in this study are listed in Table S1 and is a published library (Waespy et al., 2015).
Glycan description for undefined glycans	N/A.
Glycan modifications	Glycans were prepared in one of two ways for printing: 1. Glycans (with IDs in number/letter format; e.g. 1A, 4C, 7K) were sourced commercially from Dextra Laboratories, Elicityl and Carbosythn and were made into glycoamines using a published protocol (Day et al., 2009). 2. Glycans (with IDs in number only format) were obtained from Prof. Nicolai Bovin and were modified with spacers (Blixt et al., 2004). The library of these glycans was first published in (Huflejt et al., 2009).
2.2 Small molecule Library	
Sample description for defined compounds	Compounds printed in the amino acid/small molecule array for this study are listed in Table S1.

Supplemental Table 2.5 Cont.

3. Printing Surface; e.g., Microarray Slide	
Description of surface	Epoxy activated glass microarray slides.
Manufacturer	ArrayIt SuperEpoxy 3 (SME3).
Custom preparation of surface	N/A.
Non-covalent Immobilisation	N/A.
4. Arrayer (Printer)	
Description of Arrayer	Glycan array: SpotBot® Extreme Protein Microarray Spotter (ArrayIt, California, USA). Small molecule array: ArrayJet Argus Marathon non-contact printer.
Dispensing mechanism	Glycan array: Contact printing using 946NS6 pins with a 6 pin in a 3 columns x 2 rows configuration. Small molecule array: Non-contact jet printing
Glycan and small molecule deposition	Glycan array: Approximately 1.8 nl per spot is printed according to manufactures guidelines. Glycan were at 500 µM in 50:50 DMF:DMSO. Small molecule array: Approximately 320 nl per spot is printed according to manufactures guidelines. Samples were at 1000 µM in PBS with 2% glycerol
Printing conditions	Glycan array: Array were printed with dehumidification at a maximum humidity of 60% relative humidity (Standard laboratory starting humidity of 75-90%) at 22ºC. Glycans were left to react with the slide for at least 8 hours after the print was completed. Small molecule array: Array were printed with dehumidification at a maximum humidity of 60% relative humidity (Standard laboratory starting humidity of 75-90%) at 22ºC. Samples were left to react with the slide for at least 15 hours after the print was completed.
5.1 Glycan array with "Map"	
Array layout	The array consists of a single array of glycans split between 6 pins (3 columns x 2 rows) with 4500 µm row and column spacing. Each pin printed a 20 columns x 16 rows with 200 µm spot spacing (center to center) with a minimum spot size of 100µm. Each sample is printed in quadruplicate with each of the 6 print areas including at least three negative control samples (print solution only) and two positive control samples consisting of one sample of fluoroscienamine and one sample of a mixture of rabbit anti-mouse antibody labeled with Alexa 555 and Alexa 647. Positive controls provide proof of successful immobilization of the amine reagents and provides for orientation for analysis. The antibodies also can provide controls for secondary antibodies used in experiments (if applicable).
Glycan identification and quality control	Arrays are quality controlled by a range of measures. 1. Each printed array is post print scanned to confirm deposition of the glycans on the array surface prior to neutralization of the remaining slide surface. 2. Post neutralized slides are scanned again to monitor for remaining autofluorescence. 3. Slides are assayed with fluorescently labeled lectins: WGA-Texas Red (EY Laboratories) and ConA-FITC (EY Laboratories).

Supplemental Table 2.5 Cont.

5.2 Small molecule array with "Map"	
Array layout	The array consists of triplicate sub-arrays of amino acids and small moleucles (24 rows x 10 columns) with 400μm spot spacing (centre to centre) with a minimum spot size of 100μm. Each sample is printed six times, with each of the 3 sub-arrays including at least six negative control samples (print solution only) and a positive control samples consisting of one a mixture of rabbit anti-mouse antibody labeled with Alexa 555 and Alexa 647. Positive controls provide proof of successful immobilization of the amine reagents and provides for orientation for analysis.
Sample identification and quality control	Arrays are quality controlled by a range of measures. 1. Each printed array is post print scanned to confirm deposition of the samples on the array surface prior to neutralization of the remaining slide surface. 2. Post neutralized slides are scanned again to monitor for remaining autofluorescence.
6. Detector and Data Processing	
Scanning hardware	Inopsys InnoScan 1100AL (Lasers: 488 nM, 532 nM with two filter sets for analysis at 532 and 595 nM), 635 nM) scanner.
Scanner settings	Scanning resolution: 10 μM Laser channel: 532 nM operating 595 nM excitation / 625 nM emission filter set. PMT: 20% gain Scan powers: Low laser power.
Image analysis software	Innopsys MAPIX.
Data processing	Data was exported as a CSV file and exported to Microsoft Excel.
7. Glycan Microarray Data Presentation	
Data presentation	Glycan array: Data is presented as yes/no binding in Table 1. The full list of glycans is shown in Table S1.
8. Interpretation and Conclusion from Microarray Data	
Data interpretation	Glycan arrays: We only use glycan arrays as a yes/no binding tool. Due to this we look only at binding that is unambiguously above background vs lack of binding above background. Average background + 3x standard deviation of the background of 20 sets of 4 spots of DMF:DMSO only spots is applied to determine if binding observed is significantly above background. Only spots with values equal to or greater than this value were considered as binding from data of any tested slide. These values are slide dependert. Small molecule arrays: We only use amino acid arrays as a yes/no binding tool. Due to this we look only at binding that is unambiguously above background vs lack of binding above background. Average background + 3x standard deviation of the background of 6 spots of PBS + 2% glycerol only spots is applied to determine if binding observed is significantly above background. Only spots with values equal to or greater than this value were considered as binding from data of any tested slide. These values are slide dependert.
Conclusions	TlpA binds multiple ligands. Subsequent work showed that some of these are attractants, some elicit no response, and some are antagonists.

APPENDIX 2- Supplemental information to Chapter 3

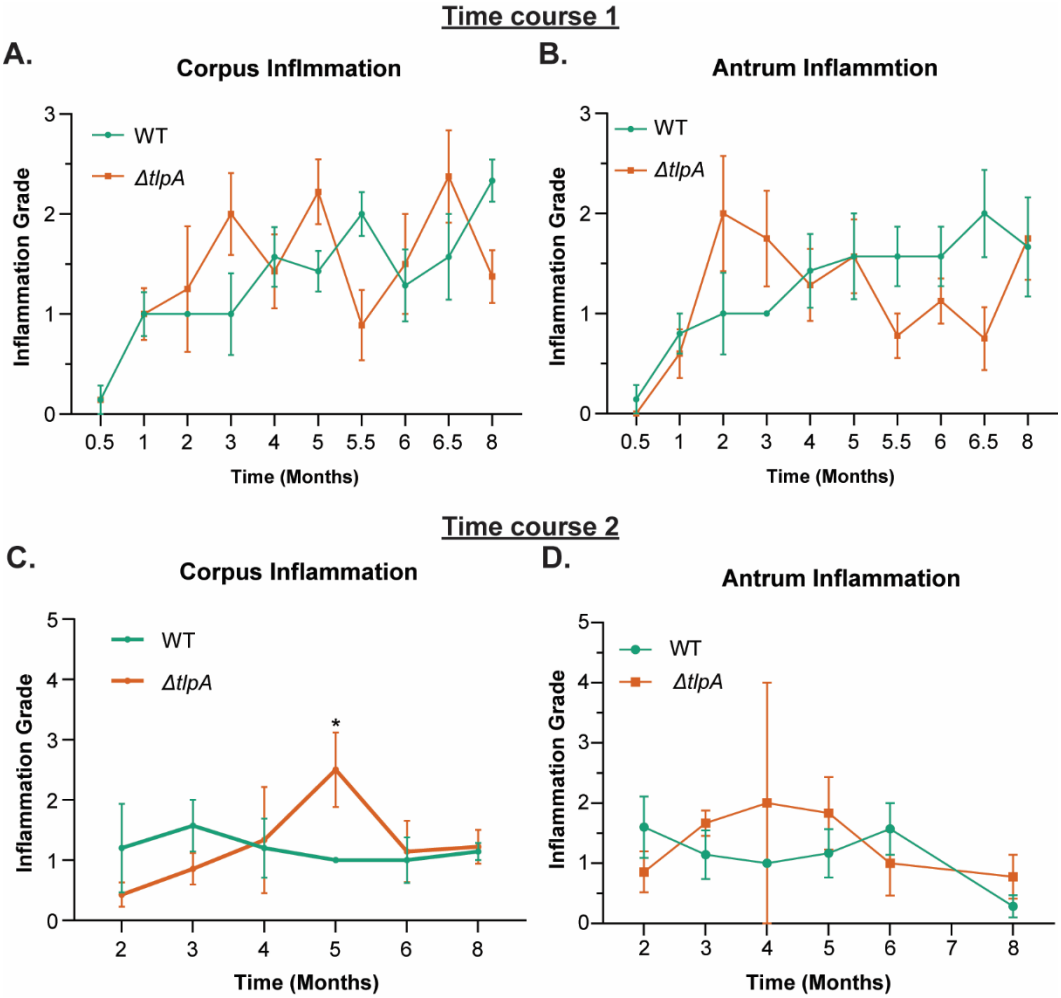

Supplemental Figure 3.1- Significantly more inflammation is induced by Δ*tlpA* *H. pylori* in a transient manner during chronic infection.
Two independent infection time courses were performed were female C57BL/6N mice orally infected with WT SS1 GFP$^+$ or Δ*tlpA* SS1 GFP$^+$. Time course 1 assessed time points at 0.5- (WT and Δ*tlpA*, n = 7), 1- (WT and Δ*tlpA*, n = 7), 2- (WT and *ΔtlpA*, n = 4), 3- (WT and Δ*tlpA*, n=4), 4- (WT and Δ*tlpA*, n=7), 5- (WT, n=7; Δ*tlpA*, n=9), 5.5- (WT, n=7; Δ*tlpA*, n=9), 6- (WT, n=7; Δ*tlpA*, n=8), 6.5- (WT, n=7; Δ*tlpA*, n=8), and 8-months (WT and Δ*tlpA,* n=6). Time course 2 assessed time points at 2- (WT and Δ*tlpA*), 3- (WT and Δ*tlpA*, n=7), 4- (WT and Δ*tlpA*, n=6), 5- (WT and Δ*tlpA*, n=6), 6- (WT and Δ*tlpA*, n=7), and 8- months (WT, n=7; Δ*tlpA*, n=9). Inflammation induced by WT SS1 GFP$^+$ or Δ*tlpA* SS1 GFP$^+$ infection groups was measured by assessing lymphocyte recruitment to the lamina propria of (A) corpus and (B) antrum via histology, as performed previously (Williams et al.,

2007). Error bars represent the standard error of the mean. *, P<0.05, comparisons between strains using two-way ANOVA, Šídák multiple comparison test.

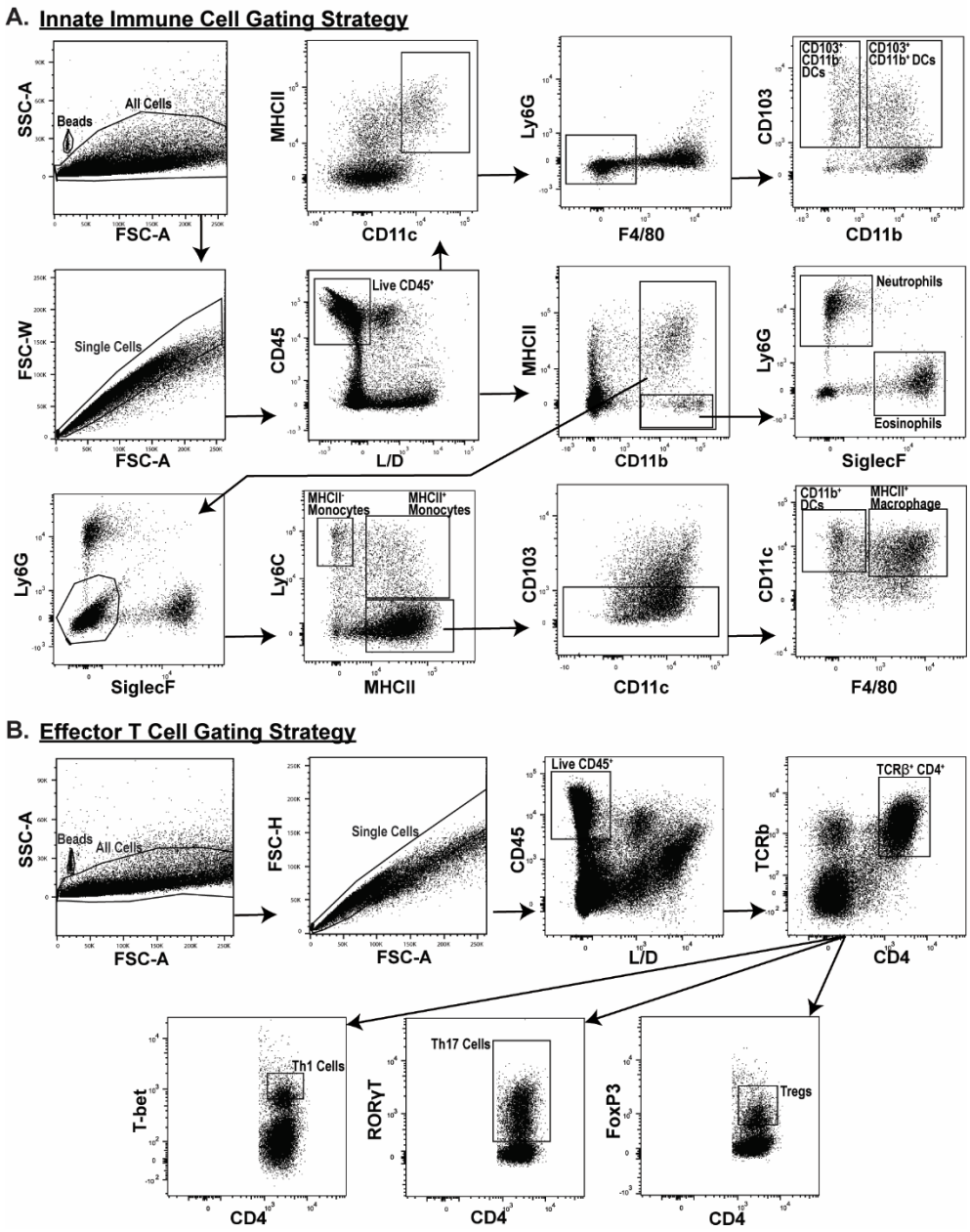

Supplemental Figure 3.2- Gating strategy used to identify innate immune and effector T cell populations.

Leukocytes were isolated from the corpus lamina propria via enzymatic digestion with collagenase IV and Percoll gradient centrifugation. Isolated leukocytes were then analyzed via flow cytometry. A) Gating strategy for innate immune cell types,

as performed by Arnold et a. 2017. B) Gating strategy for CD4$^+$ effector T cell populations.

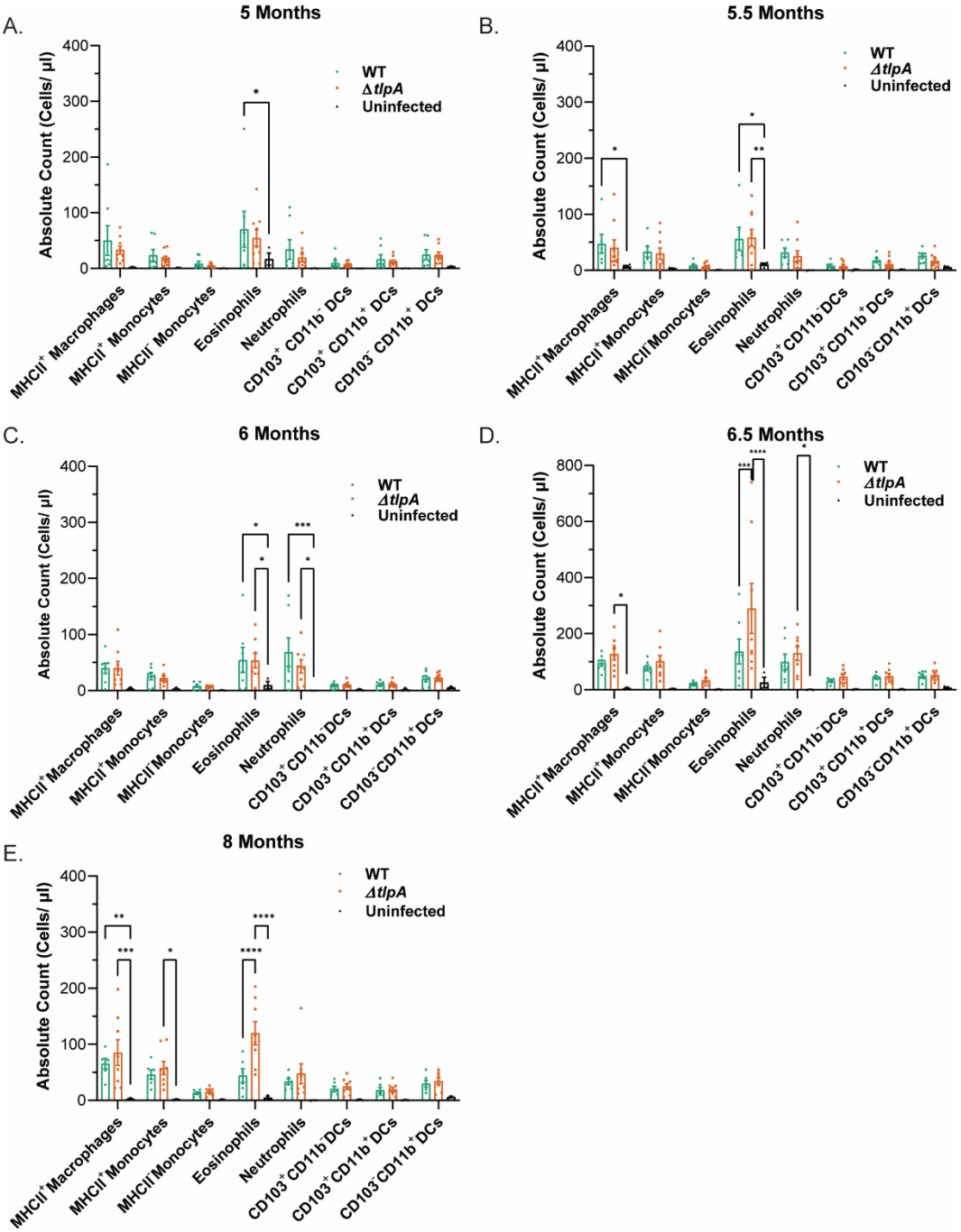

Supplemental Figure 3.3- Absolute counts of innate immune cell populations recruited to the corpus during chronic infection.

Mice were infected with WT SS1 GFP$^+$ or Δ*tlpA* SS1 GFP$^+$ and leukocytes from the corpus lamina propria were isolated at 5-, 5.5-, 6-, 6.5-, and 8-months post-

infection (n = 7- 9 per group). (A-E) neutrophils, eosinophils, $MCHII^+$ macrophages, $MCHII^-$ monocytes, $MHCII^+$ monocytes, $CD11b^+$ DCs, $CD103^+$ $CD11b^-$ DCs, and $CD103^+$ $CD11b^+$ DCs were analyzed by flow cytometry. Data are presented as the absolute count (cells/ µl) of each cell type. Error bars represent the standard error of the mean. *, $P<0.05$; **, $P<0.01$; ***, $P<0.001$; ****, $P<0.0001$, comparisons between strains using two-way ANOVA, Tukey multiple comparison test.

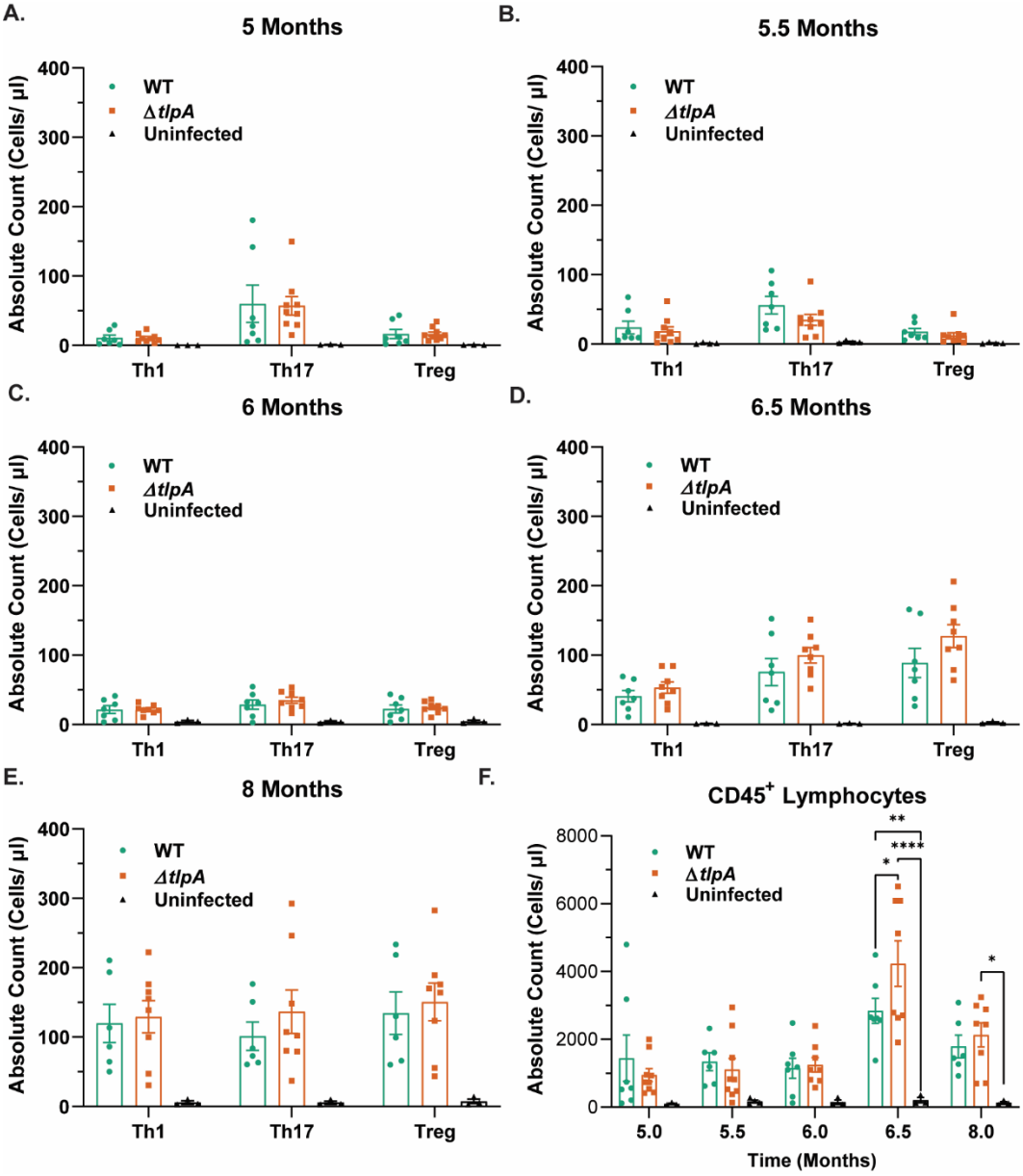

Supplemental Figure 3.4- Absolute counts of effector T cell populations and total CD45$^+$ leukocytes recruited to the stomach during chronic infection.
Mice were infected with WT SS1 GFP$^+$ or Δ*tlpA* SS1 GFP$^+$. Leukocytes from the corpus lamina propria were isolated at 5-, 5.5-, 6-, 6.5-, and 8-months post-infection (n = 7- 9 per group). (A-E) Th1, Th17, Tregs, and CD45$^+$ leukocytes were analyzed by flow cytometry. Data are presented as the absolute count (cells/ µl) of each cell type. Error bars represent the standard error of the mean. *, P<0.05; **, P<0.01; ***, P<0.001; ****, P<0.0001, comparisons between strains using two-way ANOVA, Tukey multiple comparison test.

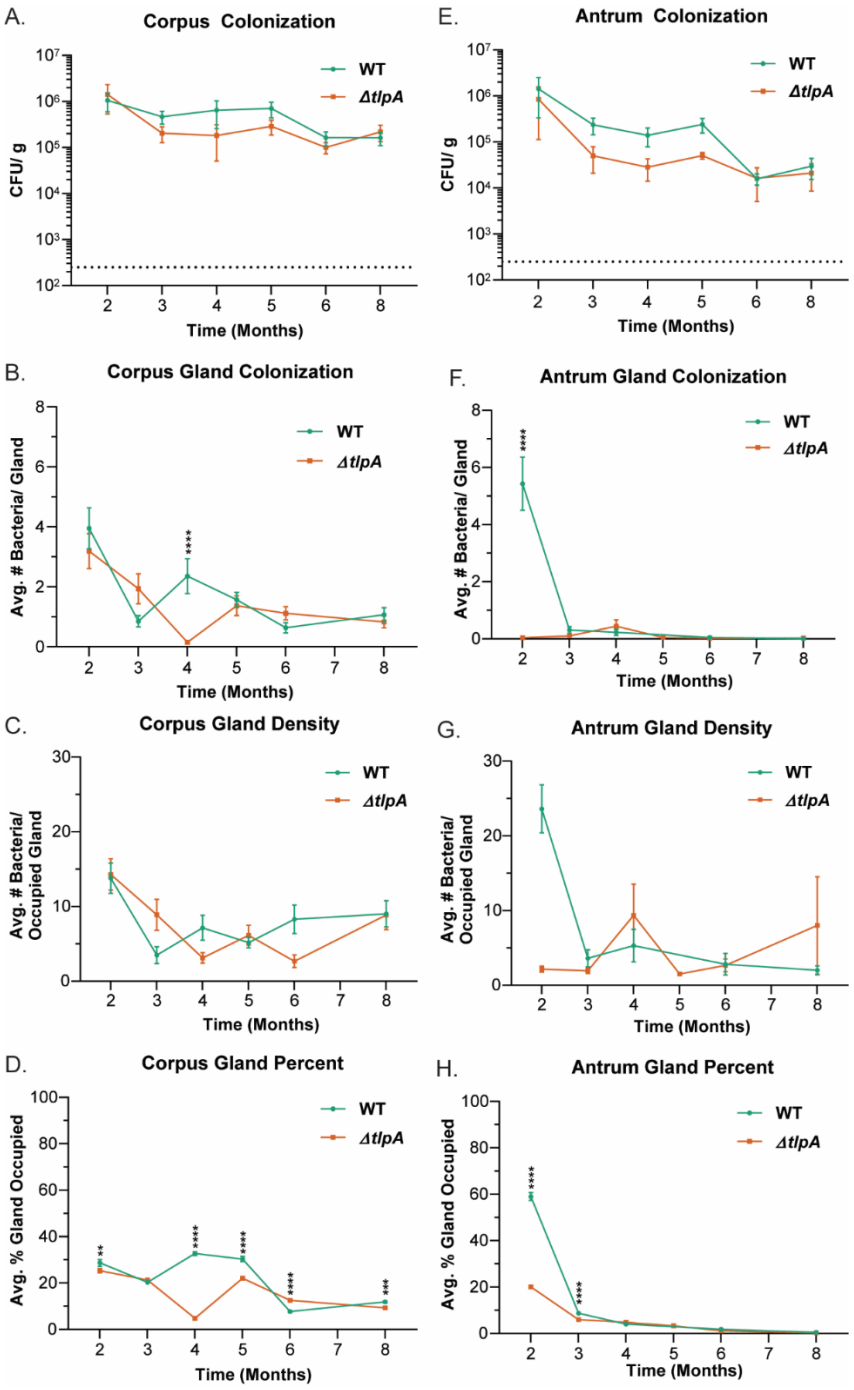

Supplemental Figure 3.5- A replicate time course infection confirms few differences in gland colonization between WT and Δ*tlpA* SS1 during the chronic stage of infection.

Female C57BL/6N mice (n ≥ 3) were orally infected with WT SS1 GFP$^+$ or Δ*tlpA* SS1 GFP$^+$ for 2-, 3-, 4-, 5-, 6-, and 8-months. Colonization of WT SS1 and Δ*tlpA*

in the corpus was assessed for (A) total colonization, (B) gland colonization, (C) gland density, and (D) gland percent. Colonization of WT SS1 and Δ*tlpA* in the antrum was assessed for (E) total colonization, (F) gland colonization, (G) gland density, and (H) gland percent. For all graphs, error bars represent the standard error of the mean. *, $P<0.05$; **, $P<0.01$; ***, $P<0.001$; ****, $P<0.0001$, comparisons between strains using two-way ANOVA, Šídák multiple comparison test.

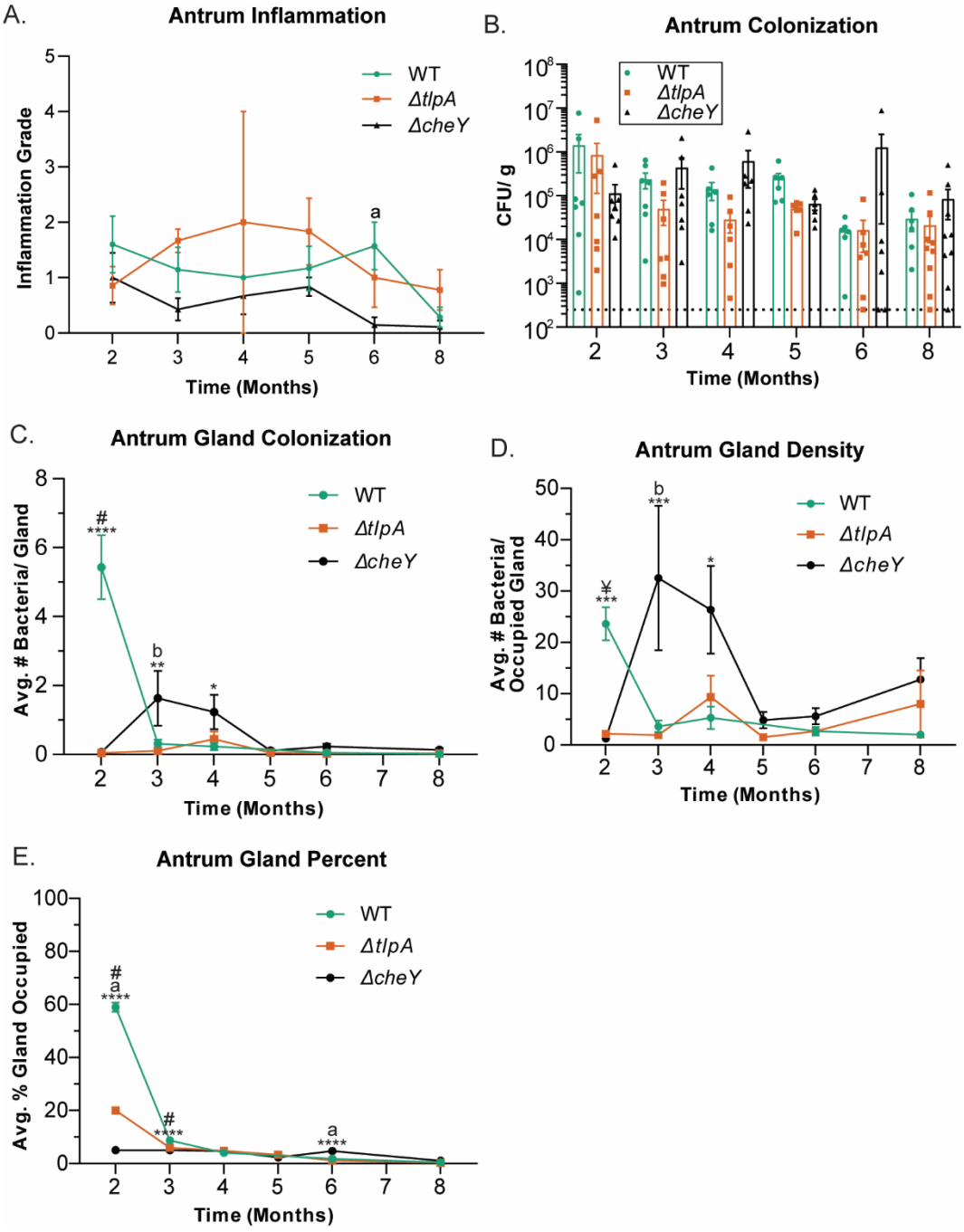

Supplemental Figure 3.6- Colonization dynamics of Δ*cheY* SS1 during the chronic stage of infection.

Colonization dynamics of WT SS1 and Δ*tlpA* SS1 within the antrum were analyzed during the chronic stage of infection. Female C57BL/6N mice (n ≥ 3) were orally infected with WT SS1 GFP$^+$ or Δ*tlpA* SS1 GFP$^+$ for 2-, 3-, 4-, 5-, 6-, and 8-months. (A) Inflammation by histology, (B) total colonization, (B) gland colonization, (C)

gland density, and (D) gland percent was assessed. For all graphs, error bars represent the standard error of the mean. Comparisons between strains were made using two-way ANOVA, Tukey multiple comparison test. WT vs. Δ*tlpA*: a, P<0.0001; b, P<0.001; c, P<0.01; d, P<0.05. WT vs. Δ*cheY*: ****, P<0.0001; ***, P<0.001; **, P<0.01; *, P<0.05. Δ*tlpA* vs. Δ*cheY*: #, P<0.0001; †, P<0.001; ‡, P<0.01; ¥, P<0.05.

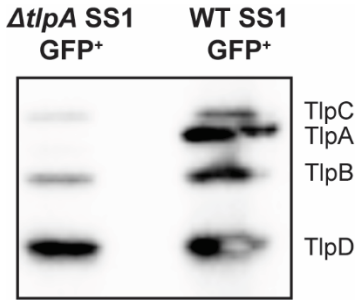

Supplemental Figure 3.7- Verification of Δ*tlpA* SS1 GFP$^+$
Verification of the generation of a Δ*tlpA* clean deletion mutant in a GFP$^+$ SS1 background was confirmed via PCR (Data not shown) and western blot. Anti-TlpA22 (Williams et al., 2007) was used to detect the conserved, cytoplasmic portion of *H. pylori* TlpA, B, C, and D. All Δ*tlpA* SS1 GFP$^+$ clones lack TlpA but express all other chemoreceptors.

REFERENCES

Abedrabbo, S., Castellon, J., Collins, K.D., Johnson, K.S., Ottemann, K.M., 2017. Cooperation of two distinct coupling proteins creates chemosensory network connections. Proc. Natl. Acad. Sci. 114, 2970–2975. https://doi.org/10.1073/pnas.1618227114

Aihara, E., Closson, C., Matthis, A.L., Schumacher, M.A., Engevik, A.C., Zavros, Y., Ottemann, K.M., Montrose, M.H., 2014. Motility and Chemotaxis Mediate the Preferential Colonization of Gastric Injury Sites by *Helicobacter pylori*. PLoS Pathog. 10. https://doi.org/10.1371/journal.ppat.1004275

Ailloud, F., Didelot, X., Woltemate, S., Pfaffinger, G., Overmann, J., Bader, R.C., Schulz, C., Malfertheiner, P., Suerbaum, S., 2019. Within-host evolution of *Helicobacter pylori* shaped by niche-specific adaptation, intragastric migrations and selective sweeps. Nat. Commun. 10, 2273. https://doi.org/10.1038/s41467-019-10050-1

Alam, M., Srivastava, A., Dutta, A., Sau, A.K., 2018. Biochemical and biophysical studies of *Helicobacter pylori* arginine decarboxylase, an enzyme important for acid adaptation in host. IUBMB Life 70, 658–669. https://doi.org/10.1002/iub.1754

Algood, H.M.S., Cover, T.L., 2006. *Helicobacter pylori* Persistence: an Overview of Interactions between *H. pylori* and Host Immune Defenses. Clin. Microbiol. Rev. 19, 597–613. https://doi.org/10.1128/CMR.00006-06

Andermann, T.M., Chen, Y.-T., Ottemann, K.M., 2002. Two Predicted Chemoreceptors of *Helicobacter pylori* Promote Stomach Infection. Infect. Immun. 70, 5877–5881. https://doi.org/10.1128/IAI.70.10.5877-5881.2002

Anderson, J.K., Huang, J.Y., Wreden, C., Goers Sweeney, E., Goers, J., James Remington, S., Guillemin, K., 2015. Chemorepulsion from the quorum signal autoinducer-2 promotes *Helicobacter pylori* biofilm dispersal. mBio 6, 1–13. https://doi.org/10.1128/mBio.00379-15

Arnold, I.C., Artola-Borán, M., Tallón de Lara, P., Kyburz, A., Taube, C., Ottemann, K., van den Broek, M., Yousefi, S., Simon, H.-U., Müller, A., 2018. Eosinophils suppress Th1 responses and restrict bacterially induced gastrointestinal inflammation. J. Exp. Med. 215, 2055–2072. https://doi.org/10.1084/jem.20172049

Arnold, I.C., Dehzad, N., Reuter, S., Martin, H., Becher, B., Taube, C., Müller, A., 2011a. *Helicobacter pylori* infection prevents allergic asthma in mouse models through the induction of regulatory T cells. J. Clin. Invest. 121, 3088–3093. https://doi.org/10.1172/JCI45041

Arnold, I.C., Lee, J.Y., Amieva, M.R., Roers, A., Flavell, R.A., Sparwasser, T., Müller, A., 2011b. Tolerance Rather Than Immunity Protects From *Helicobacter pylori* –Induced Gastric Preneoplasia. Gastroenterology 140, 199-209.e8. https://doi.org/10.1053/j.gastro.2010.06.047

Arnold, I.C., Zhang, X., Artola-Boran, M., Fallegger, A., Sander, P., Johansen, P., Müller, A., 2019. BATF3-dependent dendritic cells drive both effector and regulatory T-cell responses in bacterially infected tissues. PLOS Pathog. 15, e1007866. https://doi.org/10.1371/journal.ppat.1007866

Arnold, I.C., Zhang, X., Urban, S., Artola-Borán, M., Manz, M.G., Ottemann, K.M., Müller, A., 2017. NLRP3 Controls the Development of Gastrointestinal CD11b + Dendritic Cells in the Steady State and during Chronic Bacterial Infection. Cell Rep. 21, 3860–3872. https://doi.org/10.1016/j.celrep.2017.12.015

Atuma, C., Strugala, V., Allen, A., Holm, L., 2001. The adherent gastrointestinal mucus gel layer: thickness and physical state *in vivo*. Am. J. Physiol. Gastrointest. Liver Physiol. 280, G922–G929.

Bamford, K.B., Fan, X., Crowe, S.E., Leary, J.F., Gourley, W.K., Luthra, G.K., Brooks, E.G., Graham, D.Y., Reyes, V.E., Ernst, P.B., 1998. Lymphocytes in the human gastric mucosa during *Helicobacter pylori* have a T helper cell 1 phenotype. Gastroenterology 114, 482–492. https://doi.org/10.1016/S0016-5085(98)70531-1

Behar, J., 2013. Physiology and Pathophysiology of the Biliary Tract : The Gallbladder and Sphincter of Oddi — A Review. ISRN Physiol. 2013, 1–15.

Behrens, W., Schweinitzer, T., Bal, J., Dorsch, M., Bleich, A., Kops, F., Brenneke, B., Didelot, X., Suerbaum, S., Josenhans, C., 2013. Role of

energy sensor TlpD of *Helicobacter pylori* in Gerbil colonization and genome analyses after adaptation in the Gerbil. Infect. Immun. 81, 3534–3551. https://doi.org/10.1128/IAI.00750-13

Behrens, W., Schweinitzer, T., McMurry, J.L., Loewen, P.C., Buettner, F.F.R., Menz, S., Josenhans, C., 2016. Localisation and protein-protein interactions of the *Helicobacter pylori* taxis sensor TlpD and their connection to metabolic functions. Sci. Rep. 6, 1–20. https://doi.org/10.1038/srep23582

Bi, S., Yu, D., Si, G., Luo, C., Li, T., Ouyang, Q., Jakovljevic, V., Sourjik, V., Tu, Y., Lai, L., 2013. Discovery of novel chemoeffectors and rational design of *Escherichia coli* chemoreceptor specificity. Proc. Natl. Acad. Sci. U. S. A. 110, 16814–16819. https://doi.org/10.1073/pnas.1306811110

Biemann, H.P., Koshland, D.E., 1994. Aspartate receptors of *Escherichia coli* and Salmonella typhimurium bind ligand with negative and half-of-the-sites cooperativity. Biochemistry 33, 629–634. https://doi.org/10.1021/bi00169a002

Blaser, M.J., Chen, Y., Reibmann, J., 2008. Does *Helicobacter pylori* protect against asthma and allergy? Gut 57, 561–567. https://doi.org/10.1136/gut.2007.133462

Blosse, A., Lehours, P., Wilson, K.T., Gobert, A.P., 2018. *Helicobacter*: Inflammation, immunology, and vaccines. Helicobacter 23, e12517. https://doi.org/10.1111/hel.12517

Busch, A., Lacal, J., Martos, A., Ramos, J.L., Krell, T., 2007. Bacterial sensor kinase TodS interacts with agonistic and antagonistic signals. Proc. Natl. Acad. Sci. U. S. A. 104, 13774–13779. https://doi.org/10.1073/pnas.0701547104

Carbo, A., Olivares-Villagómez, D., Hontecillas, R., Bassaganya-Riera, J., Chaturvedi, R., Piazuelo, M.B., Delgado, A., Washington, M.K., Wilson, K.T., Algood, H.M.S., 2014. Systems Modeling of the Role of Interleukin-21 in the Maintenance of Effector CD4 $^{+}$ T Cell Responses during Chronic *Helicobacter pylori* Infection. mBio 5. https://doi.org/10.1128/mBio.01243-14

Cerda, O., Rivas, A., Toledo, H., 2003. *Helicobacter pylori* strain ATCC700392 encodes a methyl-accepting chemotaxis receptor protein (MCP) for arginine and sodium bicarbonate. FEMS Microbiol. Lett. 224, 175–181. https://doi.org/10.1016/S0378-1097(03)00423-3

Cerda, O.A., Núñez-Villena, F., Soto, S.E., Ugalde, J.M., López-Solís, R., Toledo, H., 2011. tlpA gene expression is required for arginine and bicarbonate chemotaxis in *Helicobacter pylori*. Biol. Res. 44, 277–282. https://doi.org/10.4067/S0716-97602011000300009

Chen, W., Shu, D., Chadwick, V.S., 2001. Reduced colonization of gastric mucosa by *Helicobacter pylori* in mice deficient in interleukin-101. J. Gastroenterol. Hepatol. 16, 377–383. https://doi.org/10.1046/j.1440-1746.2001.02459.x

Colin, R., Sourjik, V., 2017. Emergent properties of bacterial chemotaxis pathway. Curr. Opin. Microbiol. 39, 24–33. https://doi.org/10.1016/j.mib.2017.07.004

Collins, K.D., Andermann, T.M., Draper, J., Sanders, L., Williams, S.M., Araghi, C., Ottemann, K.M., 2016. The *Helicobacter pylori* CZB Cytoplasmic Chemoreceptor TlpD Forms an Autonomous Polar Chemotaxis Signaling Complex That Mediates a Tactic Response to Oxidative Stress. J. Bacteriol. 198, 1563–1575. https://doi.org/10.1128/JB.00071-16

Collins, K.D., Hu, S., Grasberger, H., Kao, J.Y., Ottemann, K.M., 2018. Chemotaxis Allows Bacteria To Overcome Host-Generated Reactive Oxygen Species That Constrain Gland Colonization. Infect. Immun. 86, e00878-17. https://doi.org/10.1128/IAI.00878-17

Cover, T.L., Blaser, M.J., 2009. *Helicobacter pylori* in Health and Disease. Gastroenterology 136, 1863–1873. https://doi.org/10.1053/j.gastro.2009.01.073

Creamer, B., Shorter, R.G., Bamforth, J., 1961. The turnover and shedding of epithelial cells: Part I The turnover in the gastro-intestinal tract. Gut 2, 110–116. https://doi.org/10.1136/gut.2.2.110

Croxen, M.A., Sisson, G., Melano, R., Hoffman, P.S., 2006. The *Helicobacter pylori* Chemotaxis Receptor TlpB (HP0103) Is Required for pH Taxis and for Colonization of the Gastric Mucosa. J. Bacteriol. 188, 2656–2665. https://doi.org/10.1128/JB.188.7.2656-2665.2006

Day, C.J., King, R.M., Shewell, L.K., Tram, G., Najnin, T., Hartley-Tassell, L.E., Wilson, J.C., Fleetwood, A.D., Zhulin, I.B., Korolik, V., 2016. A direct-sensing galactose chemoreceptor recently evolved in invasive strains of *Campylobacter jejuni*. Nat. Commun. 7, 13206. https://doi.org/10.1038/ncomms13206

Day, C.J., Korolik, V., 2018. Identification of Specific Ligands for Sensory Receptors by Small-Molecule Ligand Arrays and Surface Plasmon Resonance. Methods Mol. Biol. Clifton NJ 1729, 303–317. https://doi.org/10.1007/978-1-4939-7577-8_24

Debowski, A.W., Verbrugghe, P., Sehnal, M., Marshall, B.J., Benghezal, M., 2013. Development of a Tetracycline-Inducible Gene Expression System for the Study of *Helicobacter pylori* Pathogenesis. Appl. Environ. Microbiol. 79, 7351–7359. https://doi.org/10.1128/AEM.02701-13

Dixon, B.R.E.A., Hossain, R., Patel, R.V., Algood, H.M.S., 2019. Th17 Cells in *Helicobacter pylori* Infection: a Dichotomy of Help and Harm. Infect. Immun. 87, e00363-19, /iai/87/11/IAI.00363-19.atom. https://doi.org/10.1128/IAI.00363-19

Eaton, K.A., Mefford, M., Thevenot, T., 2001. The Role of T Cell Subsets and Cytokines in the Pathogenesis of *Helicobacter pylori* Gastritis in Mice. J. Immunol. 166, 7456–7461. https://doi.org/10.4049/jimmunol.166.12.7456

Eaton, K.A., Radin, M.J., Krakowka, S., 1995. An Animal Model of Gastric Ulcer Due to Bacterial Gastritis in Mice. Vet. Pathol. 32, 489–497. https://doi.org/10.1177/030098589503200506

Ehrhardt, M.K.G., Warring, S.L., Gerth, M.L., 2018. Screening Chemoreceptor-Ligand Interactions by High-Throughput Thermal-Shift Assays. Methods Mol. Biol. Clifton NJ 1729, 281–290. https://doi.org/10.1007/978-1-4939-7577-8_22

Elgamoudi, B.A., Andrianova, E.P., Shewell, L.K., Day, C.J., King, R.M., Taha, Rahman, H., Hartley-Tassell, L.E., Zhulin, I.B., Korolik, V., 2021. The *Campylobacter jejuni* chemoreceptor Tlp10 has a bimodal ligand-binding domain and specificity for multiple classes of chemoeffectors. Sci. Signal. 14, eabc8521. https://doi.org/10.1126/scisignal.abc8521

Ferlay, J., Soerjomataram, I., Dikshit, R., Eser, S., Mathers, C., Rebelo, M., Parkin, D.M., Forman, D., Bray, F., 2015. Cancer incidence and mortality worldwide: Sources, methods and major patterns in GLOBOCAN 2012. Int. J. Cancer 136, E359–E386. https://doi.org/10.1002/ijc.29210

Fimmel, C.J., Etienne, A., Cilluffo, T., Ritter, C., Gasser, T., Rey, J., Caradonna-moscatelli, P., Sabbatini, F., Pace, F., Buhler, H.W., Bauerfeind, P., Blum, A.L., 1985. Long-Term Ambulatory Gastric pH Monitoring : Validation of a New Method and Effect of Hz-Antagonists. Gastroenterology 88, 1842–1851.

Foynes, S., Dorrell, N., Ward, S.J., Stabler, R.A., McColm, A.A., Rycroft, A.N., Wren, B.W., 2000. *Helicobacter pylori* possesses two CheY response regulators and a histidine kinase sensor, CheA, which are essential for chemotaxis and colonization of the gastric mucosa. Infect. Immun. 68, 2016–2023. https://doi.org/10.1128/IAI.68.4.2016-2023.2000

Fung, C., Tan, S., Nakajima, M., Skoog, E.C., Camarillo-Guerrero, L.F., Klein, J.A., Lawley, T.D., Solnick, J.V., Fukami, T., Amieva, M.R., 2019. High-resolution mapping reveals that microniches in the gastric glands control *Helicobacter pylori* colonization of the stomach. PLOS Biol. 17, e3000231. https://doi.org/10.1371/journal.pbio.3000231

Ge, Z., Feng, Y., Dangler, C.A., Xu, S., Taylor, N.S., Fox, J.G., 2000. Fumarate reductase is essential for *Helicobacter pylori* colonization of the mouse stomach. Microb. Pathog. 29, 279–287. https://doi.org/10.1006/mpat.2000.0391

Gobert, A.P., Wilson, K.T., 2016. The Immune Battle against *Helicobacter pylori* Infection: NO Offense. Trends Microbiol. 24, 366–376. https://doi.org/10.1016/j.tim.2016.02.005

Goers Sweeney, E., Henderson, J.N., Goers, J., Wreden, C., Hicks, K.G., Foster, J.K., Parthasarathy, R., Remington, S.J., Guillemin, K., 2012. Structure and Proposed Mechanism for the pH-Sensing *Helicobacter pylori* Chemoreceptor TlpB. Structure 20, 1177–1188. https://doi.org/10.1016/j.str.2012.04.021

Goyal, R.K., Guo, Y., Mashimo, H., 2019. Advances in the physiology of gastric emptying. Neurogastroenterol. Motil. 31, e13546. https://doi.org/10.1111/nmo.13546

Grasberger, H., El-Zaatari, M., Dang, D.T., Merchant, J.L., 2013. Dual oxidases control release of hydrogen peroxide by the gastric epithelium to prevent *Helicobacter felis* infection and inflammation in mice. Gastroenterology 145, 1045–1054. https://doi.org/10.1053/j.gastro.2013.07.011

Gray, B.M., Fontaine, C.A., Poe, S.A., Eaton, K.A., 2013. Complex T Cell Interactions Contribute to *Helicobacter pylori* Gastritis in Mice. Infect. Immun. 81, 740–752. https://doi.org/10.1128/IAI.01269-12

Handa, O., Naito, Y., Yoshikawa, T., 2010. *Helicobacter pylori*: A ROS-inducing bacterial species in the stomach. Inflamm. Res. 59, 997–1003. https://doi.org/10.1007/s00011-010-0245-x

Hänninen, M.L., 1991. Sensitivity of *Helicobacter pylori* to Different Bile Salts. Eur. J. Clin. Microbiol. Infect. Dis. 10, 515–518.

Harris, P.R., Smythies, L.E., Smith, P.D., Perez-Perez, G.I., 2013. Role of childhood infection in the sequelae of *H. pylori* disease. Gut Microbes 4, 426–438. https://doi.org/10.4161/gmic.26943

Hartley-Tassell, L.E., Shewell, L.K., Day, C.J., Wilson, J.C., Sandhu, R., Ketley, J.M., Korolik, V., 2010. Identification and characterization of the aspartate chemosensory receptor of *Campylobacter jejuni*: The aspartate receptor of

Campylobacter jejuni. Mol. Microbiol. 75, 710–730. https://doi.org/10.1111/j.1365-2958.2009.07010.x

Haselhorst, T., Lamerz, A.-C., Itzstein, M. von, 2009. Saturation Transfer Difference NMR Spectroscopy as a Technique to Investigate Protein-Carbohydrate Interactions in Solution, in: Packer, N.H., Karlsson, N.G. (Eds.), Glycomics. Humana Press, Totowa, NJ, pp. 375–396. https://doi.org/10.1007/978-1-59745-022-5_26

Hooi, J.K.Y., Lai, W.Y., Ng, W.K., Suen, M.M.Y., Underwood, F.E., Tanyingoh, D., Malfertheiner, P., Graham, D.Y., Wong, V.W.S., Wu, J.C.Y., Chan, F.K.L., Sung, J.J.Y., Kaplan, G.G., Ng, S.C., 2017a. Global Prevalence of *Helicobacter pylori* Infection: Systematic Review and Meta-analysis. Gastroenterology 153, 420–429. https://doi.org/10.1053/j.gastro.2017.04.022

Hooi, J.K.Y., Lai, W.Y., Ng, W.K., Suen, M.M.Y., Underwood, F.E., Tanyingoh, D., Malfertheiner, P., Graham, D.Y., Wong, V.W.S., Wu, J.C.Y., Chan, F.K.L., Sung, J.J.Y., Kaplan, G.G., Ng, S.C., 2017b. Global Prevalence of *Helicobacter pylori* Infection: Systematic Review and Meta-Analysis. Gastroenterology 153, 420–429. https://doi.org/10.1053/j.gastro.2017.04.022

Howitt, M.R., Lee, J.Y., Lertsethtakarn, P., Vogelmann, R., Joubert, L.-M., Ottemann, K.M., Amieva, M.R., 2011. ChePep Controls *Helicobacter pylori* Infection of the Gastric Glands and Chemotaxis in the

Epsilonproteobacteria. mBio 2, e00098-11. https://doi.org/10.1128/mBio.00098-11

Huang, J.Y., Goers Sweeney, E., Guillemin, K., Amieva, M.R., 2017. Multiple Acid Sensors Control *Helicobacter pylori* Colonization of the Stomach. PLOS Pathog. 13, e1006118. https://doi.org/10.1371/journal.ppat.1006118

Huang, J.Y., Sweeney, E.G., Sigal, M., Zhang, H.C., Remington, S.J., Cantrell, M.A., Kuo, C.J., Guillemin, K., Amieva, M.R., 2015. Chemodetection and Destruction of Host Urea Allows *Helicobacter pylori* to Locate the Epithelium. Cell Host Microbe 18, 147–156. https://doi.org/10.1016/j.chom.2015.07.002

Javed, S., Skoog, E.C., Solnick, J.V., 2019. Impact of *Helicobacter pylori* Virulence Factors on the Host Immune Response and Gastric Pathology. Curr. Top. Microbiol. Immunol. 421, 21–52. https://doi.org/10.1007/978-3-030-15138-6_2

Jiménez-Pearson, M.A., Delany, I., Scarlato, V., Beier, D., 2005. Phosphate flow in the chemotactic response system of *Helicobacter pylori*. Microbiology 151, 3299–3311. https://doi.org/10.1099/mic.0.28217-0

Johnson, K.S., Elgamoudi, B.A., Jen, F.E.-C., Day, C.J., Sweeney, E.G., Pryce, M.L., Guillemin, K., Haselhorst, T., Korolik, V., Ottemann, K.M., 2021. The dCache Chemoreceptor TlpA of *Helicobacter pylori* Binds Multiple Attractant and Antagonistic Ligands via Distinct Sites. mBio 12.

Johnson, K.S., Ottemann, K.M., 2018. Colonization, localization, and inflammation: the roles of *H. pylori* chemotaxis *in vivo*. Curr. Opin. Microbiol. 41, 51–57. https://doi.org/10.1016/j.mib.2017.11.019

Josefowicz, S.Z., Lu, L.-F.F., Rudensky, A.Y., 2012. Regulatory T Cells: Mechanisms of Differentiation and Function. Annu. Rev. Immunol. 30, 531–564. https://doi.org/10.1146/annurev.immunol.25.022106.141623

Keilberg, D., Ottemann, K.M., 2016. How *H elicobacter pylori* senses, targets and interacts with the gastric epithelium: *H. pylori* -gastric epithelium interaction. Environ. Microbiol. 18, 791–806. https://doi.org/10.1111/1462-2920.13222

Keilberg, D., Steele, N., Fan, S., Yang, C., Zavros, Y., Ottemann, K.M., 2020. Gastric Metabolomics Detects *Helicobacter pylori* Correlated Loss of Numerous Metabolites in Both the Corpus and Antrum. Infect. Immun. 89, e00690-20, /iai/89/2/IAI.00690-20.atom. https://doi.org/10.1128/IAI.00690-20

Keilberg, D., Zavros, Y., Shepherd, B., Salama, N.R., Ottemann, K.M., 2016. Spatial and Temporal Shifts in Bacterial Biogeography and Gland Occupation during the Development of a Chronic Infection. mBio 7, e01705-16, /mbio/7/5/e01705-16.atom. https://doi.org/10.1128/mBio.01705-16

Krell, T., 2015. Tackling the bottleneck in bacterial signal transduction research: high-throughput identification of signal molecules: High-throughput

identification of signal molecules. Mol. Microbiol. 96, 685–688. https://doi.org/10.1111/mmi.12975

Krieger, E., Koraimann, G., Vriend, G., 2002. Increasing the precision of comparative models with YASARA NOVA-a self-parameterizing force field. Proteins Struct. Funct. Bioinforma. 47, 393–402. https://doi.org/10.1002/prot.10104

Lam, K.H., Ling, T.K.W., Au, S.W.N., 2010. Crystal structure of activated CheY1 from *Helicobacter pylori*. J. Bacteriol. 192, 2324–2334. https://doi.org/10.1128/JB.00603-09

Larussa, T., Leone, I., Suraci, E., Imeneo, M., Luzza, F., 2015. *Helicobacter pylori* and T Helper Cells: Mechanisms of Immune Escape and Tolerance. J. Immunol. Res. 2015. https://doi.org/10.1155/2015/981328

Lazar, V., Ditu, L.-M., Pircalabioru, G.G., Gheorghe, I., Curutiu, C., Holban, A.M., Picu, A., Petcu, L., Chifiriuc, M.C., 2018. Aspects of Gut Microbiota and Immune System Interactions in Infectious Diseases, Immunopathology, and Cancer. Front. Immunol. 9, 1830. https://doi.org/10.3389/fimmu.2018.01830

Lee, A., O'Rourke, J., De Ungria, M.C., Robertson, B., Daskalopoulos, G., Dixon, M.F., 1997. A standardized mouse model of *Helicobacter pylori* infection: introducing the Sydney strain. Gastroenterology 112, 1386–1397. https://doi.org/10.1016/s0016-5085(97)70155-0

Lee, W.C., Goh, K.L., Loke, M.F., Vadivelu, J., 2017. Elucidation of the Metabolic Network of *Helicobacter pylori* J99 and Malaysian Clinical Strains by Phenotype Microarray. Helicobacter 22, e12321. https://doi.org/10.1111/hel.12321

Lertsethtakarn, P., Draper, J., Ottemann, K.M., 2012. Chemotactic signal transduction in *Helicobacter pylori*, in: Gross, R., Beierm, D. (Eds.), Two-Component Systems in Bacteria. Horizon Scientific Press, pp. 355–370.

Lertsethtakarn, P., Howitt, M.R., Castellon, J., Amieva, M.R., Ottemann, K.M., 2015. *Helicobacter pylori* CheZHP and ChePep form a novel chemotaxis-regulatory complex distinct from the core chemotaxis signaling proteins and the flagellar motor: *H. pylori* CheZ HP and ChePep form a distinct complex. Mol. Microbiol. 97, 1063–1078. https://doi.org/10.1111/mmi.13086

Lertsethtakarn, P., Ottemann, K.M., 2010. A remote CheZ orthologue retains phosphatase function. Mol. Microbiol. 77, 225–235. https://doi.org/10.1111/j.1365-2958.2010.07200.x

Lertsethtakarn, P., Ottemann, K.M., Hendrixson, D.R., 2011. Motility and Chemotaxis in *Campylobacter* and *Helicobacter*. Annu. Rev. Microbiol. 65, 389–410. https://doi.org/10.1146/annurev-micro-090110-102908

Liu, Y., McBride, R., Stoll, M., Palma, A.S., Silva, L., Agravat, S., Aoki-Kinoshita, K.F., Campbell, M.P., Costello, C.E., Dell, A., Haslam, S.M., Karlsson, N.G., Khoo, K.-H., Kolarich, D., Novotny, M.V., Packer, N.H.,

Ranzinger, R., Rapp, E., Rudd, P.M., Struwe, W.B., Tiemeyer, M., Wells, L., York, W.S., Zaia, J., Kettner, C., Paulson, J.C., Feizi, T., Smith, D.F., 2017. The minimum information required for a glycomics experiment (MIRAGE) project: improving the standards for reporting glycan microarray-based data. Glycobiology 27, 280–284. https://doi.org/10.1093/glycob/cww118

Lowenthal, Andrew C., Hill, M., Sycuro, L.K., Mehmood, K., Salama, N.R., Ottemann, K.M., 2009. Functional analysis of the *Helicobacter pylori* flagellar switch proteins. J. Bacteriol. 191, 7147–7156. https://doi.org/10.1128/JB.00749-09

Lowenthal, Andrew C, Simon, C., Fair, A.S., Mehmood, K., Terry, K., Anastasia, S., Ottemann, K.M., 2009. A fixed-time diffusion analysis method determines that the three cheV genes of *Helicobacter pylori* differentially affect motility. Microbiology 155, 1181–1191. https://doi.org/10.1099/mic.0.021857-0

Lundgren, A., Trollmo, C., Edebo, A., Svennerholm, A.-M., Lundin, B.S., 2005. *Helicobacter pylori*-Specific CD4♌ T Cells Home to and Accumulate in the Human Helicobacter pylori-Infected Gastric Mucosa. INFECT IMMUN 73, 8.

Machuca, M.A., Johnson, K.S., Liu, Y.C., Steer, D.L., Ottemann, K.M., Roujeinikova, A., 2017. *Helicobacter pylori* chemoreceptor TlpC

mediates chemotaxis to lactate. Sci. Rep. 7, 14089. https://doi.org/10.1038/s41598-017-14372-2

Martinez, L.E., O'Brien, V.P., Leverich, C., Knoblaugh, S.E., Salama, N.R., 2018. Non-helical *Helicobacter pylori* show altered gland colonization and elicit less gastric pathology during chronic infection (preprint). Microbiology. https://doi.org/10.1101/505107

Martín-Mora, D., Ortega, Á., Pérez-Maldonado, F.J., Krell, T., Matilla, M.A., 2018. The activity of the C4-dicarboxylic acid chemoreceptor of *Pseudomonas aeruginosa* is controlled by chemoattractants and antagonists. Sci. Rep. 8, 2102. https://doi.org/10.1038/s41598-018-20283-7

Matilla, M.A., Krell, T., 2018. The effect of bacterial chemotaxis on host infection and pathogenicity. FEMS Microbiol. Rev. 42, 40–67. https://doi.org/10.1093/femsre/fux052

Mayer, M., Meyer, B., 1999. Characterization of Ligand Binding by Saturation Transfer Difference NMR Spectroscopy. Angew. Chem. Int. Ed Engl. 38, 1784–1788. https://doi.org/10.1002/(SICI)1521-3773(19990614)38:12<1784::AID-ANIE1784>3.0.CO;2-Q

McGee, D.J., Langford, M.L., Watson, E.L., Carter, J.E., Chen, Y.-T., Ottemann, K.M., 2005. Colonization and inflammation deficiencies in Mongolian gerbils infected by *Helicobacter pylori* chemotaxis mutants. Infect. Immun. 73, 1820–1827. https://doi.org/10.1128/IAI.73.3.1820-1827.2005

Mcgee, D.J., Radcliff, F.J., Mendz, G.L., Ferrero, R.L., Mobley, H.L.T., 1999. *Helicobacter pylori* rocF Is Required for Arginase Activity and Acid Protection In Vitro but Is Not Essential for Colonization of Mice or for Urease Activity. J BACTERIOL 181, 9.

Mckellar, J.L.O., Minnell, J.J., Gerth, M.L., 2015. A high-throughput screen for ligand binding reveals the specificities of three amino acid chemoreceptors from *Pseudomonas syringae pv. actinidiae*. Mol. Microbiol. 96, 694–707. https://doi.org/10.1111/mmi.12964

Mendz, G.L., Hazell, S.L., Srinivasan, S., 1995. Fumarate reductase: a target for therapeutic intervention against *Helicobacter pylori*. Arch. Biochem. Biophys. 321, 153–159. https://doi.org/10.1006/abbi.1995.1380

Mizote, T., Yoshiyama, H., Nakazawa, T., 1997. Urease-independent chemotactic responses of *Helicobacter pylori* to urea, urease inhibitors, and sodium bicarbonate. Infect. Immun. 65, 1519–1521.

Naito, Y., Yoshikawa, T., 2002. Molecular and Cellular Mechanisms Involved in *Helicobacter pylori*-Induced Inflammation and Oxidative Stress. Free Radic. Biol. Med. 33, 323–336.

Nakamura, H., Yoshiyama, H., Takeuchi, H., Mizote, T., Okita, K., Nakazawa, T., 1998. Urease plays an important role in the chemotactic motility of *Helicobacter pylori* in a viscous environment. Infect. Immun. 66, 4832–4837.

Nedenskov, P., 1994. Nutritional requirements for growth of *Helicobacter pylori*. Appl. Environ. Microbiol. 60, 3450–3453.

Neithercut, W.D., Rowe, P.A., El Nujumi, A.M., Dahill, S., McColl, K.E.L., 1993. Effect of *Helicobacter pylori* Infection on Intragastric Urea and Ammonium Concentrations in Patients with Chronic Renal Failure. J. Clin. Pathol. 46, 544–547. https://doi.org/Doi 10.1136/Jcp.46.6.544

Nishiumi, S., Yoshida, M., Azuma, T., 2017. Alterations in metabolic pathways in stomach of mice infected with *Helicobacter pylori*. Microb. Pathog. 109, 78–85. https://doi.org/10.1016/j.micpath.2017.05.027

Oertli, M., Sundquist, M., Hitzler, I., Engler, D.B., Arnold, I.C., Reuter, S., Maxeiner, J., Hansson, M., Taube, C., Quiding-Järbrink, M., Müller, A., 2012. DC-derived IL-18 drives Treg differentiation, murine *Helicobacter pylori*–specific immune tolerance, and asthma protection. J. Clin. Invest. 122, 1082–1096. https://doi.org/10.1172/JCI61029

Parsonnet, J., 2014. Are there benefits of *Helicobacter pylori* infection?, in: *Helicobacter Pylori* Eradication as a Strategy for Preventing Gastric Cancer IARC Working Group Report Volume 8. pp. 72–79.

Peek, R.M., Fiske, C., Wilson, K.T., 2010. Role of Innate Immunity in *Helicobacter pylori* -Induced Gastric Malignancy. Physiol Rev 90, 831–858.

Perkins, A., Tudorica, D.A., Amieva, M.R., Remington, S.J., Guillemin, K., 2019. *Helicobacter pylori* senses bleach (HOCl) as a chemoattractant using a

cytosolic chemoreceptor. PLOS Biol. 17, e3000395. https://doi.org/10.1371/journal.pbio.3000395

Pittman, M.S., Goodwin, M., Kelly, D.J., 2001. Chemotaxis in the human gastric pathogen *Helicobacter pylori*: different roles for CheW and the three CheV paralogues, and evidence for CheV2 phosphorylation. Microbiology 147, 2493–2504.

Plummer, M., Franceschi, S., Vignat, J., Forman, D., de Martel, C., 2015. Global burden of gastric cancer attributable to *Helicobacter pylori*. Int. J. Cancer J. Int. Cancer 136, 487–490. https://doi.org/10.1002/ijc.28999

Polk, D.B., Peek, R.M., 2010. *Helicobacter pylori*: gastric cancer and beyond. Nat. Rev. Cancer 10, 403–14. https://doi.org/10.1038/nrc2857

Rader, B.A., Wreden, C., Hicks, K.G., Sweeney, E.G., Ottemann, K.M., Guillemin, K., 2011. *Helicobacter pylori* perceives the quorum-sensing molecule AI-2 as a chemorepellent via the chemoreceptor TlpB. Microbiology 157, 2445–2455. https://doi.org/10.1099/mic.0.049353-0

Rahman, H., King, R.M., Shewell, L.K., Semchenko, E.A., Hartley-Tassell, L.E., Wilson, J.C., Day, C.J., Korolik, V., 2014. Characterisation of a Multi-ligand Binding Chemoreceptor CcmL (Tlp3) of *Campylobacter jejuni*. PLoS Pathog. 10, 1–14. https://doi.org/10.1371/journal.ppat.1003822

Reynolds, D.J., Penn, C.W., 1994. Characteristics of *Helicobacter pylori* growth in a defined medium and determination of its amino acid requirements.

Microbiology 140, 2649–2656. https://doi.org/10.1099/00221287-140-10-2649

Rolig, A.S., Carter, J.E., Ottemann, K.M., 2011. Bacterial chemotaxis modulates host cell apoptosis to establish a T-helper cell, type 17 (Th17)-dominant immune response in *Helicobacter pylori* infection. Proc. Natl. Acad. Sci. 108, 19749–19754. https://doi.org/10.1073/pnas.1104598108

Rolig, A.S., Shanks, J., Carter, J.E., Ottemann, K.M., 2012. *Helicobacter pylori* Requires TlpD-Driven Chemotaxis To Proliferate in the Antrum. Infect. Immun. 80, 3713–3720. https://doi.org/10.1128/IAI.00407-12

Rugge, M., Correa, P., Dixon, M.F., Fiocca, R., Hattori, T., Lechago, J., Leandro, G., Price, A.B., Sipponen, P., Solcia, E., Watanabe, H., Genta, R.M., 2002. Gastric mucosal atrophy: interobserver consistency using new criteria for classification and grading. Aliment. Pharmacol. Ther. 16, 1249–1259. https://doi.org/10.1046/j.1365-2036.2002.01301.x

Salama, N.R., Hartung, M.L., Müller, A., 2013. Life in the human stomach: persistence strategies of the bacterial pathogen *Helicobacter pylori*. Nat. Rev. Microbiol. 11, 385–399. https://doi.org/10.1038/nrmicro3016

Sanders, L., Andermann, T.M., Ottemann, K.M., 2013. A supplemented soft agar chemotaxis assay demonstrates the *Helicobacter pylori* chemotactic response to zinc and nickel. Microbiology 159, 46–57. https://doi.org/10.1099/mic.0.062877-0

Schreiber, S., Bucker, R., Groll, C., Azevedo-Vethacke, M., Garten, D., Scheid, P., Friedrich, S., Gatermann, S., Josenhans, C., Suerbaum, S., 2005. Rapid Loss of Motility of *Helicobacter pylori* in the Gastric Lumen In Vivo. Infect. Immun. 73, 1584–1589. https://doi.org/10.1128/IAI.73.3.1584-1589.2005

Schreiber, S., Konradt, M., Groll, C., Scheid, P., Hanauer, G., Werling, H.-O., Josenhans, C., Suerbaum, S., 2004. The spatial orientation of *Helicobacter pylori* in the gastric mucus. Proc. Natl. Acad. Sci. 101, 5024–5029. https://doi.org/10.1073/pnas.0308386101

Schreiber, S., Scheid, P., 1997. Gastric mucus of the guinea pig: proton carrier and diffusion barrier. Am. J. Physiol.-Gastrointest. Liver Physiol. 272, G63–G70. https://doi.org/10.1152/ajpgi.1997.272.1.G63

Schweinitzer, T., Mizote, T., Ishikawa, N., Dudnik, A., Inatsu, S., Schreiber, S., Suerbaum, S., Aizawa, S.-I., Josenhans, C., 2008. Functional Characterization and Mutagenesis of the Proposed Behavioral Sensor TlpD of *Helicobacter pylori*. J. Bacteriol. 190, 3244–3255. https://doi.org/10.1128/JB.01940-07

Serrano, C., Wright, S.W., Bimczok, D., Shaffer, C.L., Cover, T.L., Venegas, A., Salazar, M.G., Smythies, L.E., Harris, P.R., Smith, P.D., 2013. Downregulated Th17 responses are associated with reduced gastritis in *Helicobacter pylori*–infected children. Mucosal Immunol. 6, 950–959. https://doi.org/10.1038/mi.2012.133

Sgouras, D.N., Trang, T.T.H., Yamaoka, Y., 2015. Pathogenesis of *Helicobacter pylori* Infection. Helicobacter 20, 8–16. https://doi.org/10.1111/hel.12251

Shiomi, S., Toriie, A., Imamura, S., Konishi, H., Mitsufuji, S., Iwakura, Y., Yamaoka, Y., Ota, H., Yamamoto, T., Imanishi, J., Kita, M., 2008. IL-17 is Involved in *Helicobacter pylori* -Induced Gastric Inflammatory Responses in a Mouse Model. Helicobacter 13, 518–524. https://doi.org/10.1111/j.1523-5378.2008.00629.x

Shiu, J., Blanchard, T.G., 2013. Dendritic cell function in the host response to *Helicobacter pylori* infection of the gastric mucosa. Pathog. Dis. 67, 46–53. https://doi.org/10.1111/2049-632X.12014

Sigal, M., Rothenberg, M.E., Logan, C.Y., Lee, J.Y., Honaker, R.W., Cooper, R.L., Passarelli, B., Camorlinga, M., Bouley, D.M., Alvarez, G., Nusse, R., Torres, J., Amieva, M.R., 2015. *Helicobacter pylori* Activates and Expands Lgr5+ Stem Cells Through Direct Colonization of the Gastric Glands. Gastroenterology 148, 1392-1404.e21. https://doi.org/10.1053/j.gastro.2015.02.049

Soehnlein, O., Lindbom, L., 2010. Phagocyte partnership during the onset and resolution of inflammation. Nat. Rev. Immunol. 10, 427–439. https://doi.org/10.1038/nri2779

Sweeney, E.G., Perkins, A., Kallio, K., Remington, S.J., Guillemin, K., 2018. Structures of the Ligand-Binding Domain of *Helicobacter pylori*

Chemoreceptor TlpA. Protein Sci. 27, 1961–1968. https://doi.org/10.1002/pro.3503

Terry, K., Go, A.C., Ottemann, K.M., 2006. Proteomic mapping of a suppressor of non-chemotactic cheW mutants reveals that *Helicobacter pylori* contains a new chemotaxis protein. Mol. Microbiol. 61, 871–882. https://doi.org/10.1111/j.1365-2958.2006.05283.x

Terry, K., Williams, S.M., Connolly, L., Ottemann, K.M., 2005. Chemotaxis Plays Multiple Roles during *Helicobacter pylori* Animal Infection. Infect. Immun. 73, 803–811. https://doi.org/10.1128/IAI.73.2.803-811.2005

Thompson, L.J., Danon, S.J., Wilson, J.E., O'Rourke, J.L., Salama, N.R., Falkow, S., Mitchell, H., Lee, A., 2004. Chronic *Helicobacter pylori* Infection with Sydney Strain 1 and a Newly Identified Mouse-Adapted Strain (Sydney Strain 2000) in C57BL/6 and BALB/c Mice. Infect. Immun. 72, 4668–4679. https://doi.org/10.1128/IAI.72.8.4668-4679.2004

Tomb, J.-F., White, O., Kerlavage, A.R., Clayton, R.A., Sutton, G.G., Fleischmann, R.D., Ketchum, K.A., Klenk, H.P., Gill, S., Dougherty, B.A., Nelson, K., Quackenbush, J., Zhou, L., Kirkness, E.F., Peterson, S., Loftus, B., Richardson, D., Dodson, R., Khalak, H.G., Glodek, A., McKenney, K., Fitzegerald, L.M., Lee, N., Adams, M.D., Hickey, E.K., Berg, D.E., Gocayne, J.D., Utterback, T.R., Peterson, J.D., Kelley, J.M., Cotton, M.D., Weidman, J.M., Fujii, C., Bowman, C., Watthey, L., Wallin, E., Hayes, W.S., Borodovsky, M., Karp, P.D., Smith, H.O., Fraser,

C.M., Venter, J.C., 1997. The complete genome sequence of the gastric pathogen *Helicobacter pylori*. Nature 388, 539–547. https://doi.org/10.1038/41483

Torchinsky, M.B., Garaude, J., Martin, A.P., Blander, J.M., 2009. Innate immune recognition of infected apoptotic cells directs T(H)17 cell differentiation. Nature 458, 78–82. https://doi.org/10.1038/nature07781

Trott, O., Olson, A.J., 2009. AutoDock Vina: Improving the speed and accuracy of docking with a new scoring function, efficient optimization, and multithreading. J. Comput. Chem. NA-NA. https://doi.org/10.1002/jcc.21334

Ud-Din, A.I.M.S., Khan, M.F., Roujeinikova, A., 2020. Broad Specificity of Amino Acid Chemoreceptor CtaA of *Pseudomonas fluorescens* Is Afforded by Plasticity of Its Amphipathic Ligand-Binding Pocket. Mol. Plant-Microbe Interactions® 33, 612–623. https://doi.org/10.1094/MPMI-10-19-0277-R

Upadhyay, A.A., Fleetwood, A.D., Adebali, O., Finn, R.D., Zhulin, I.B., 2016. Cache Domains That are Homologous to, but Different from PAS Domains Comprise the Largest Superfamily of Extracellular Sensors in Prokaryotes. PLoS Comput. Biol. 12, 1–21. https://doi.org/10.1371/journal.pcbi.1004862

Valenzuela, M., Cáceres, A., Almarza, O., Bravo, D., Soto, S., Cerda, O., Toledo, H., 2014. Characterization of the Arginine Decarboxylase Gene (ORF

HP0422, *speA*) Involved in Acid Tolerance in *Helicobacter pylori*. Helicobacter 19, 182–193. https://doi.org/10.1111/hel.12115

Wadhams, G.H., Armitage, J.P., 2004. Making sense of it all: bacterial chemotaxis. Nat. Rev. Mol. Cell Biol. 5, 1024–1037. https://doi.org/10.1038/nrm1524

Wagner, A., Wang, C., Fessler, J., DeTomaso, D., Avila-Pacheco, J., Kaminski, J., Zaghouani, S., Christian, E., Thakore, P., Schellhaass, B., Akama-Garren, E., Pierce, K., Singh, V., Ron-Harel, N., Douglas, V.P., Bod, L., Schnell, A., Puleston, D., Sobel, R.A., Haigis, M., Pearce, E.L., Soleimani, M., Clish, C., Regev, A., Kuchroo, V.K., Yosef, N., 2021. Metabolic modeling of single Th17 cells reveals regulators of autoimmunity. Cell S0092867421007005. https://doi.org/10.1016/j.cell.2021.05.045

Wang, Z., Sun, H., Yao, X., Li, D., Xu, L., Li, Y., Tian, S., Hou, T., 2016. Comprehensive evaluation of ten docking programs on a diverse set of protein–ligand complexes: the prediction accuracy of sampling power and scoring power. Phys. Chem. Chem. Phys. 18, 12964–12975. https://doi.org/10.1039/C6CP01555G

White, J.R., Winter, J.A., Robinson, K., 2015. Differential inflammatory response to *Helicobacter pylori* infection: Etiology and clinical outcomes. J. Inflamm. Res. 8, 137–147. https://doi.org/10.2147/JIR.S64888

Williams, S.M., Chen, Y.-T., Andermann, T.M., Carter, J.E., McGee, D.J., Ottemann, K.M., 2007. *Helicobacter pylori* chemotaxis modulates

inflammation and bacterium-gastric epithelium interactions in infected mice. Infect. Immun. 75, 3747–3757. https://doi.org/10.1128/IAI.00082-07

Wilson, K.T., Crabtree, J.E., 2007. Immunology of *Helicobacter pylori*: Insights Into the Failure of the Immune Response and Perspectives on Vaccine Studies. Gastroenterology 133, 288–308. https://doi.org/10.1053/j.gastro.2007.05.008

Worku, M.L., Karim, Q.N., Spencer, J., Sidebotham, R.L., 2004. Chemotactic response of *Helicobacter pylori* to human plasma and bile. J. Med. Microbiol. 53, 807–811. https://doi.org/10.1099/jmm.0.45636-0

Wroblewski, L.E., Peek, R.M., Wilson, K.T., 2010. *Helicobacter pylori* and Gastric Cancer: Factors That Modulate Disease Risk. Clin. Microbiol. Rev. 23, 713–739. https://doi.org/10.1128/CMR.00011-10

Wuichet, K., Zhulin, I.B., 2010. Origins and Diversification of a Complex Signal Transduction System in Prokaryotes. Sci. Signal. 3, ra50–ra50. https://doi.org/10.1126/scisignal.2000724

Wunder, C., Churin, Y., Winau, F., Warnecke, D., Vieth, M., Lindner, B., Zähringer, U., Mollenkopf, H.-J., Heinz, E., Meyer, T.F., 2006. Cholesterol glucosylation promotes immune evasion by *Helicobacter pylori.* Nat. Med. 12, 1030–1038. https://doi.org/10.1038/nm1480

Yang, C., Ottemann, K.M., 2019. Control of bacterial colonization in the glands and crypts. Curr. Opin. Microbiol. 47, 38–44. https://doi.org/10.1016/j.mib.2018.11.004

Zhang, X., 2020. Mechanisms of persistence, innate immune activation and immunomodulation by the gastric pathogen *Helicobacter pylori.* Curr. Opin. Microbiol. 10.